Aalto University
School of Electrical
Engineering

E4230
Microwave EO Instrumetation

(5 cr)

Jaan Praks
Aalto University

Aalto University
School of Electrical
Engineering

Radiative transfer

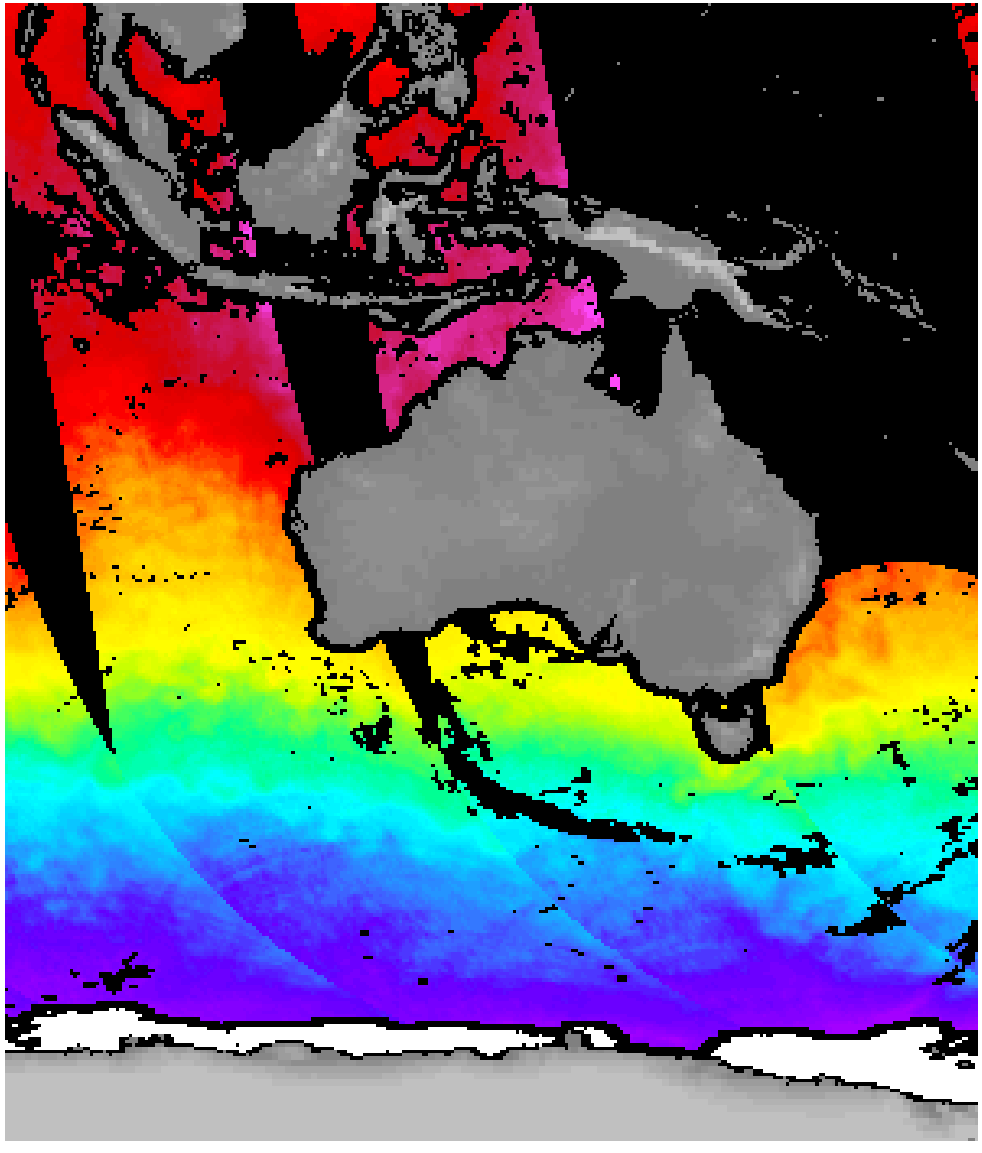

Emission: All substances at finite temperatures radiate EM energy

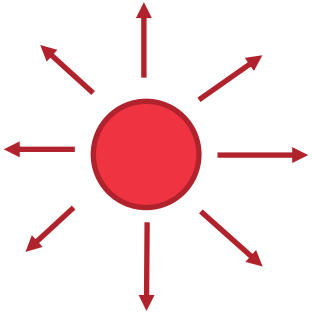

Absorption: Energy into heat

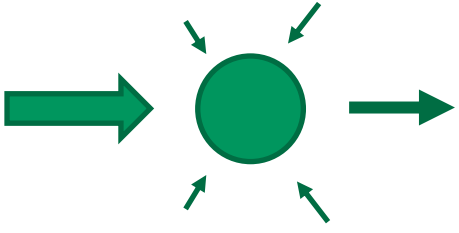

Scattering: Energy to other directions due to particles in the propagation path

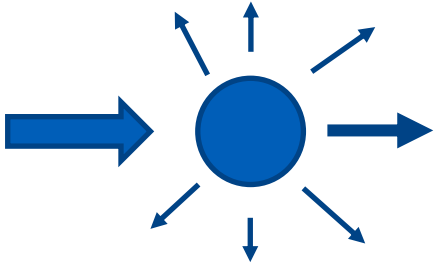

causing attenuation or **extinction** of the radiation

Radiative Transfer Equation 1/4

Absorption: Energy into heat

Scattering: Energy to other directions due to particles in the propagation path

Emission: All substances at finite temperatures radiate EM energy

Extinction: Intensity of brightness decreases during propagation in a medium (absorption and scattering)

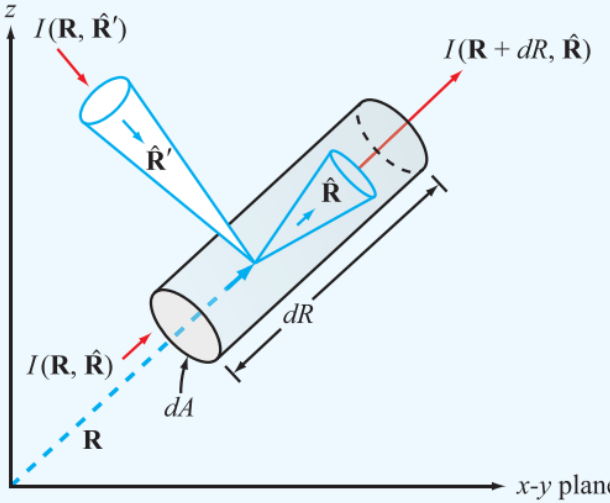

Figure 6-12: Radiation transfer through an infinitesimal cylinder.

Emission and extinction take place simultaneously in every point

Extinction: The **loss in brightness intensity *I(R)*** by extinction due to propagation over distance dr is:

$$dI_{extinction} = \kappa_e I \, dR$$

Extinction coefficient (power attenuation) = κ_e

(Note: Brightness = spectral brightness x bandwidth)

$$\kappa_e = \kappa_a + \kappa_s$$

κ_e = extinxtion coefficient

κ_a = absorption coefficient

κ_s = scattering coefficient

Radiative Transfer Equation 2/4

Emission by a small volume:

J_s and J_a: emission (absorption) and scattering source functions into direction R

$$dI_{emission} = \left(\kappa_a J_a + \kappa_s J_s\right) dR$$

We define **albedo**:

$$a = \frac{\kappa_s}{\kappa_e} = \frac{\kappa_s}{\kappa_a + \kappa_s}$$

=> Emission:

$$dI_{emission} = \kappa_e \left[\frac{\kappa_a}{\kappa_e} J_a + \frac{\kappa_s}{\kappa_e} J_s \right] dR = \kappa_e \left[(1-a) J_a + a J_s \right] dR$$

If J is the effective total source function

$$J = (1-a) J_a + a J_s$$

then emission by small volume =>

$$dI_{emission} = \kappa_e J \, dr$$

Emission and extinction together:

$$dI = I(R + dR) - I(R) = dI_{emission} - dI_{extinction}$$

By inserting emission and extinction:

$$dI = \kappa_e dR (J - I)$$

Radiative Transfer Equation 3/4

Insert optical depth, defined as: $d\tau = \kappa_e dR$

=>

Radiative transfer equation: $\frac{dI}{d\tau} + I = J$

At the boundary z = 0 we have $I(R=0)$

What is $I(R)$ in direction R ?

We define **optical depth** between points R_1 and R_2 :

$$\tau(R_1, R_2) = \int_{R_1}^{R_2} \kappa_e dR$$

Optical depth = total attenuation

Solution (not derived here):

T_B from Rayleigh-Jeans law:

(note the use of bandwidth here**)**

$$I(R) = I(0)e^{-\tau(0,R)} + \int_0^R \kappa_e(R')J(R')e^{-\tau(R',R)}dR'$$

$$I(R) = \frac{k\Delta f}{\lambda^2} T_B(R)$$

Radiative Transfer Equation 4/4

Thermodynamic balance=>

J_a is isotropic, follows Planck's law

$$J_a(R) = \frac{k}{\lambda^2} T(R) \Delta f$$

Analogous to absorption source function, J_s can be defined as follows:

$$J_s(R) = \frac{k}{\lambda^2} T_{VS}(R) \Delta f$$

where *volume scattered* brightness temperature T_{VS}

$$T_{VS}(R) = \frac{1}{4\pi} \iint_{4\pi} \phi(R; R_i) T_B(R_i) \, d\Omega_i$$

$\phi(R;R_i)$ is the phase function; accounts for energy scattered from direction R_i into direction R

Radiative transfer equation (using T_B):

$$T_B(r) = T_B(0) e^{-\tau(0,R)} + \int_0^R \kappa_e(R') \left[(1-a) T(R') + a T_{SC}(R') \right] e^{-\tau(r',r)} dR'$$

In a **scatter-free** medium:

($\kappa_s = 0; a = 0$)

This is the result we mostly use in radiative transfer problems

$$T_B(R) = T_B(0) e^{-\tau(0,R)} + \int_0^R \kappa_a(R') T(R') e^{-\tau(R',R)} dR'$$

Brightness temperature radiative transfer equation

$$\frac{dT_B}{d\tau} + T_B = (1-a)T + aT_{VS}.$$

(brightness temperature radiative transfer equation)

T – is the physical temperature

T_B - is the brightness temperature

T_{VS} - is the volume scattering temperature

a – albedo

τ– is the optical depth

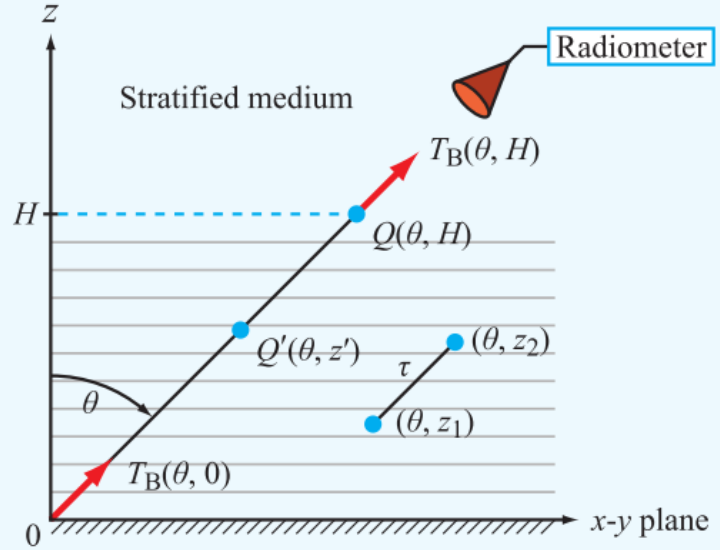

Figure 6-13: Geometry for brightness temperature radiative transfer equation.

Atmosphere

Interesting reading:
http://bencraven.org.uk/2016/01/17/how-high-is-the-sky/

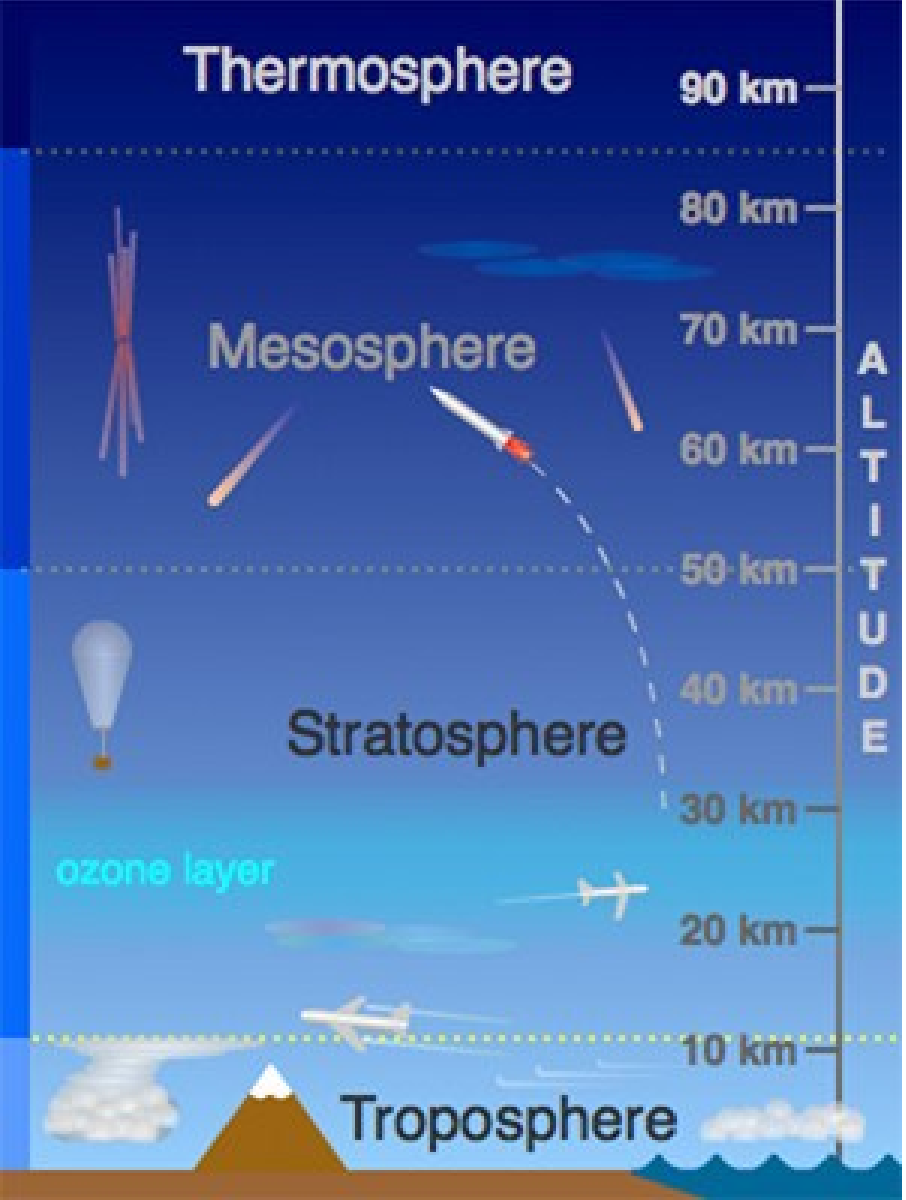

Sea level pressure atmosphere

Liquid atmosphere

Atmospheric composition

Except for water-vapor variations, the relative composition of the atmosphere essentially is constant up to 90 km above sea level.

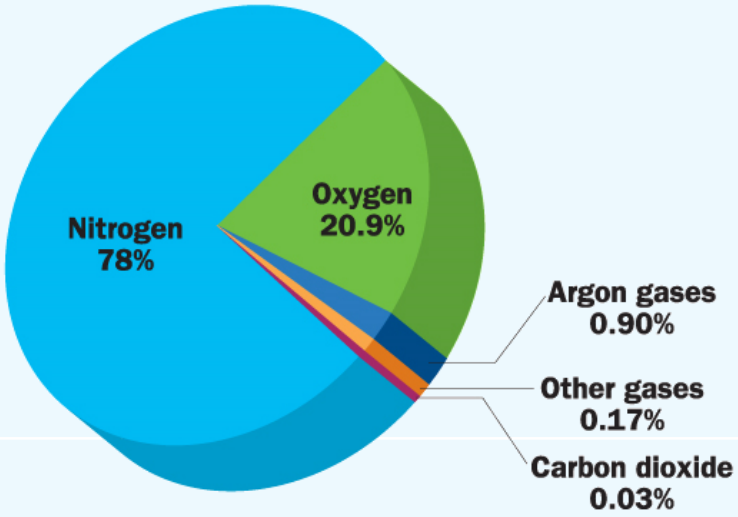

Table 8-1: Composition of clean, dry atmospheric air near sea level [from Hering, 1965].

Constituent gas	Gas symbol	Content (% by volume)	Molecular weight
Nitrogen	N_2	78.084	28.0134
Oxygen	O_2	20.9476	31.9988
Argon	Ar	0.932	39.948
Carbon dioxide	CO_2	0.0314	44.00995
Neon	Ne	0.001818	20.183
Helium	He	0.000524	4.0026
Krypton	Kr	0.000114	83.80
Xenon	Xe	0.0000087	131.30
Hydrogen	H_2	0.00005	2.01594
Methane	CH_4	0.0002	16.04303
Nitrous oxide	N_2O	0.00005	44.0128
Ozone	O_3	Summer: $0–7 \times 10^{-6}$	47.9982
		Winter: $0–2 \times 10^{-6}$	47.9982
Sulfur dioxide	SO_2	0 to 0.0001	64.0628
Nitrogen dioxide	NO_2	0 to 0.000002	46.0055
Ammonia	NH_3	0 to trace	17.03061
Carbon monoxide	CO	0 to trace	28.01055
Iodine	I_2	0 to 0.000001	253.8088

From: Microwave Radar and Radiometric Remote Sensing, by Ulaby and Long, 2014, with permission.

Standard Atmosphere

Pressure

Atmospheric pressure *P(z)* and decreases approximately exponentially with increasing geometric height *z* (Fig. 8-2).

Although its variation with height is somewhat irregular and is strongly dependent on time of day, season, geographic location, and atmospheric activity.

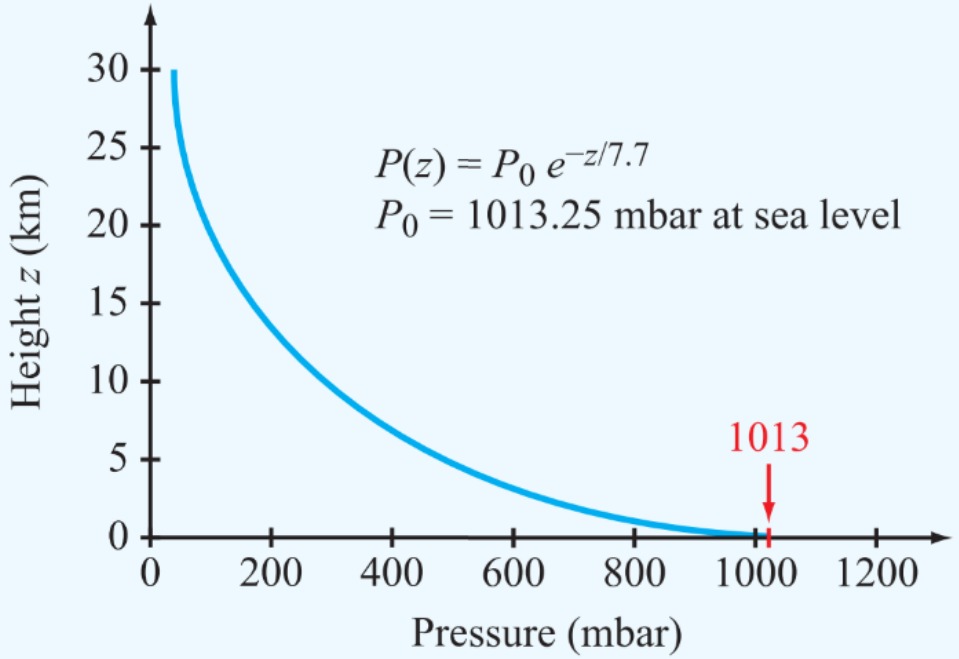

Figure 8-2: Atmospheric pressure decreases exponentially with height.

From: Microwave Radar and Radiometric Remote Sensing, by Ulaby and Long, 2014, with permission.

Standard Atmosphere

Temperature

The variation of atmospheric temperature with height, *T(z)*, exhibits a cyclic pattern that subdivides the Earth's atmosphere into a number of atmospheric layers

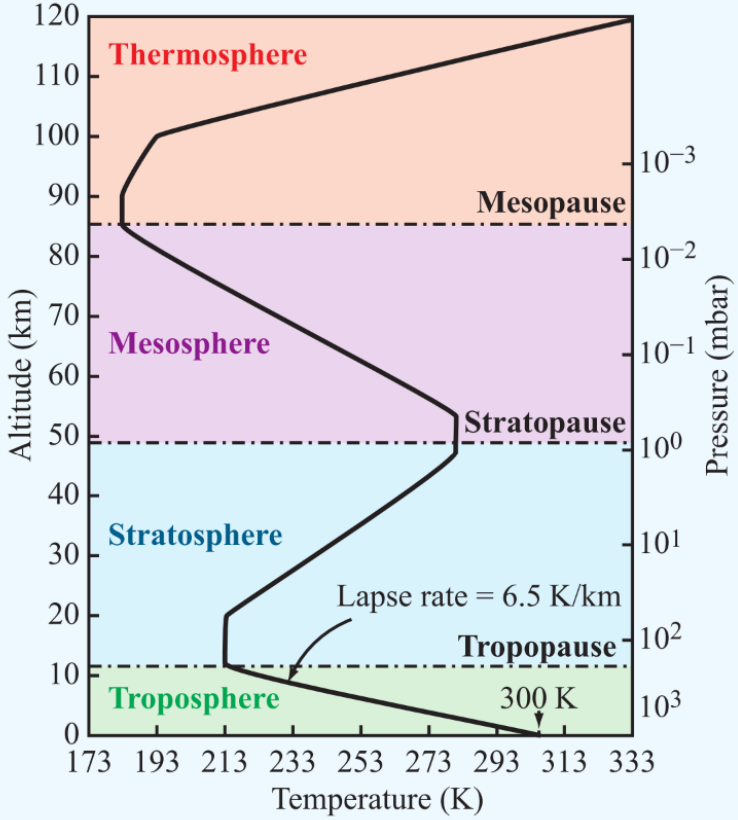

Figure 8-3: Atmospheric temperature height profile according to the Standard Atmosphere model.

From: Microwave Radar and Radiometric Remote Sensing, by Ulaby and Long, 2014, with permission.

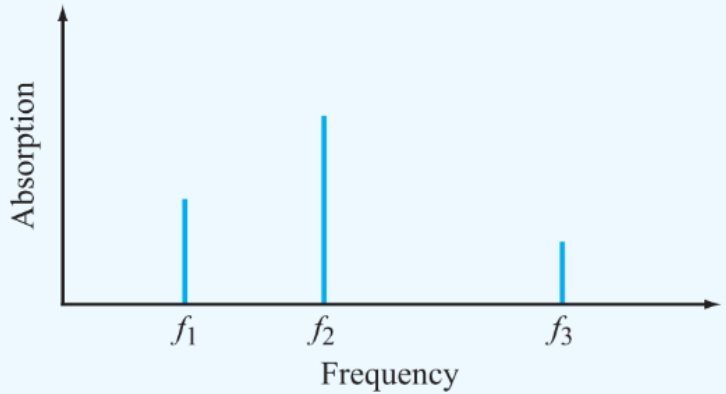

(a) Absorption spectrum of an isolated molecule

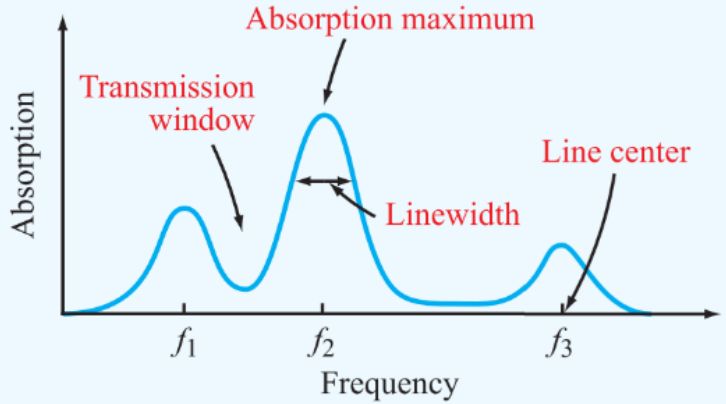

(b) Absorption spectrum of a gas

Figure 8-4: Absorption spectrum of (a) a single isolated molecule and (b) a gas containing many molecules.

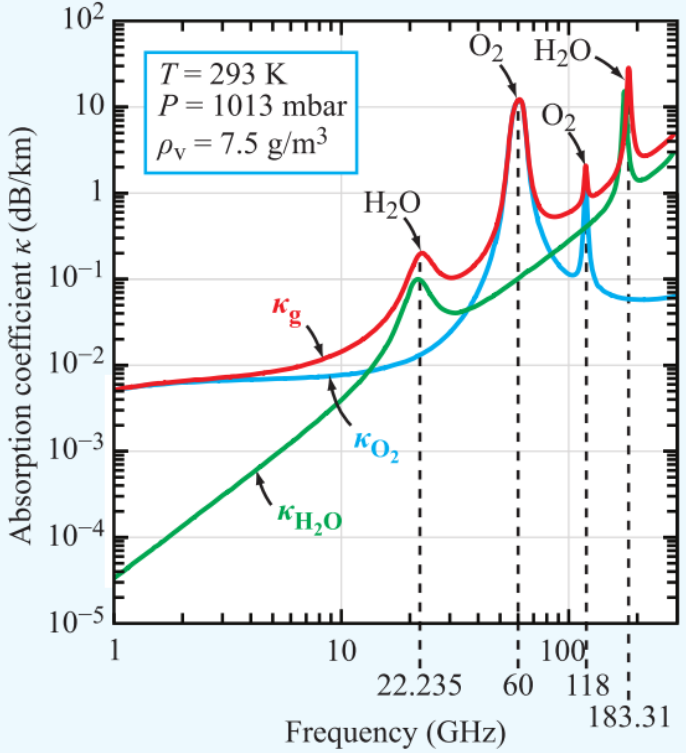

Figure 8-7: Absorption spectra of oxygen, water vapor, and their sum at sea level.

From: Microwave Radar and Radiometric Remote Sensing, by Ulaby and Long, 2014, with permission.

Oxygen and **water vapor** are the **only atmospheric constituents** that exhibit **significant absorption** bands in the microwave spectrum.

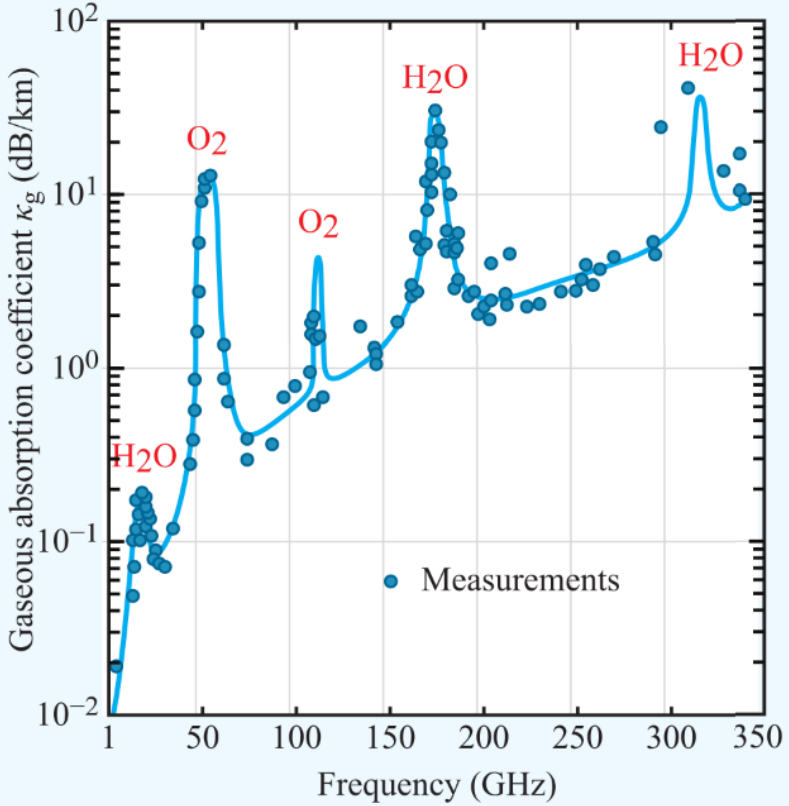

Figure 8-8: Microwave absorption spectrum due to atmospheric gases, $\kappa_g(f)$, at sea level for surface conditions $P_0 = 1013$ mb, $T_0 = 293$ K, and $\rho_0 = 7.5$ g/m^3. Solid curves are calculated according to theory, and dots are measured values [Crane, 1981].

From: Microwave Radar and Radiometric Remote Sensing, by Ulaby and Long, 2014, with permission.

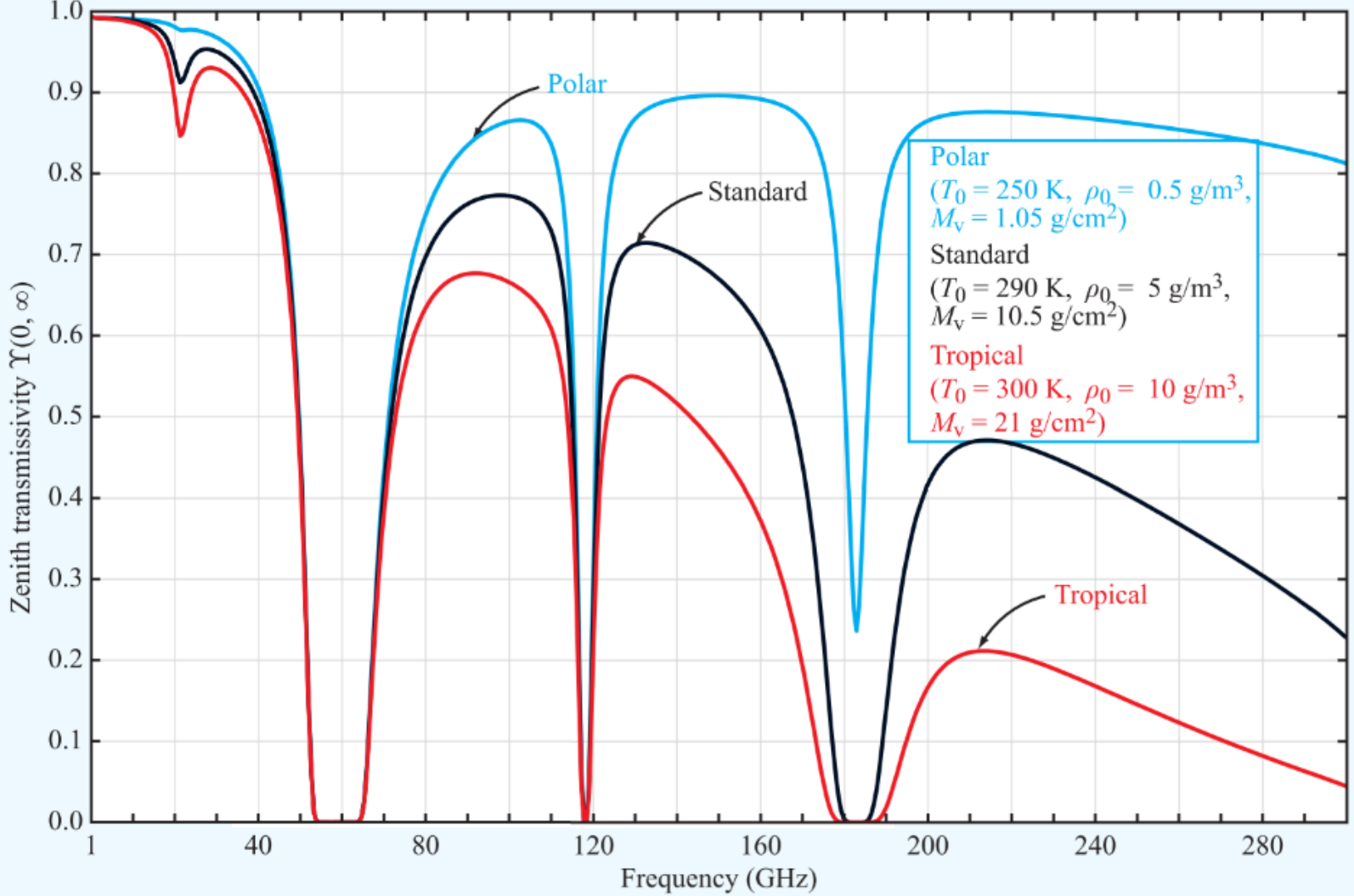

Figure 8-14: Atmosphere transmissivity as characterized by different surface temperatures T_0 and integrated water-vapor content M_v.

From:

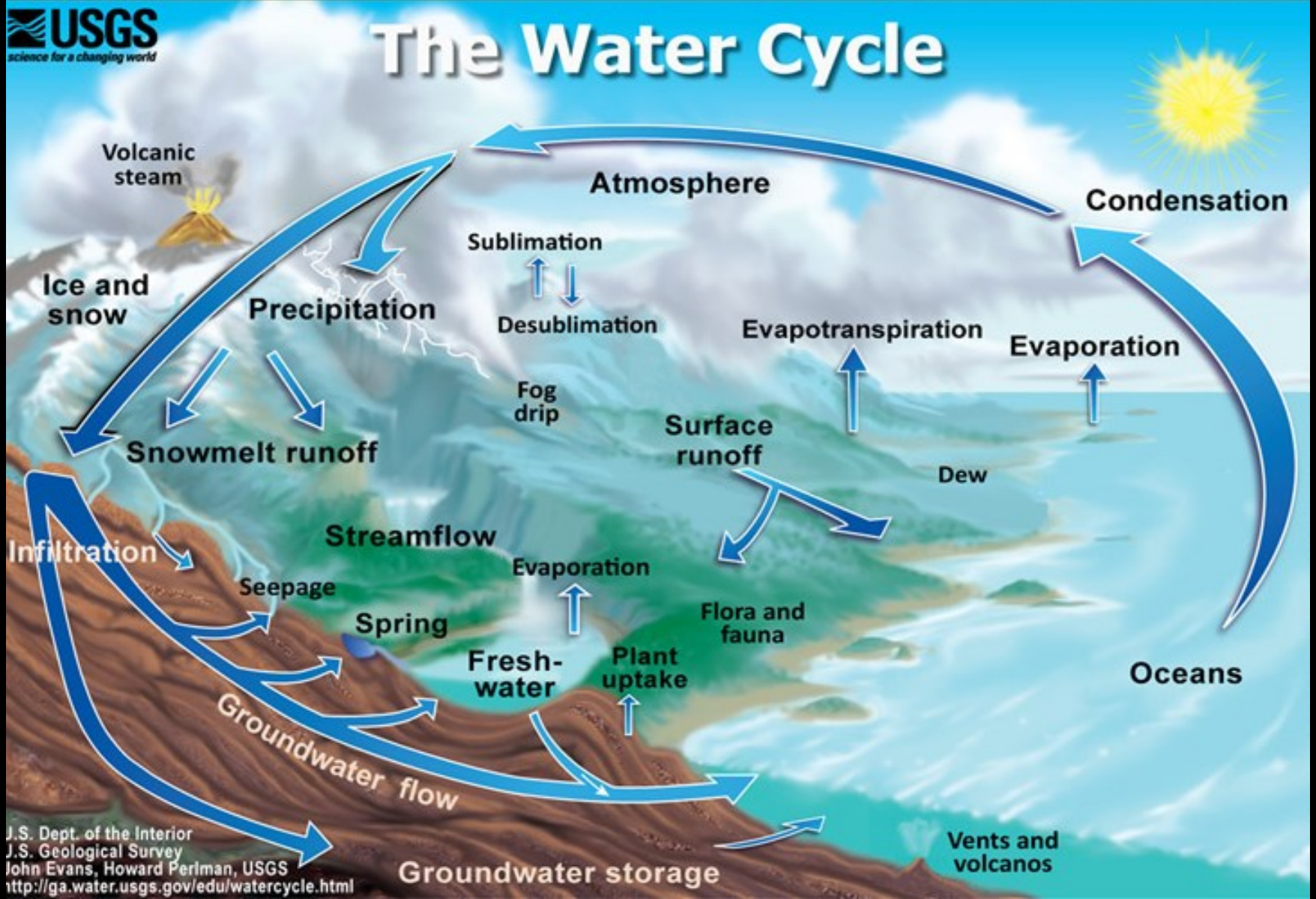
USGS
science for a changing world
The Water Cycle
Volcanic steam
Atmosphere
Condensation
Sublimation
Desublimation
Ice and snow
Precipitation
Evapotranspiration
Evaporation
Fog drip
Surface runoff
Snowmelt runoff
Dew
Streamflow
Infiltration
Evaporation
Seepage
Flora and fauna
Spring
Fresh-water
Plant uptake
Oceans
Groundwater flow
Vents and volcanos
Groundwater storage
U.S. Dept. of the Interior
U.S. Geological Survey
John Evans, Howard Perlman, USGS
http://ga.water.usgs.gov/edu/watercycle.html

Aalto University
School of Electrical
Engineering

Atmospheric absorption and radiometer measurement

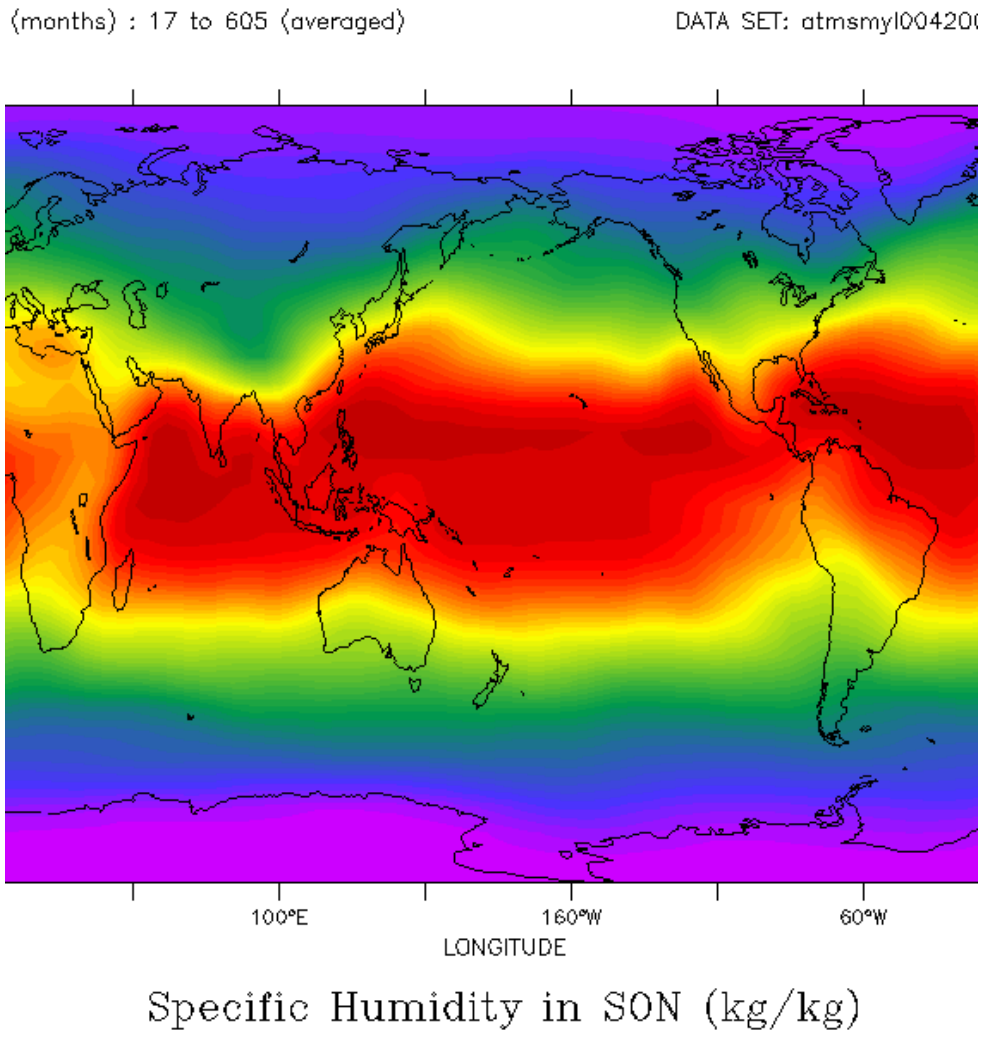

Upward looking radiometer

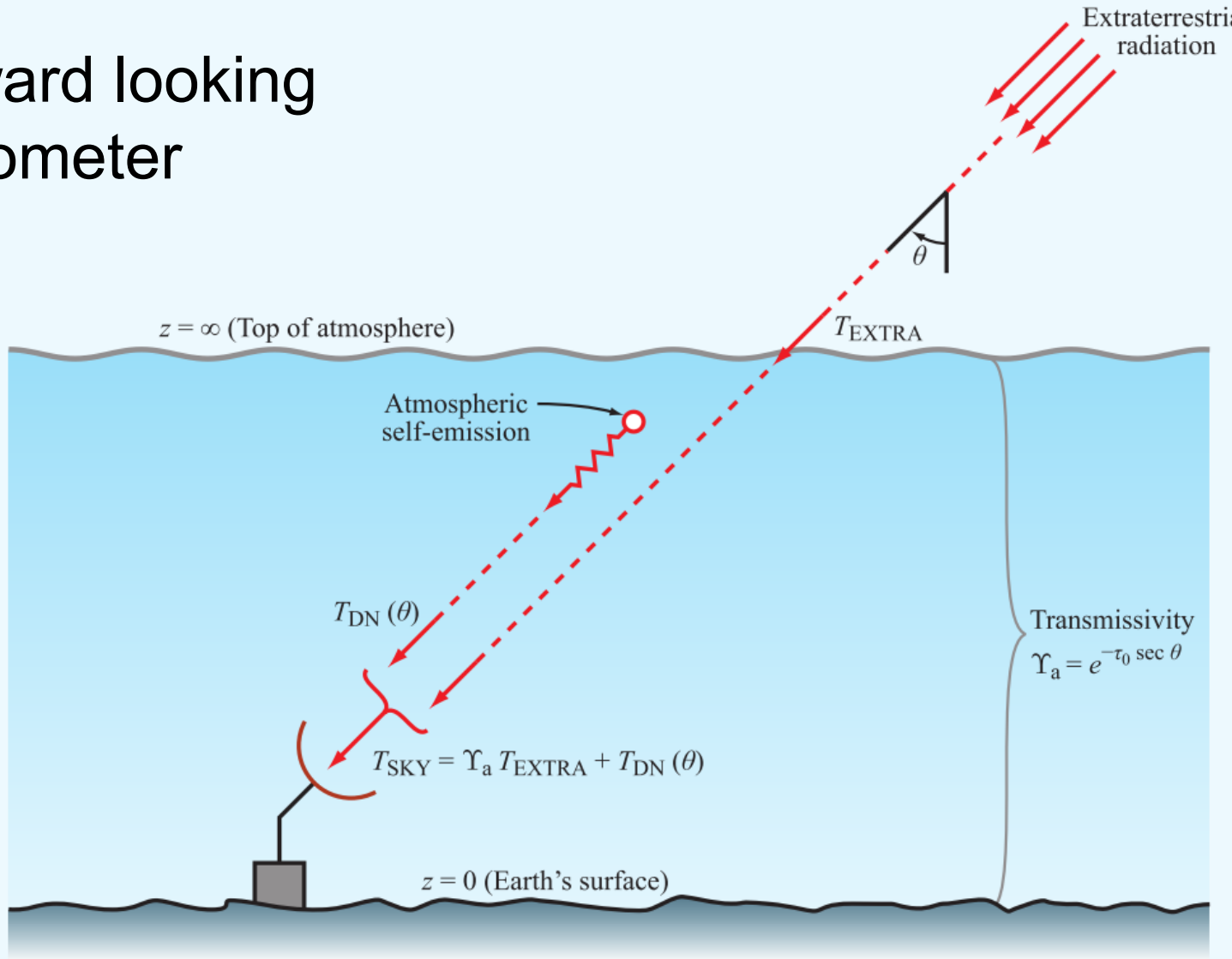

From: Microwave Radar and Radiometric Remote Sensing, by Ulaby and Long, 2014, with permission.

(a) direct and (b) inverse problems in atmospheric remote sensing

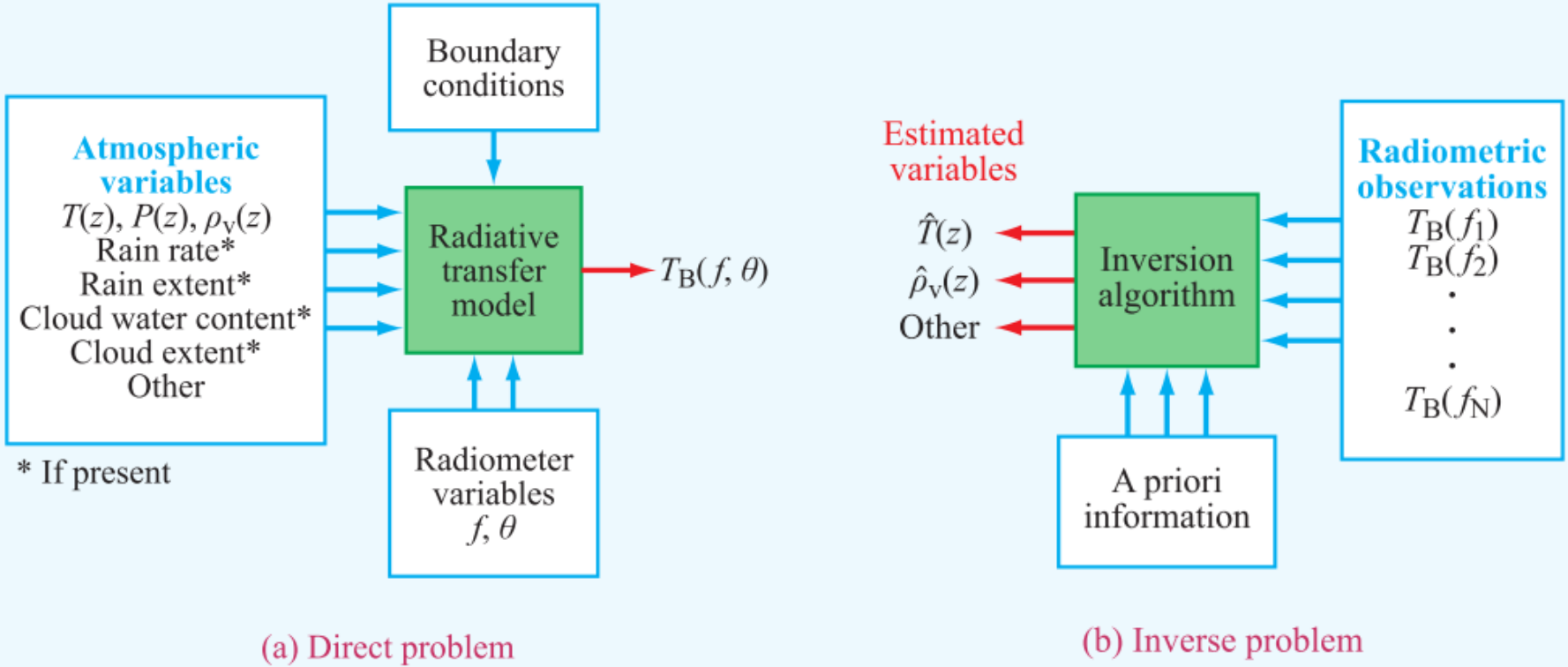

From: Microwave Radar and Radiometric Remote Sensing, by Ulaby and Long, 2014, with permission.

Optical thickness of atmosphere

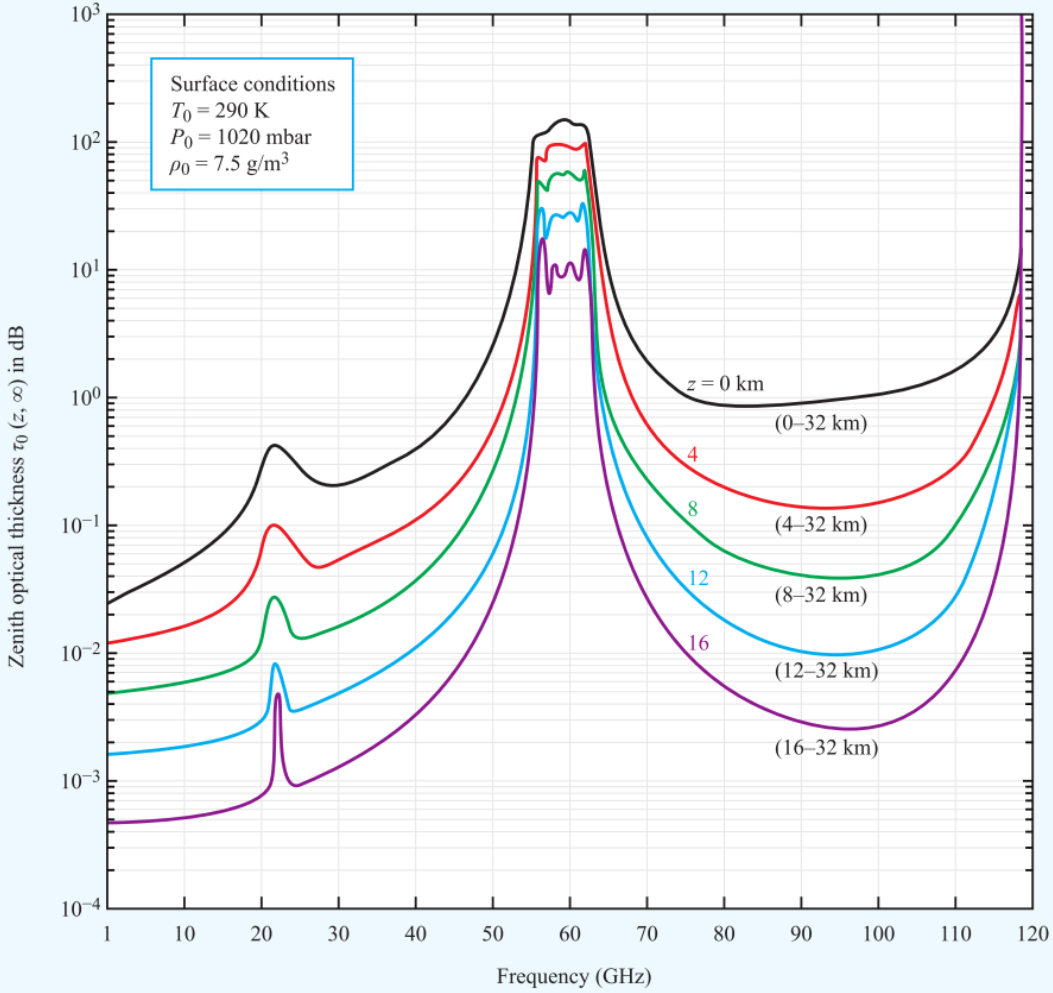

Figure 8-12: Zenith optical thickness $\tau_0(z, \infty)$ for five values of z [from Smith, 1982].

From: Microwave Radar and Radiometric Remote Sensing, by Ulaby and Long, 2014, with permission.

Downward emitted brightness temperature

For an upward-directed antenna beam, the sky brightness temperature is given by

$$T_{\mathrm{SKY}}(f,\theta) = T_{\mathrm{EXTRA}} e^{-\tau_0 \sec\theta} + T_{\mathrm{DN}}(f,\theta), \qquad (9.1)$$

$$T_{\mathrm{DN}}(f,\theta) = \sec\theta \int_0^{\infty} \kappa_{\mathrm{a}}(f,z)\, T(z)\, e^{-\tau_0(0,z)\sec\theta}\, dz, \qquad (9.2)$$

were $\kappa_a(f, z)$ and $T(z)$ are the absorption coefficient and thermometric temperature,

Absorbtion components:

$$\kappa_{\mathrm{a}}(f,z) = \kappa_{\mathrm{g}}(f,z) + \kappa_{\mathrm{c}}(f,z) + \kappa_{\mathrm{p}}(f,z), \qquad (9.3)$$

zenith optical thickness

$$\tau_0(0,z) = \int_0^{z} \kappa_{\mathrm{a}}(f,z')\, dz' \qquad (\mathrm{Np}). \qquad (9.4)$$

where $W_T(f,\theta, z)$ is the temperature weighting function

$$W_{\mathrm{T}}(f,\theta,z) = \kappa_{\mathrm{a}}(f,z)\, e^{-\tau_0(0,z)\sec\theta} \sec\theta, \qquad (9.6)$$

Weighting function

Estimating the state of the atmosphere includes generating height profiles for atmospheric temperature, pressure, and water vapor, measuring cloud liquid-water content and rain rate, and profiling the concentrations of atmospheric gases of interest. The estimation process is realized through the application of inversion algorithms that are formulated in terms of atmospheric **weighting functions**.

A weighting function is specific to the physical quantity being estimated.

Temperature weighting function and height

Oblique transmissivity

$$\Upsilon(0,z) = e^{-\tau(0,z)} = e^{-\tau_0(0,z)\sec\theta}, \qquad (9.7)$$

$$\begin{aligned}\frac{\partial\Upsilon(0,z)}{\partial z} &= \frac{\partial\Upsilon(0,z)}{\partial\tau}\cdot\frac{\partial\tau}{\partial z}\\ &= -e^{-\tau(0,z)}\cdot\kappa_a(z)\sec\theta\\ &= -\kappa_a(z)\, e^{-\tau_0(0,z)\sec\theta}\sec\theta, \qquad (9.10)\end{aligned}$$

The temperature weighting function W_T is the derivative of the atmospheric transmittance with respect to altitude z.

$$W_T(f,\theta,z) = -\frac{\partial\Upsilon(0,z)}{\partial z}. \qquad (9.11)$$

And when pressure is taken into account

$$T_{DN}(f,\theta) = \int_{-\infty}^{\ln P_s} W_T(f,\theta,P)\, T(P)\, d(\ln P) \qquad (9.16)$$

$$W_T(f,\theta,P) = \frac{\partial\Upsilon(P_s,P)}{\partial(\ln P)}, \qquad (9.17)$$

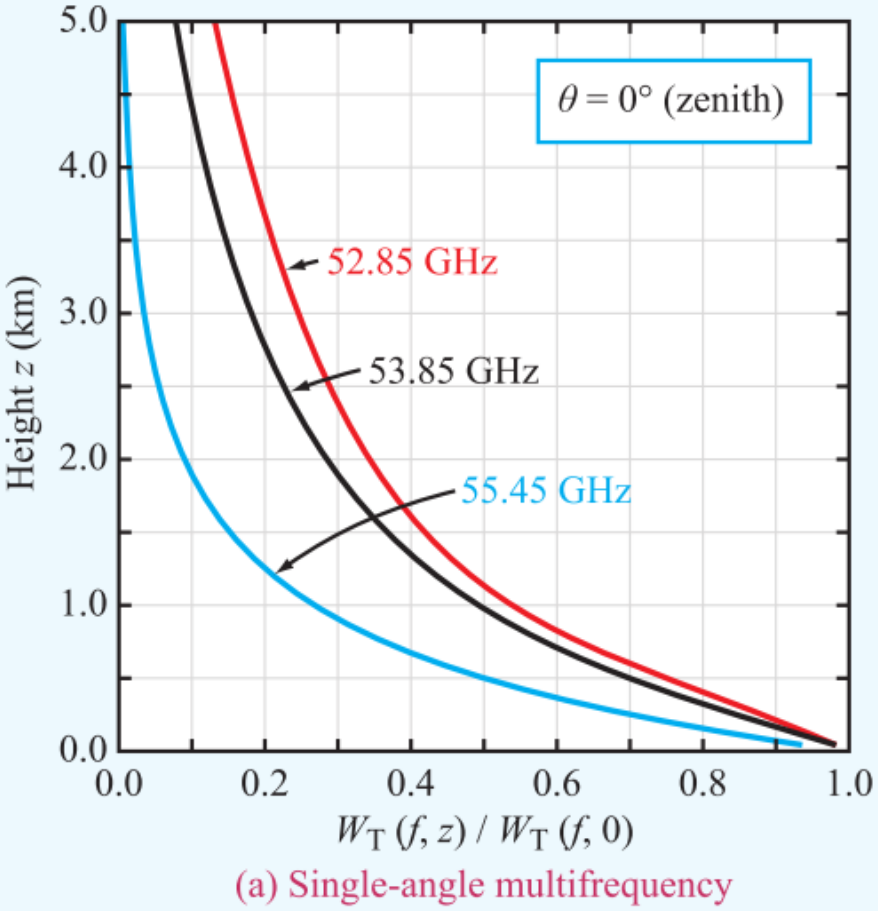

(a) Single-angle multifrequency

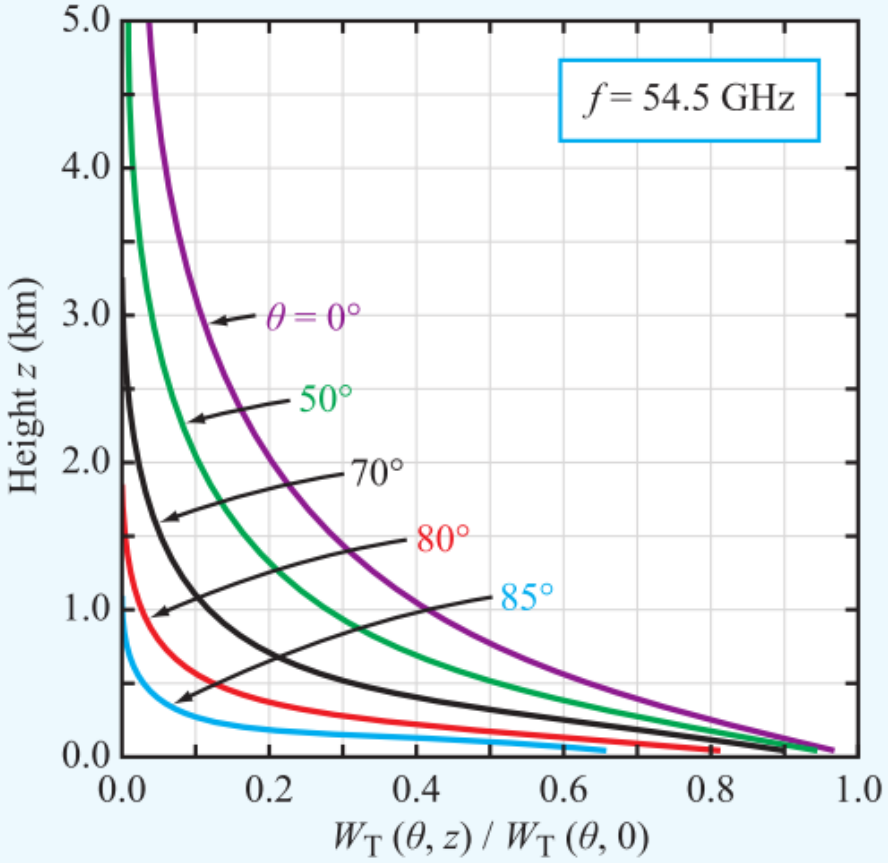

(b) Single-frequency multiangle

Normalized temperature weighting function for ground-based sensing at (a) several Nimbus 6/SCAMS frequencies along the zenith (θ = 0), and (b) several angles θ at 54.5 GHz (from Westwater and Decker, 1977).

From: Microwave Radar and Radiometric Remote Sensing, by Ulaby and Long, 2014, with permission.

Retrieving parameters from atmospheric sounding data

- Forward model
- Model inversion

- Linearisation
- Least-Squares solution
- Constrained solution
- Statistical inversion
- etc.

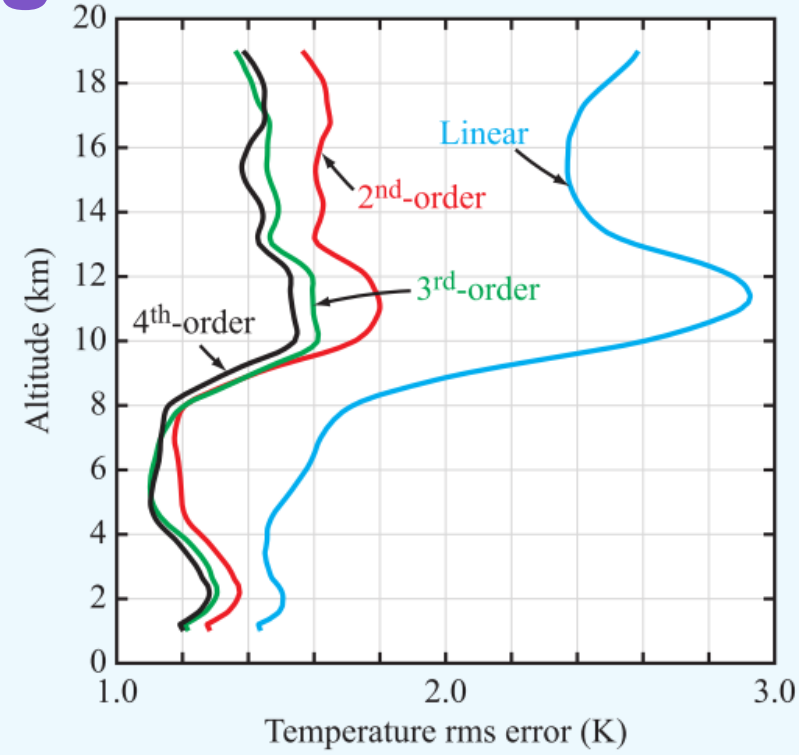

Figure 9-9: RMS temperature-retrieval error for linear regression and nonlinear (polynomial) regression for ATMS over ocean.

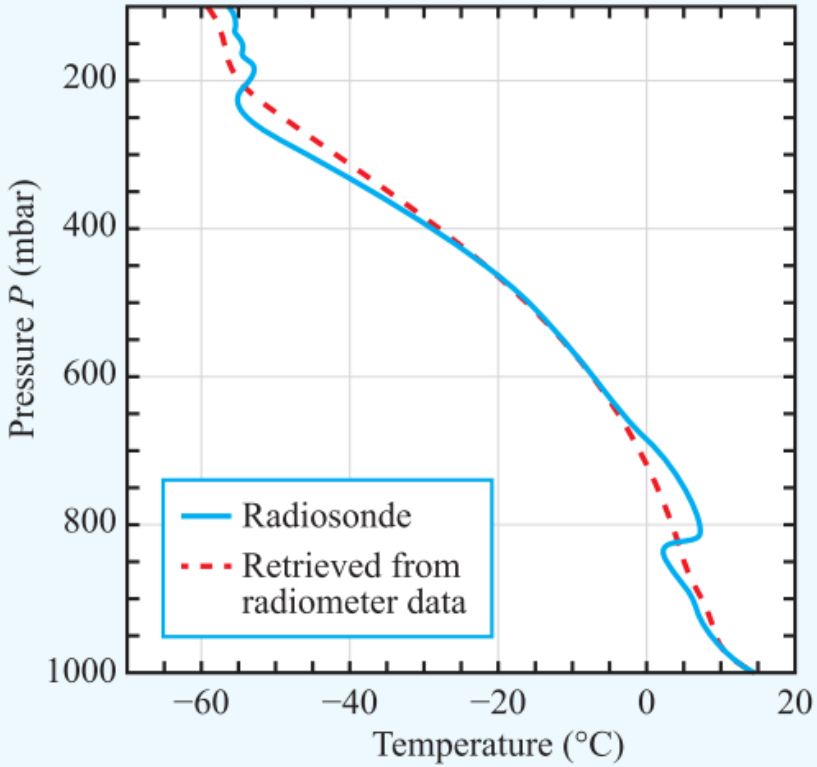

Figure 9-14: An example of a temperature profile retrieved from SCAMS radiometric data (dashed line) compared with concurrent radiosondes (solid line) (from Decker et al., 1978).

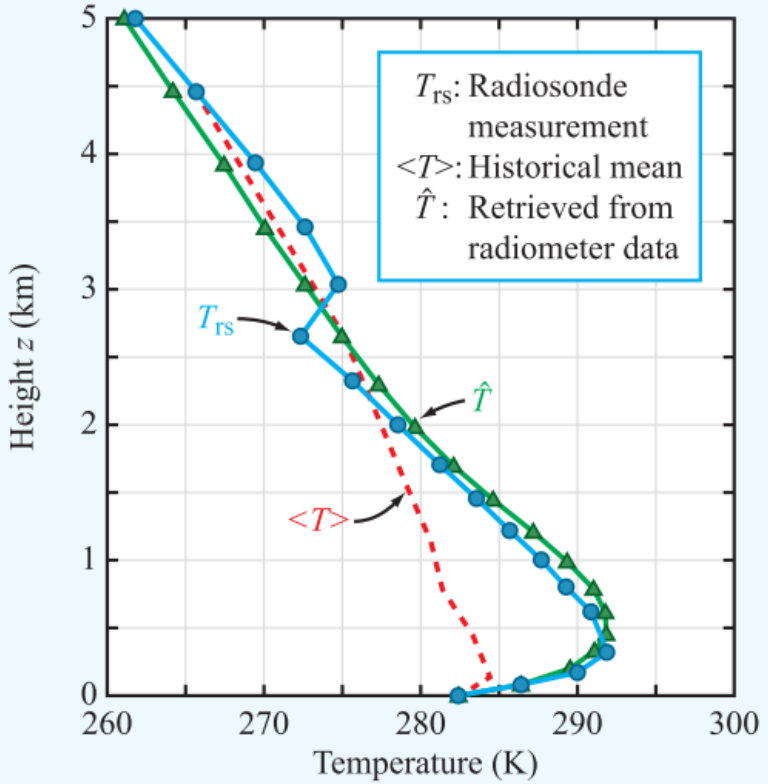

Figure 9-13: Typical example of a temperature profile derived from single-frequency (54.5 GHz) angular scanned radiometer data at Cincinnati, Ohio. T_{rs} = radiosonde profile, $\langle T \rangle$ = mean profile for constrained surface conditions, $\hat{T}$ = inferred profile (from Westwater and Decker, 1977).

Microwave Radiometer (MWR) by Radiometrics.
Water vapor and liquid water measurements at frequencies: 23.8 and 31.4 GHz

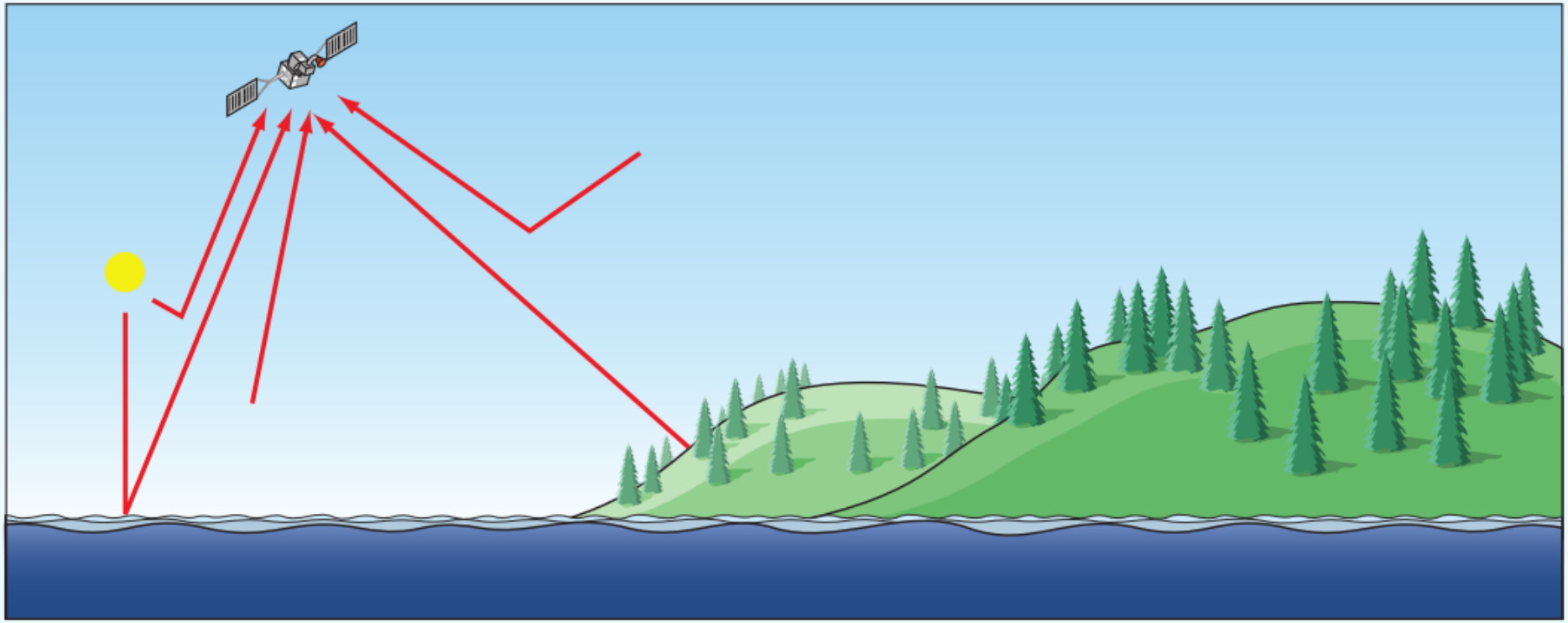

Figure 9-1: Typical measurement scenario for spaceborne atmospheric remote sensing. Electromagnetic radiation that reaches the sensor is emitted by the sun, atmosphere, surface, clouds, and cosmic background. This radiation can also be reflected or scattered by the surface, atmosphere, or clouds; some of these interactions are indicated with arrows in the figure. The spectral radiances measured by the sensor are related to geophysical quantities such as the vertical temperature profile of the atmosphere. An appropriate retrieval algorithm is necessary to convert these radiances into a geophysical quantity of interest.

From: Microwave Radar and Radiometric Remote Sensing, by Ulaby and Long, 2014, with permission.

Scattering by atmospheric particles

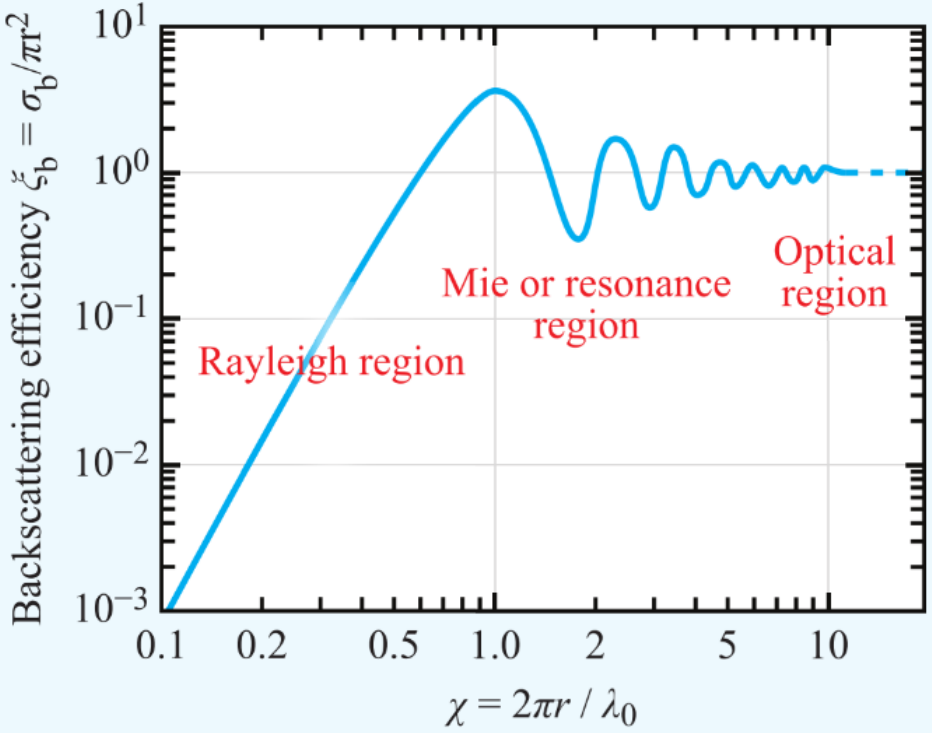

Figure 8-21: Backscattering efficiency of a perfectly conducting sphere.

From: Microwave Radar and Radiometric Remote Sensing, by Ulaby and Long, 2014, with permission.

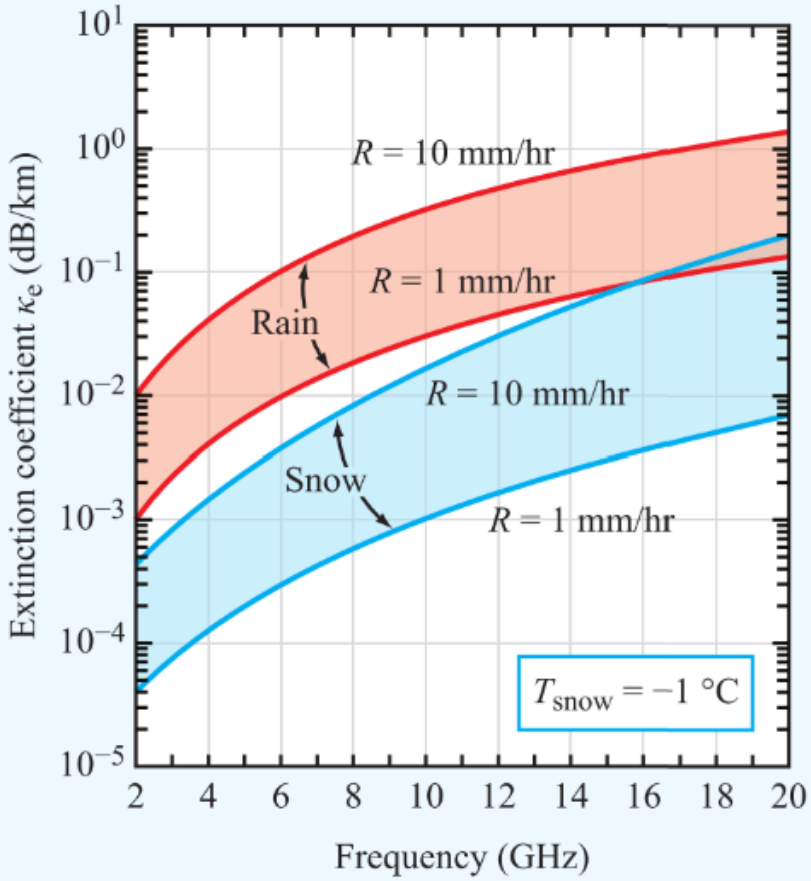

Figure 8-36: Extinction coefficient of rain and snow as a function of frequency [adapted from Barton, 1974].

From: Microwave Radar and Radiometric Remote Sensing, by Ulaby and Long, 2014, with permission.

Aalto University
School of Electrical
Engineering

Land Observations with radiometer

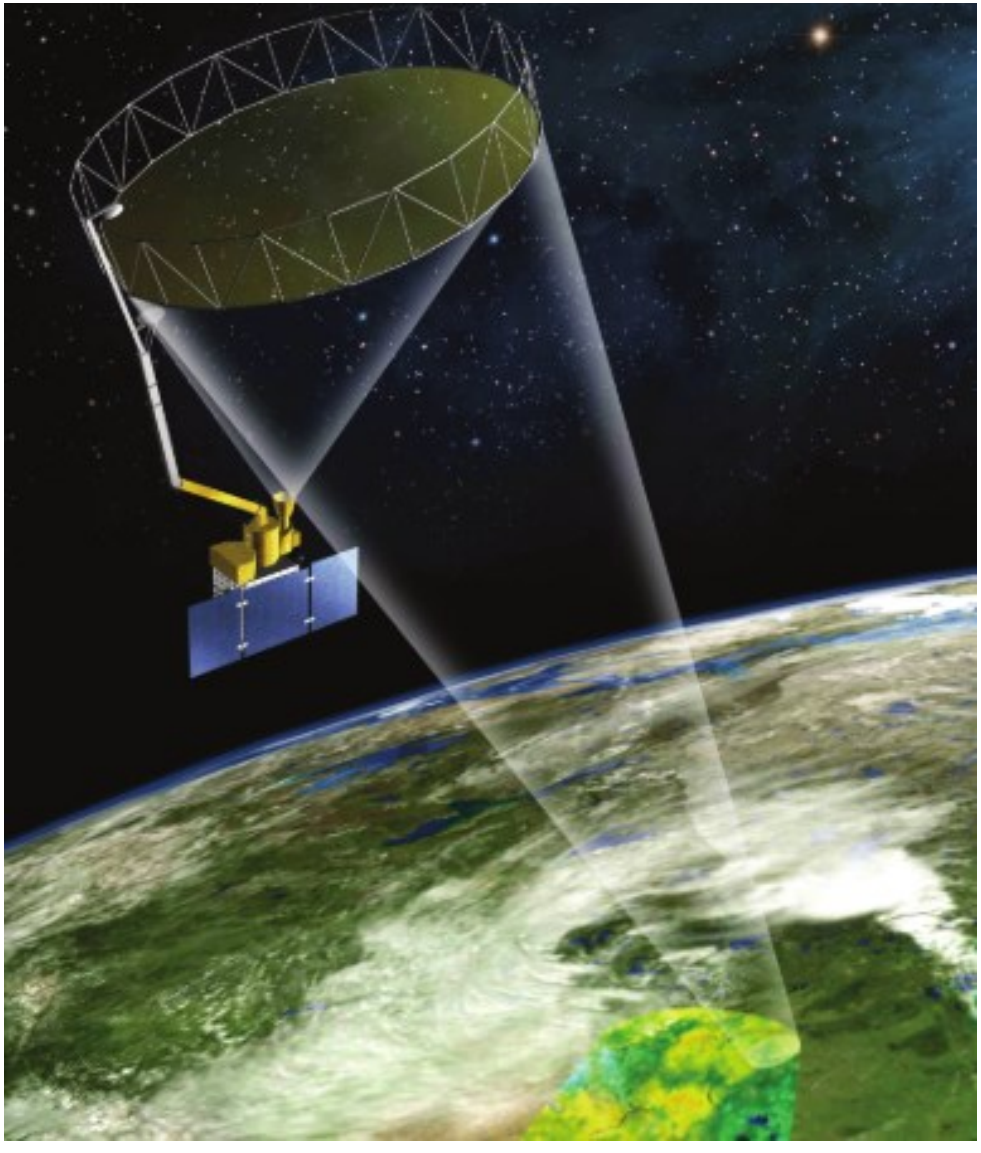

Downward looking radiometer

$$T_B(\text{satellite}) = T_{UP}(F,\theta) + T_{SKY}(F,\theta)\,\Gamma\,\Upsilon(0,\infty) + T_{SE}\,\Upsilon(0,\infty), \quad (9.18)$$

Where Γ is the reflectivity of the ground (or ocean) surface, $(0,\infty)$ is the one-way transmissivity of the atmosphere along direction θ, and T_{SE} is the brightness temperature of the surface when observed in the absence of the atmosphere.

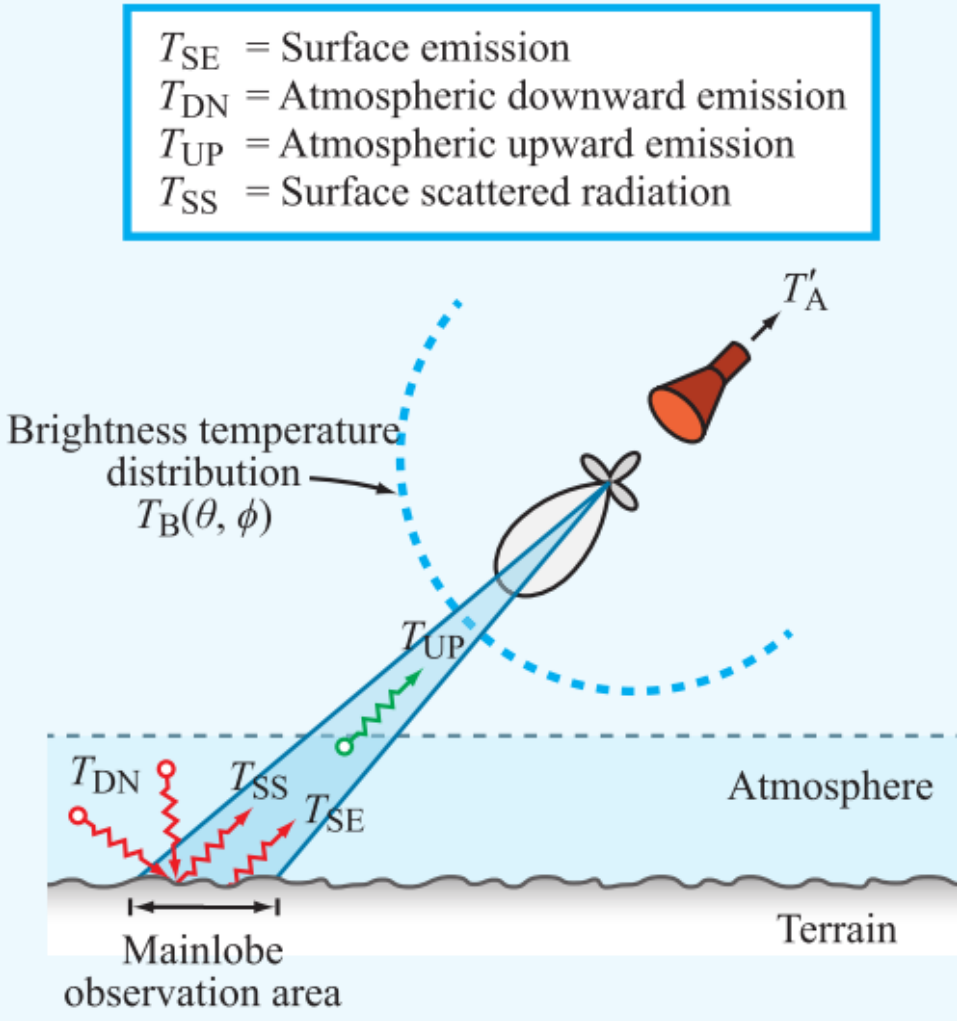

(a) Emission by surface and atmosphere

The brightness temperature T_B incident upon the radiometer antenna includes emission contributions from the atmosphere and the ground cell observed by the antenna field of view.

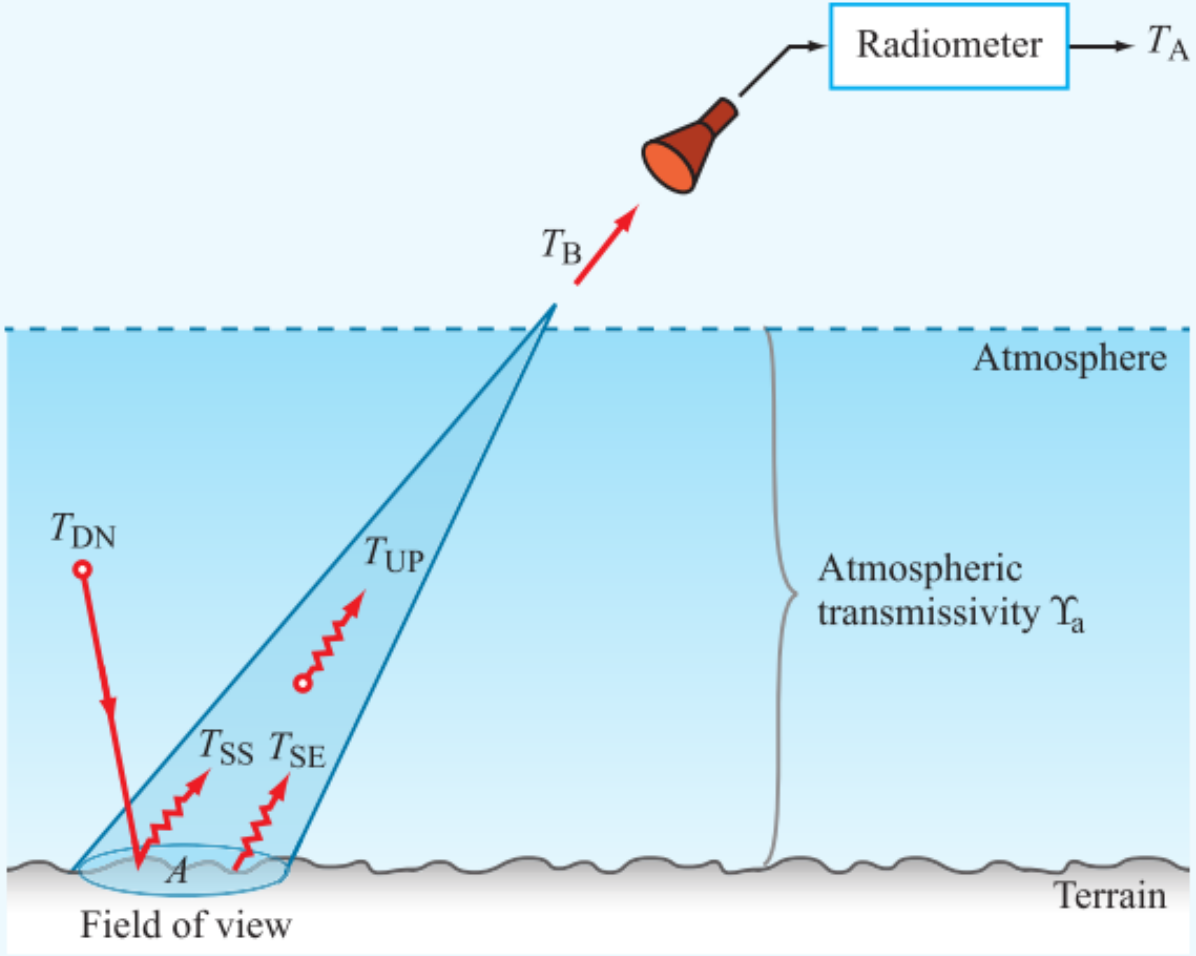

From: Microwave Radar and Radiometric Remote Sensing, by Ulaby and Long, 2014, with permission.

Surface emission

Our interest is in T^p_{SE}, the p-polarized brightness temperature due to surface emission by the cell viewed by the beam of the p-polarized antenna.

$$T_B^p = \Upsilon_a (T_{SE}^p + T_{SS}^p) + T_{UP} \qquad (p = \text{v or h}), \qquad (12.1)$$

Where Υ_a is the transmissivity of the atmospheric layer between the ground cell and the antenna, T_{UP} is the upwelling atmospheric emission by the same layer, and T^p_{SS} is the fraction of the downward-emitted atmospheric radiation that gets surface scattered by the ground cell into the direction of the radiometer.

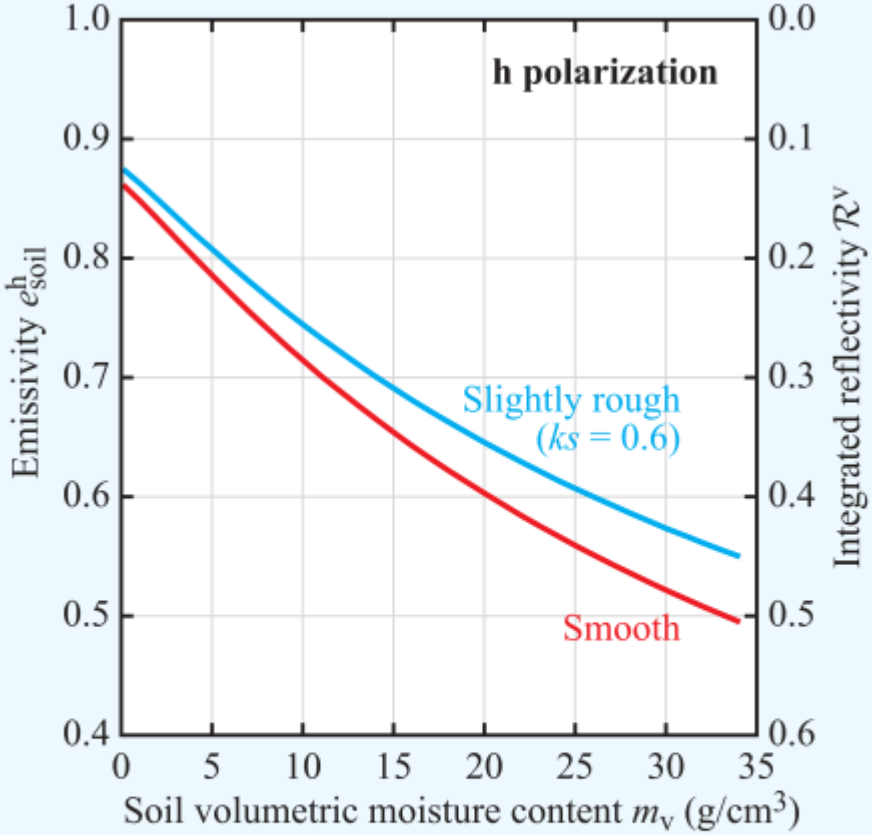

(b) h polarization

Figure 12-3: Variations of e^v and e^h at $\theta = 40°$ with m_v for two different surface roughnesses, both computed using I^{2}EM.

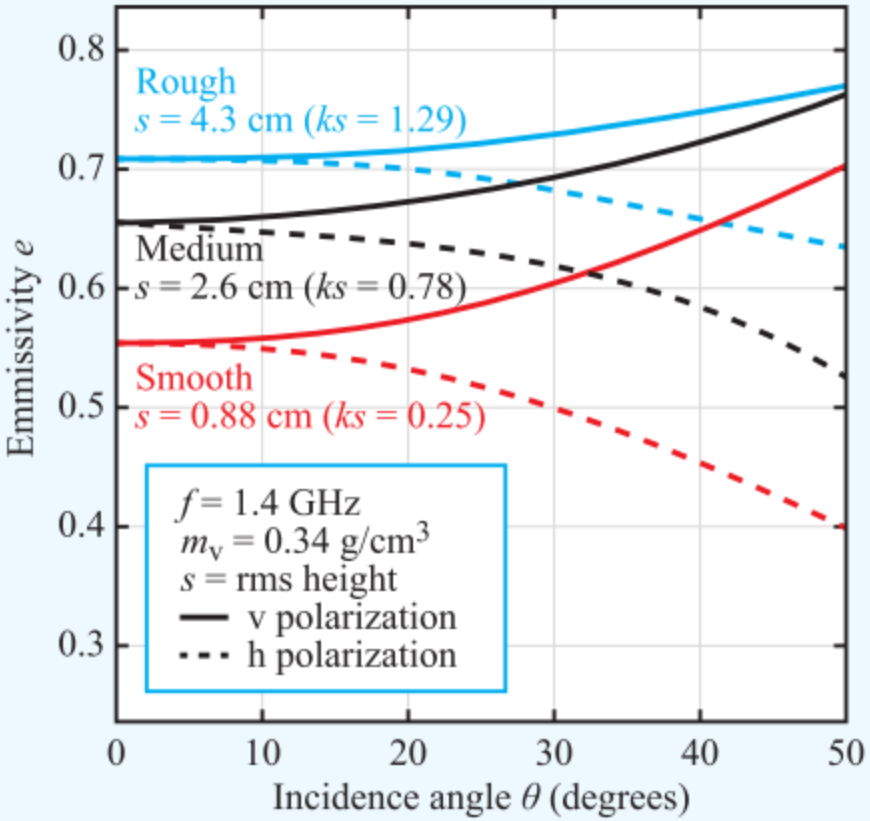

Figure 12-4: Angular patterns of the emissivity measured at 1.4 GHz for three bare-soil fields with different surface roughnesses [Newton and Rouse, 1980].

From: Microwave Radar and Radiometric Remote Sensing, by Ulaby and Long, 2014, with permission.

Vegetation

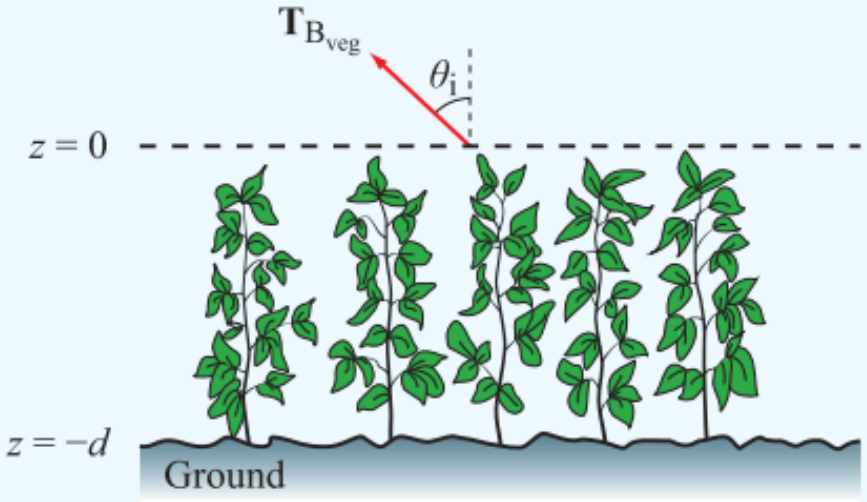

Figure 12-14: Microwave emission by a vegetation layer over a ground surface.

① Direct emission by soil $\Upsilon_{veg}\, e_s$
(includes one-way attenuation by canopy)

② Direct upward emission by plants $(1 - a)(1 - \Upsilon_{veg})$

③ Plant emission downward, followed by reflection
$\Gamma_{coh}(1 - a)(1 - \Upsilon_{veg})\,\Upsilon_{veg}$

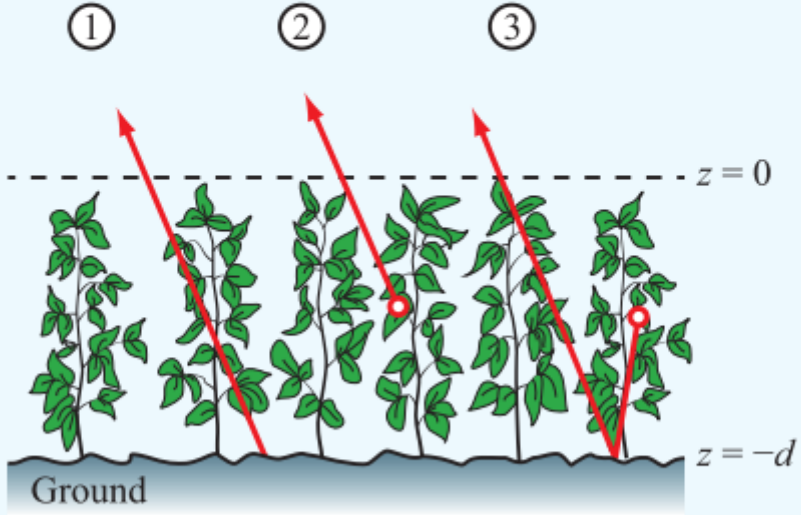

Figure 12-16: Emission contributions in a weakly scattering vegetation canopy.

From: Microwave Radar and Radiometric Remote Sensing, by Ulaby and Long, 2014, with permission.

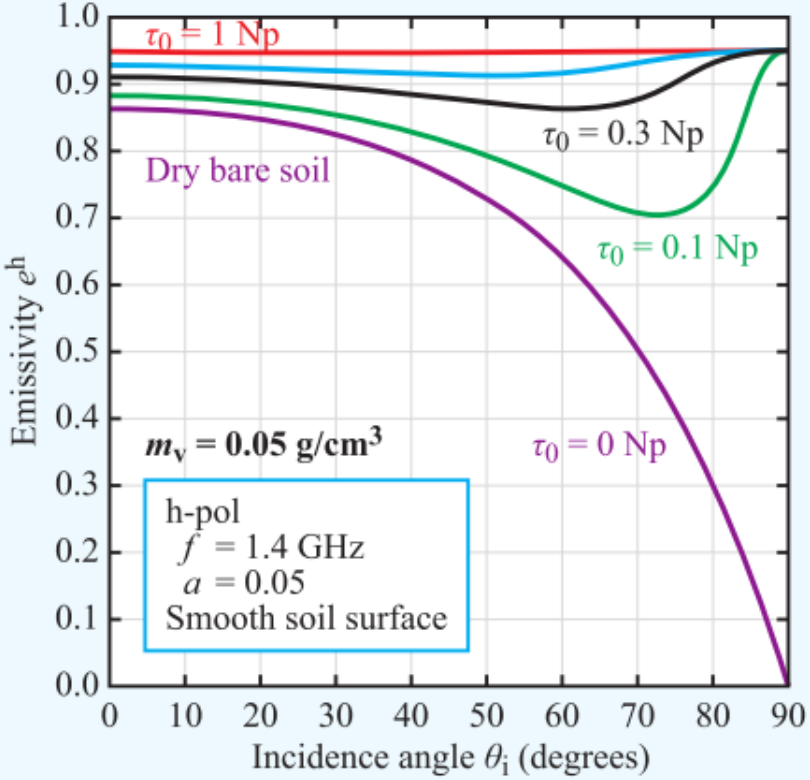

(a) Dry soil

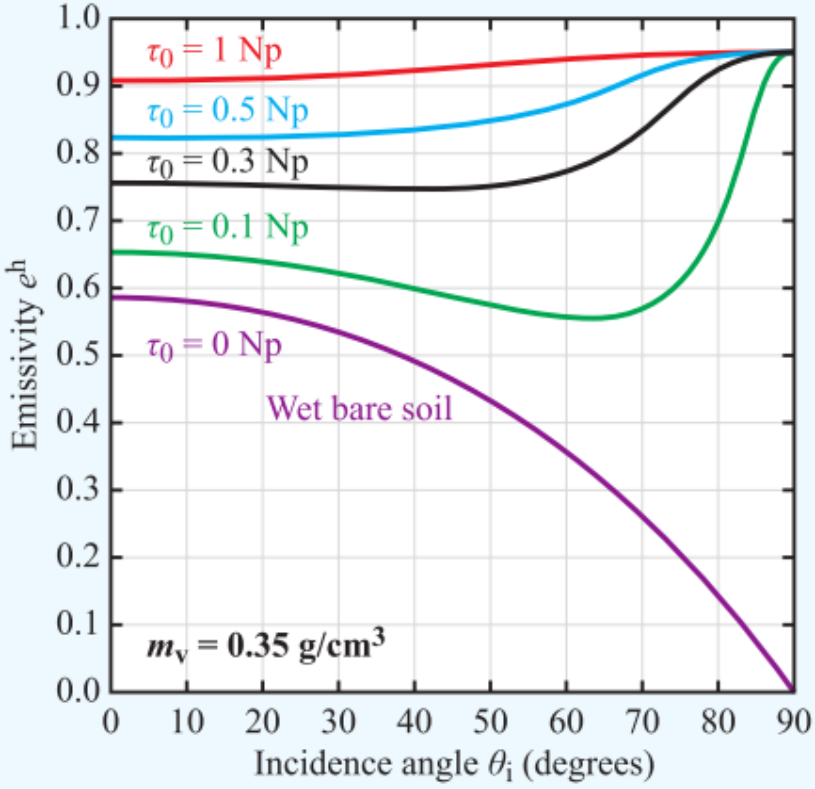

(b) Wet soil

Figure 12-18: Angular plots of the h-polarized emissivity for (a) a dry soil surface and (b) a very wet soil surface, covered with vegetation of nadir optical thickness τ_0. The soil surface is perfectly smooth.

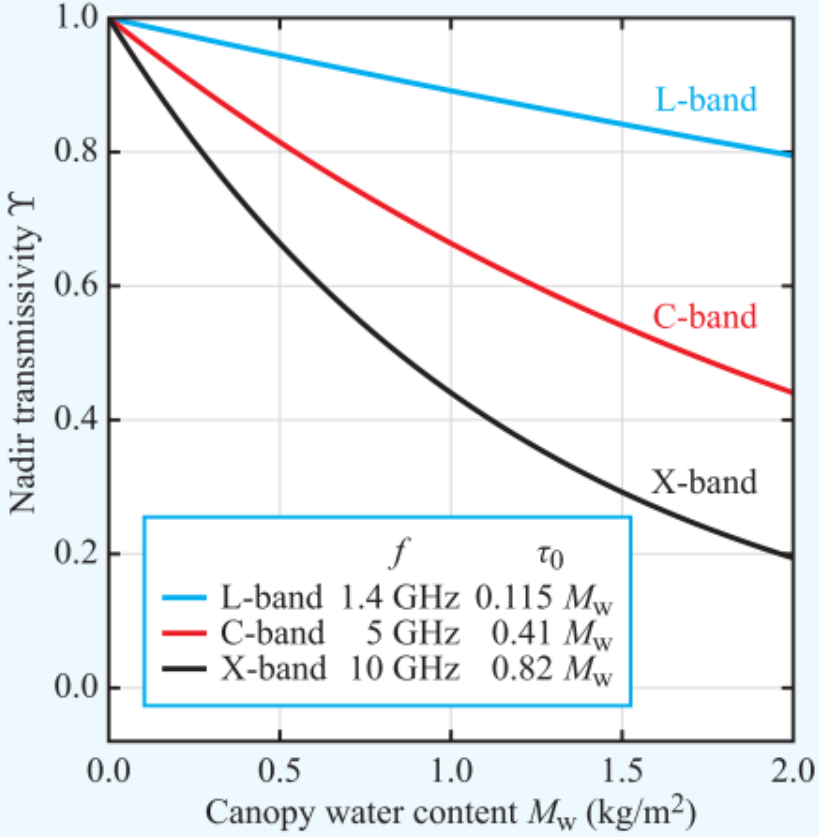

Figure 12-27: Representative canopy transmissivity for a grass canopy at three microwave frequencies.

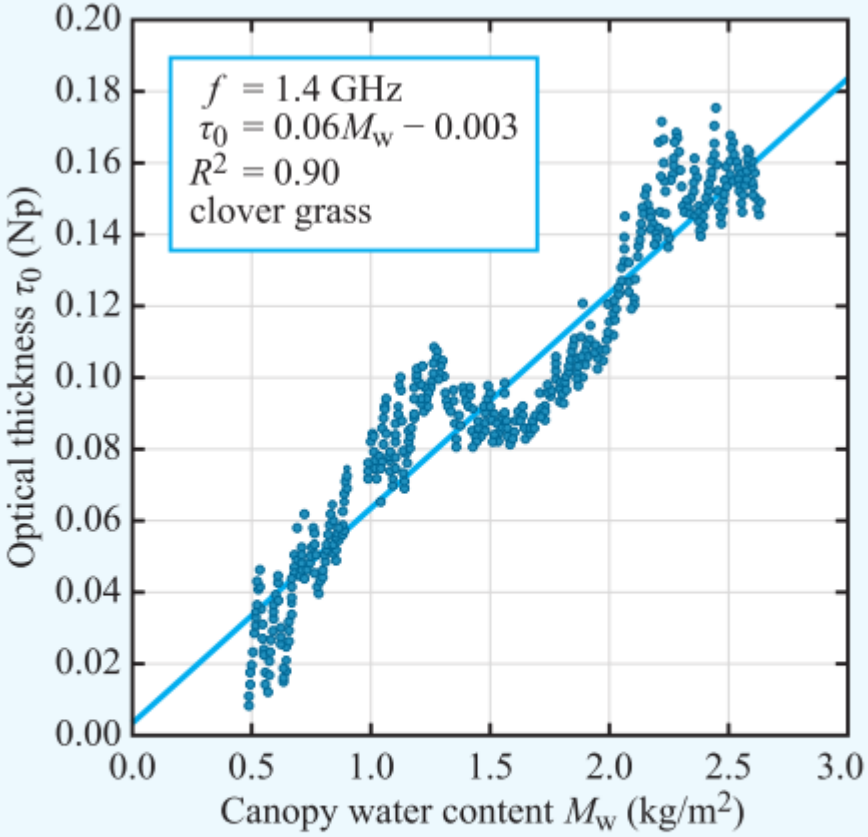

Figure 12-26: Attenuation (optical thickness) τ_0 versus vegetation water content for a site covered with clover grass [Saleh et al., 2007].

Aalto University
School of Electrical
Engineering

Radiometer usage and instrument examples

Radiometers in remote sensing

Operating frequencies presently 1.2, 6.9, 18, 22, 37, and 89 GHz, vertical and horizontal polarizations at each frequency

- Poor spatial resolution from satellite (5 -100 km)
- Swath width up to 1500 km
- Data time series available since 1978 (various satellites) – Regional coverage excellent due to continuous operation
- Can measure through clouds (rain affects data)
- Day / night measurement capability
- Data interpretation not simple
- Radiometer measurement outcome is proportional to target temperature
- Penetration depth smaller than for radar (higher operating frequencies)
  - ”Penetration depth” ~1 cm – 0.5 m, mostly <30 cm
  - ”Penetration depth”: Emission still reaches air (and sensor)

Freely available passive microwave data

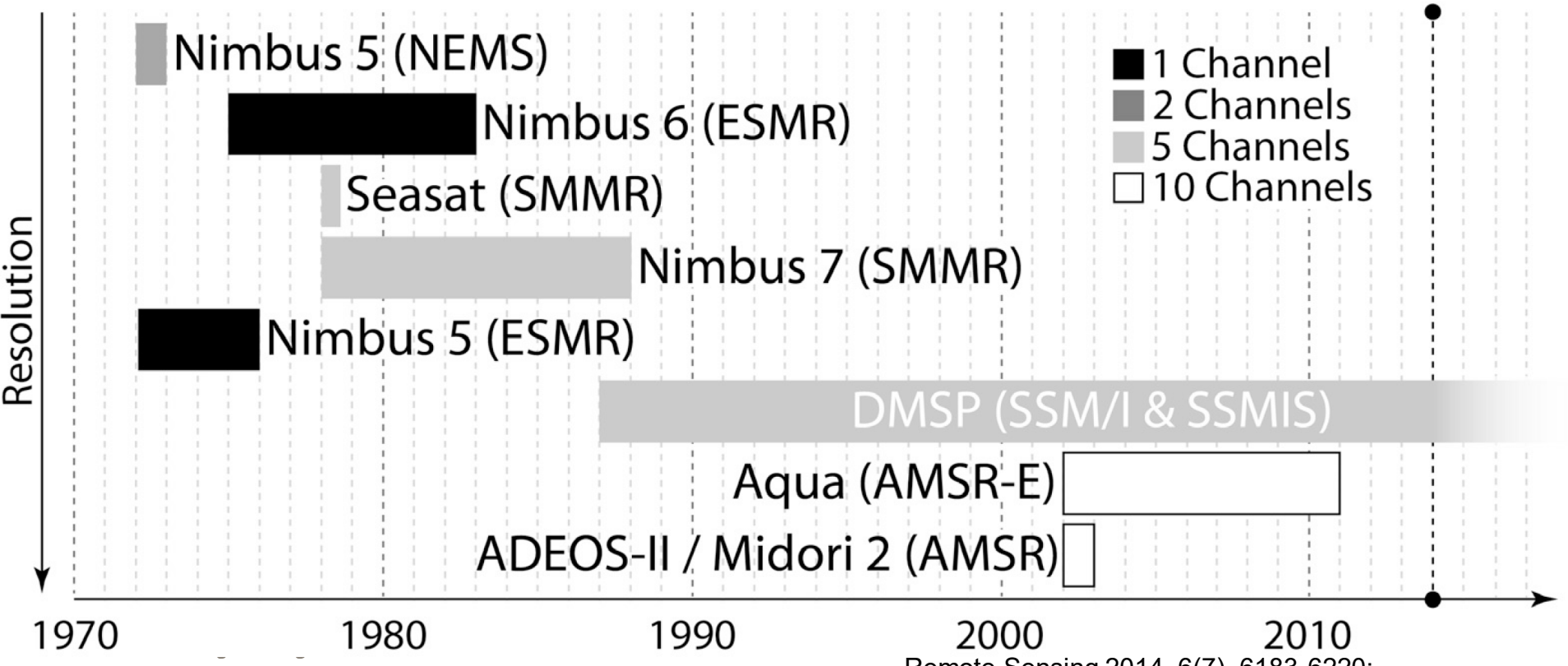

Remote Sensing 2014, 6(7), 6183-6220; doi:10.3390/rs6076183

Atmospheric applications

Aalto University
School of Electrical
Engineering

The deployed SSMIS instrument showing the main canister, reflector antenna, and calibration load assembly [Kunkee et al., 2008]. The sensor is approximately 1.2 m tall when deployed with a mass of approximately 96 kg.

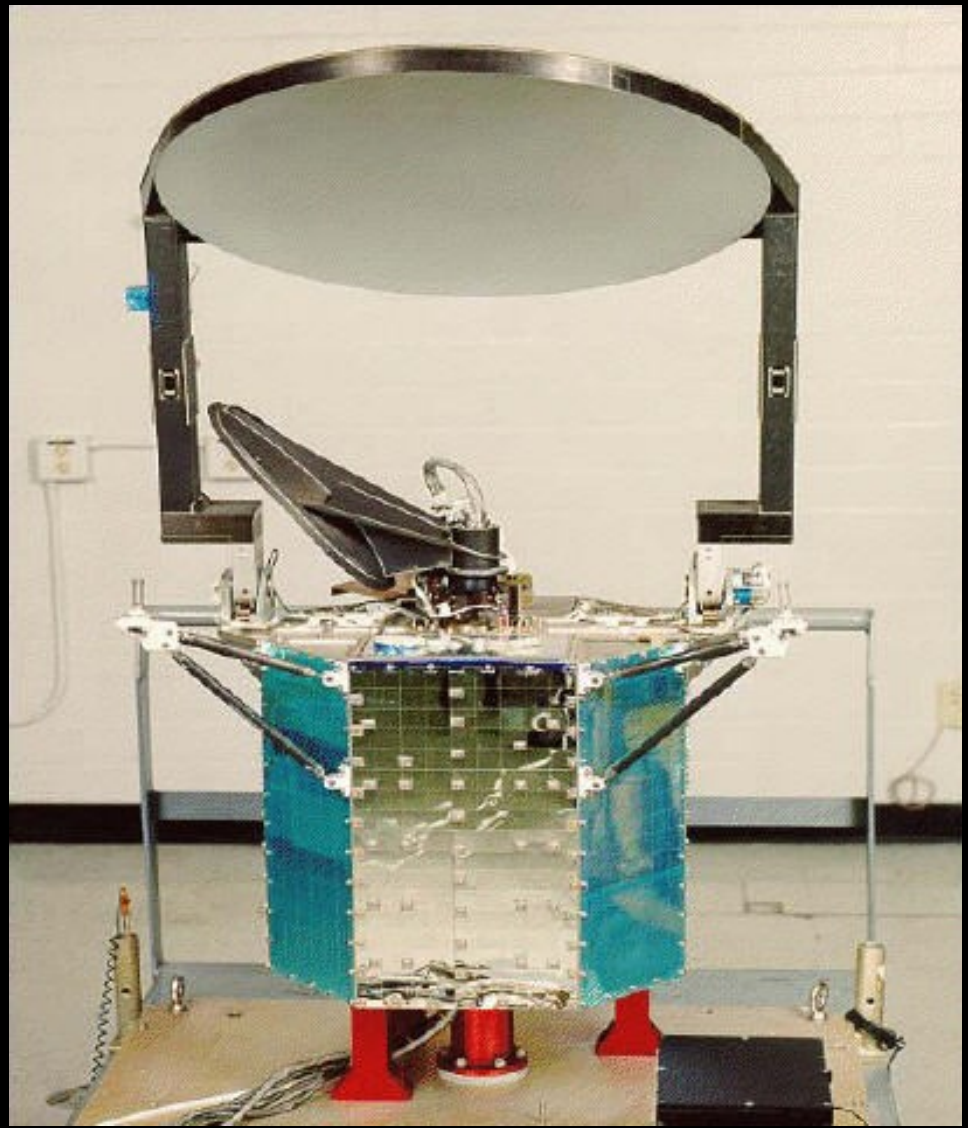

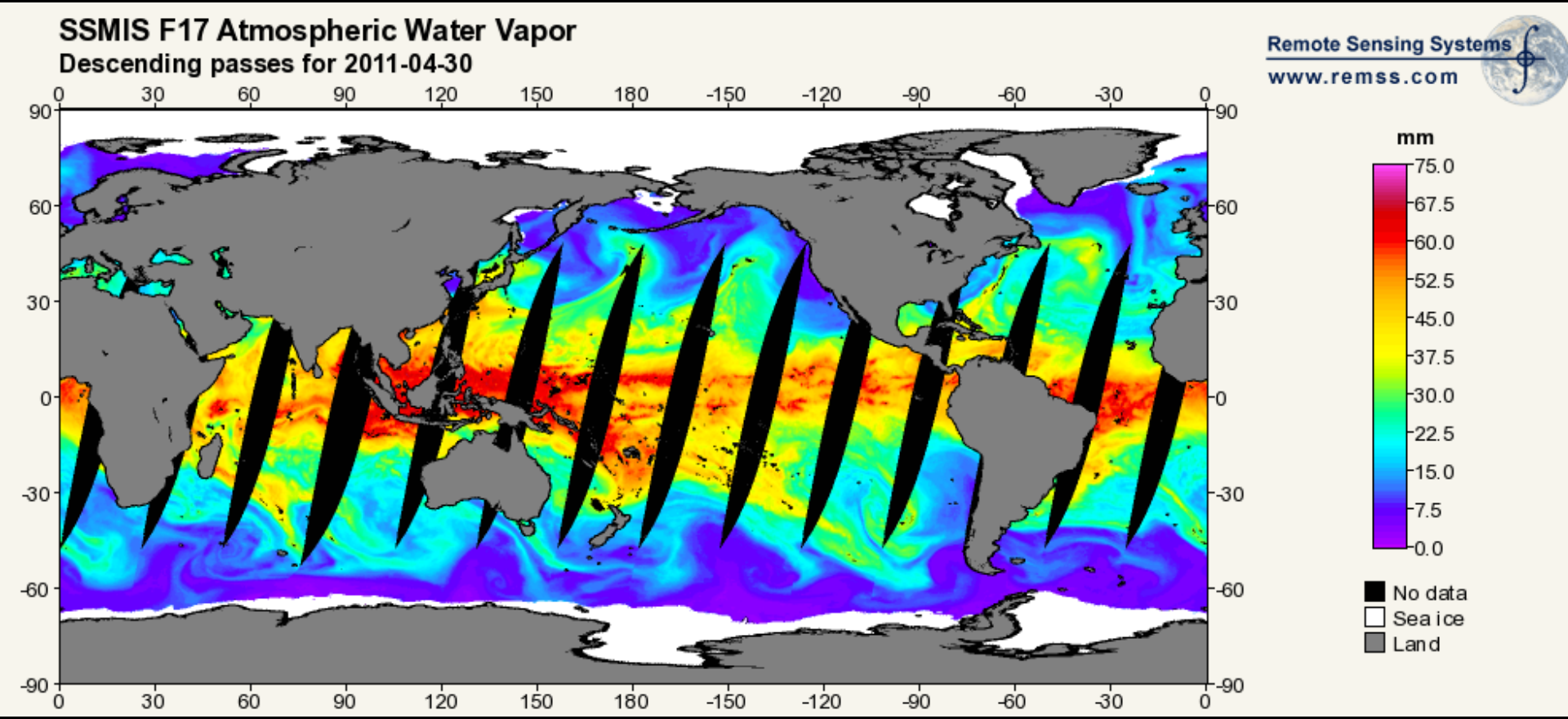
SSMIS F17 Atmospheric Water Vapor
Descending passes for 2011-04-30
Remote Sensing Systems
www.remss.com
mm
75.0
67.5
60.0
52.5
45.0
37.5
30.0
22.5
15.0
7.5
0.0
No data
Sea ice
Land
0 30 60 90 120 150 180 -150 -120 -90 -60 -30 0
90 60 30 0 -30 -60 -90

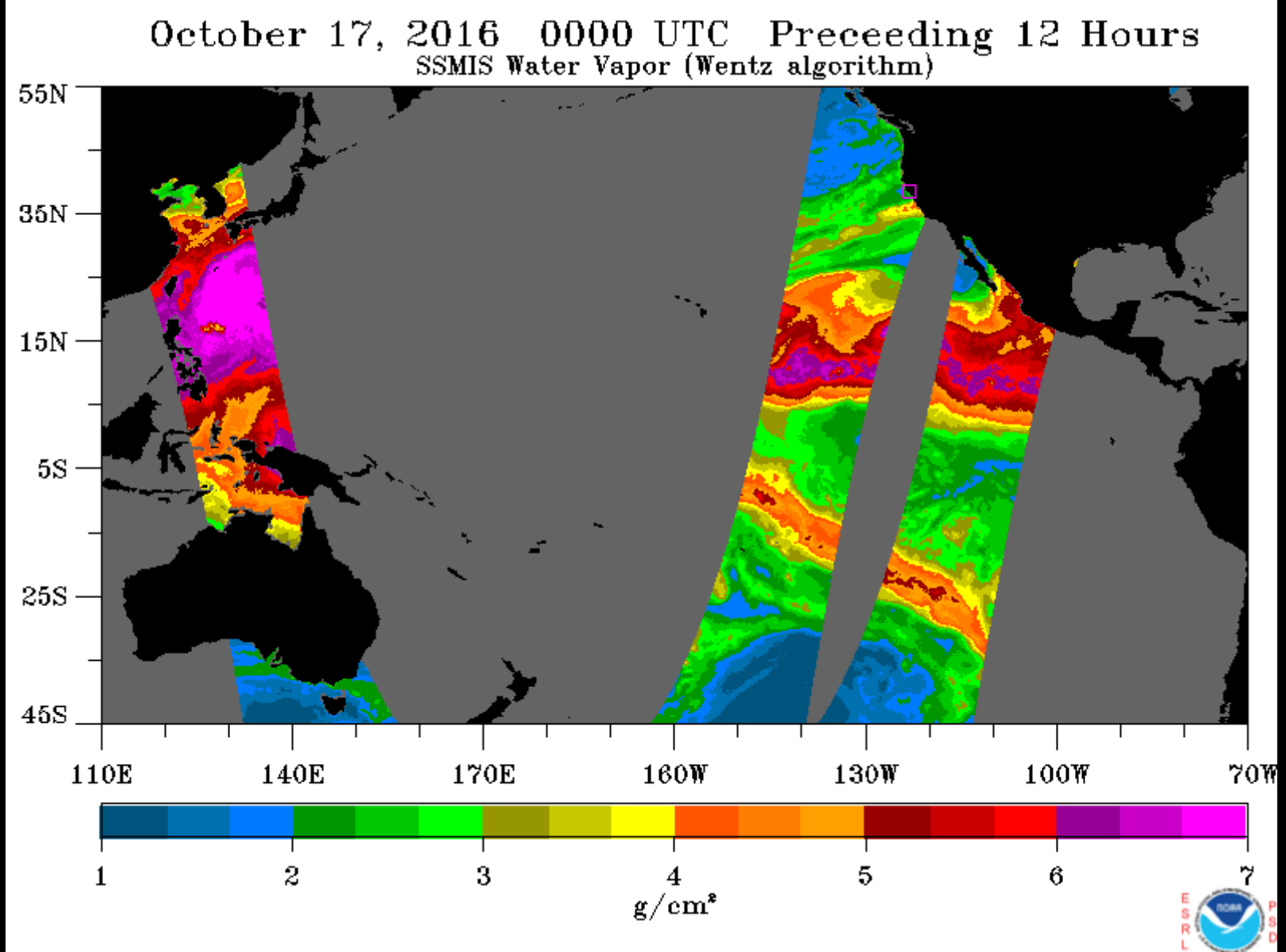
October 17, 2016 0000 UTC Preceeding 12 Hours
SSMIS Water Vapor (Wentz algorithm)
55N
35N
15N
5S
25S
45S
110E
140E
170E
160W
130W
100W
70W
1
2
3
4
5
6
7
g/cm²

Suomi NPP

Suomi NPP

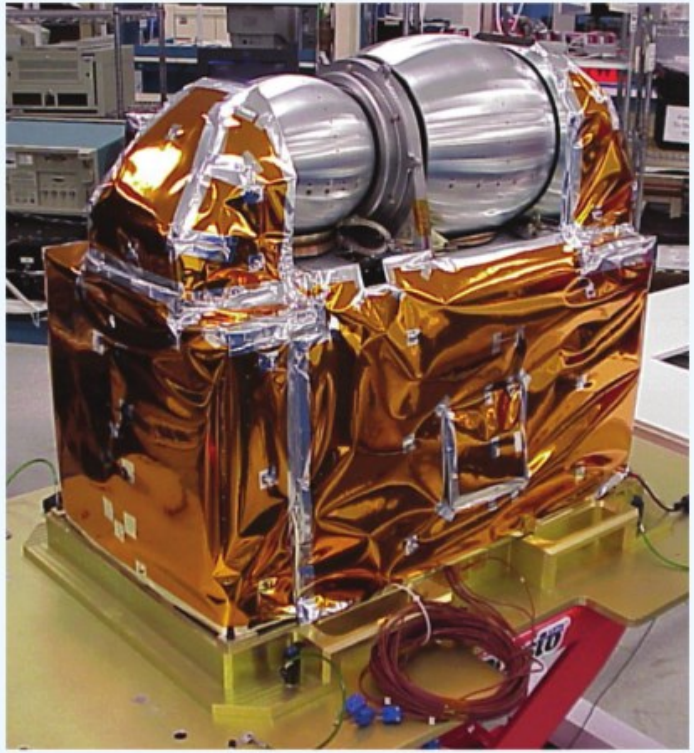

Figure 9-31: The Advanced Technology Microwave Sounder (ATMS) ready for integration on the Suomi NPP satellite. The sensor dimensions are $70 \times 60 \times 40$ cm and mass is 74.1 kg. [Courtesy of Northrop Grumman Electronic Systems.]

Table 9-1: AMSU instrument characteristics.

Channel number	Center frequency (GHz)	Band-width (MHz)	Radiometric sensitivity ΔT
1	23.80	251	0.30
2	31.40	161	0.30
3	50.30	161	0.40
4	52.80	380	0.25
5	53.59 ± 0.115	168	0.25
6	54.40	380	0.25
7	54.94	380	0.25
8	55.50	310	0.25
9	$57.29 = f_0$	310	0.25
10	$f_0 \pm 0.217$	76	0.40
11	$f_0 \pm 0.322 \pm 0.048$	34	0.40
12	$f_0 \pm 0.322 \pm 0.022$	15	0.60
13	$f_0 \pm 0.322 \pm 0.010$	8	0.80
14	$f_0 \pm 0.322 \pm 0.004$	3	1.20
15	89.00	2000	0.50
16	89.00	5000	2.00
17	150	4000	2.00
18	183 ± 1	1000	2.00
19	183 ± 3	2000	2.00
20	183 ± 7	4000	2.00

From: Microwave Radar and Radiometric Remote Sensing, by Ulaby and Long, 2014, with permission.

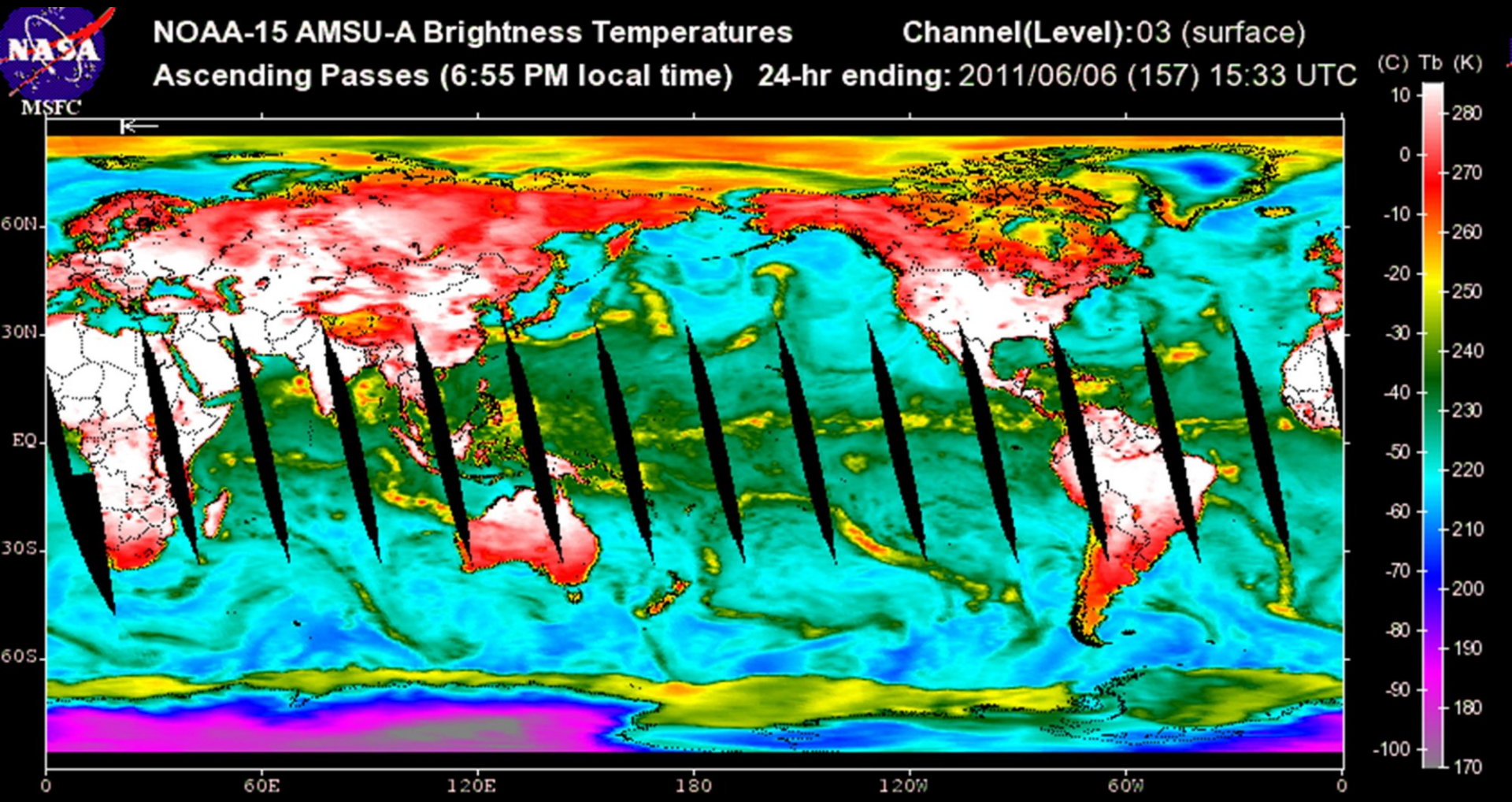
NOAA-15 AMSU-A Brightness Temperatures
Channel(Level):03 (surface)
Ascending Passes (6:55 PM local time)
24-hr ending: 2011/06/06 (157) 15:33 UTC
MSFC
(C) Tb (K)
10 280
0 270
-10 260
-20 250
-30 240
-40 230
-50 220
-60 210
-70 200
-80 190
-90 180
-100 170
60N
30N
EQ
30S
60S
0
60E
120E
180
120W
60W
0

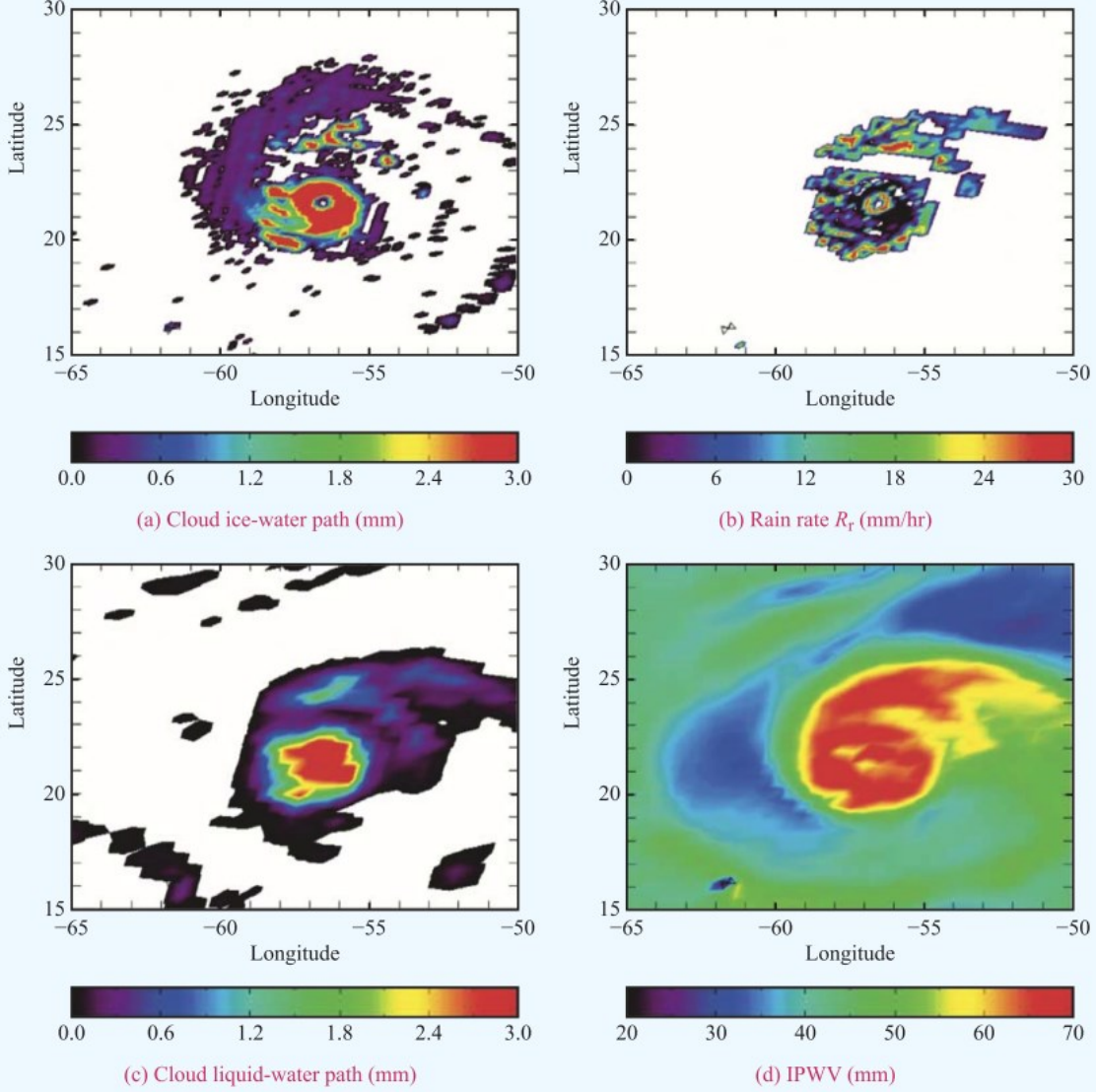

(a) Cloud ice-water path (mm)

(b) Rain rate R_r (mm/hr)

(c) Cloud liquid-water path (mm)

(d) IPWV (mm)

Figure 9-39: AMSU-retrieved (a) ice-water path, (b) surface rain rate, (c) cloud liquid water, and (d) integrated precipitable water vapor (IPWV) for Hurricane Isabel on September 12, 2003 [Liu and Weng, 2005].

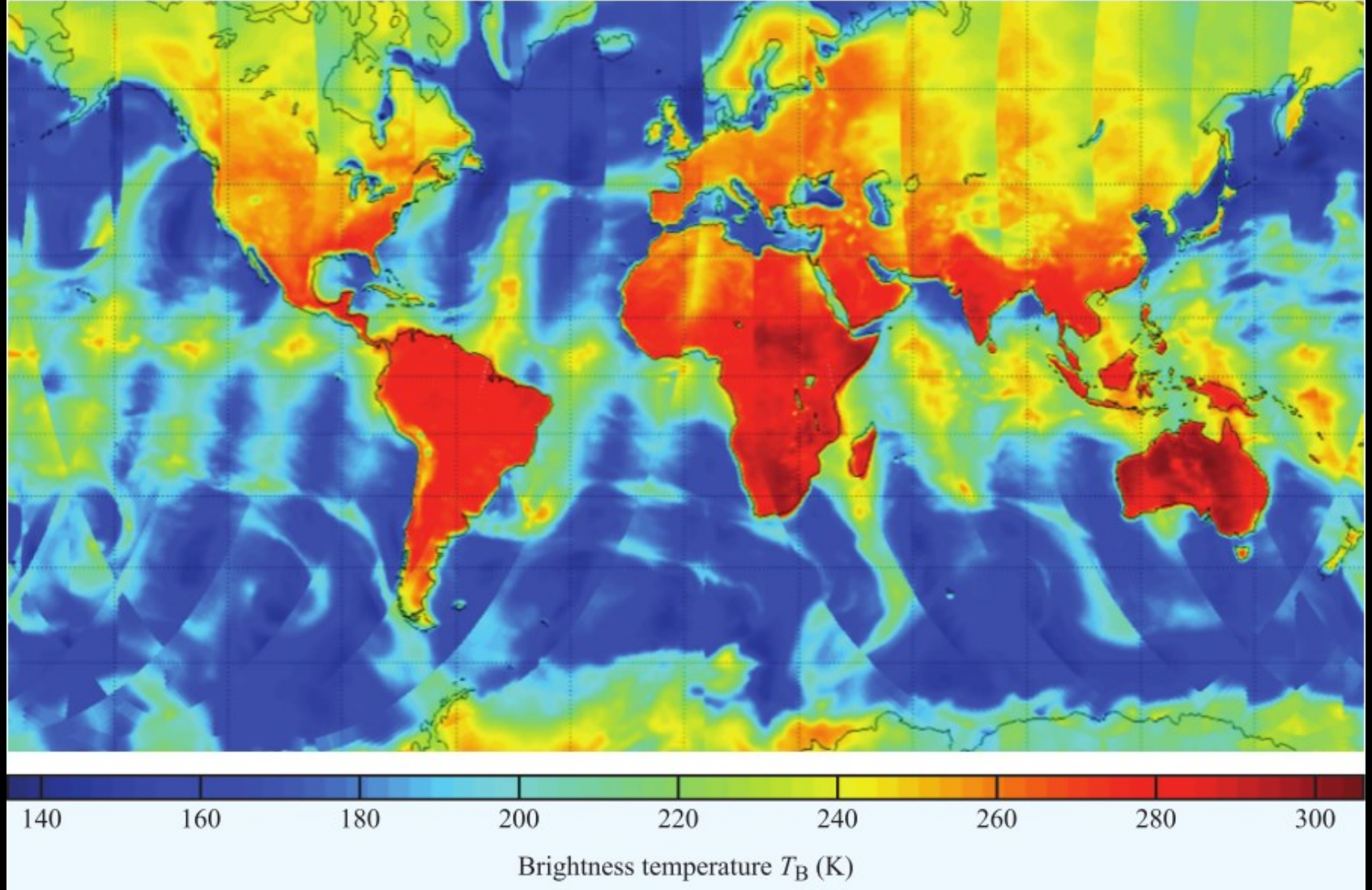

Figure 9-32: A global mosaic of ATMS 23.8 GHz brightness temperatures observed on December 16, 2011.

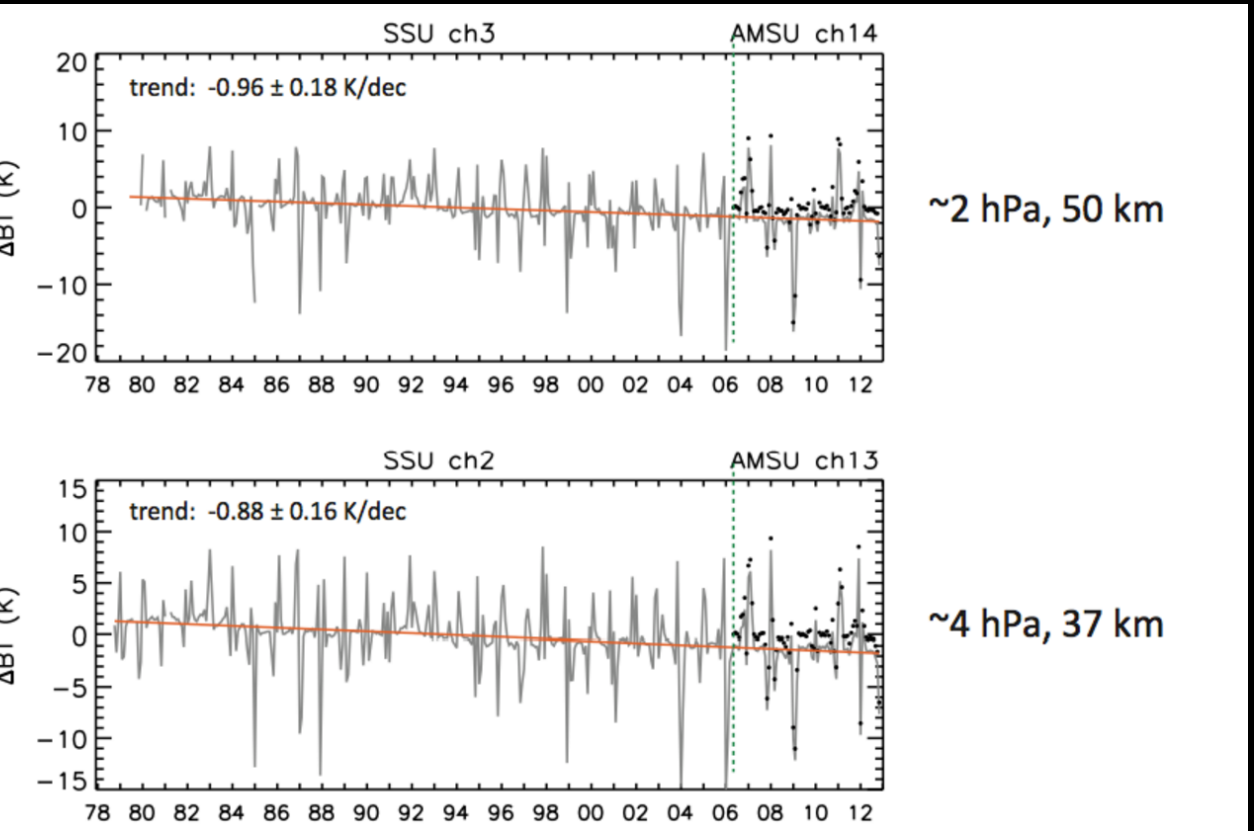

~2 hPa, 50 km

~4 hPa, 37 km

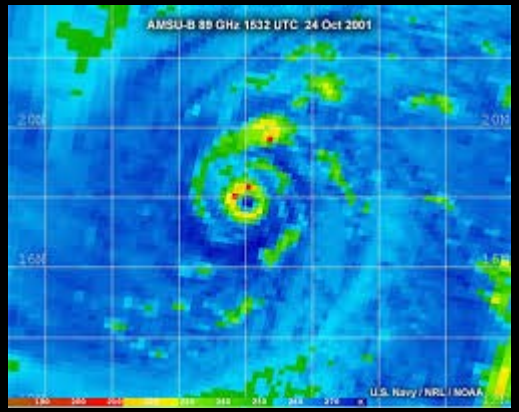

METOP AMSU-A

Microwave radiometer

15 channels

23-90 GHz

Atmospheric Temperature and water

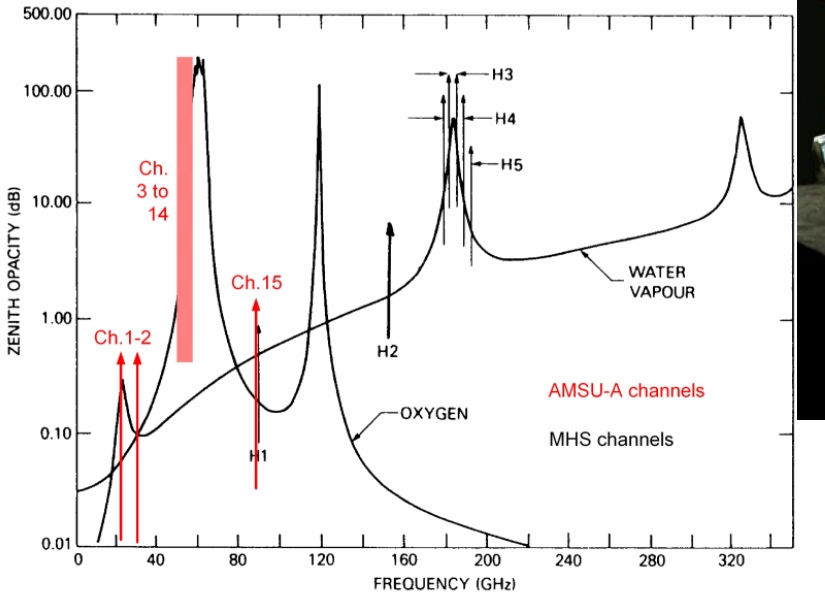

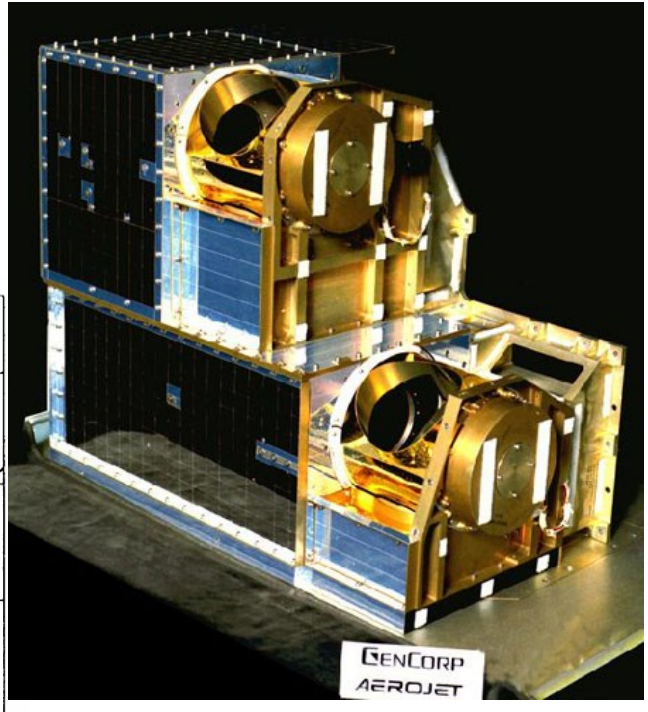

Aalto University
School of Electrical
Engineering

METOP

EUMETSAT

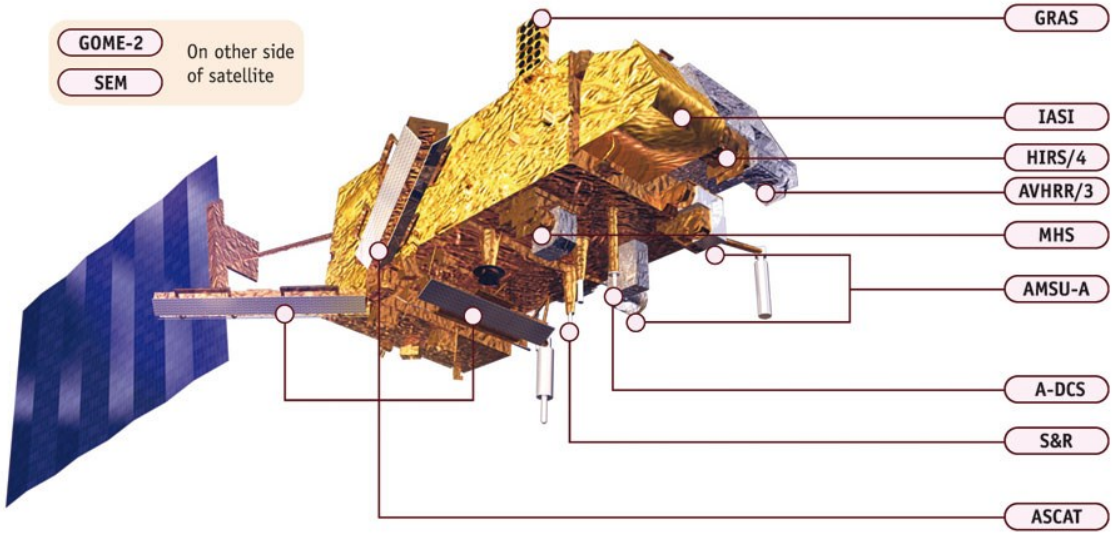

GPM Constellation of Satellites

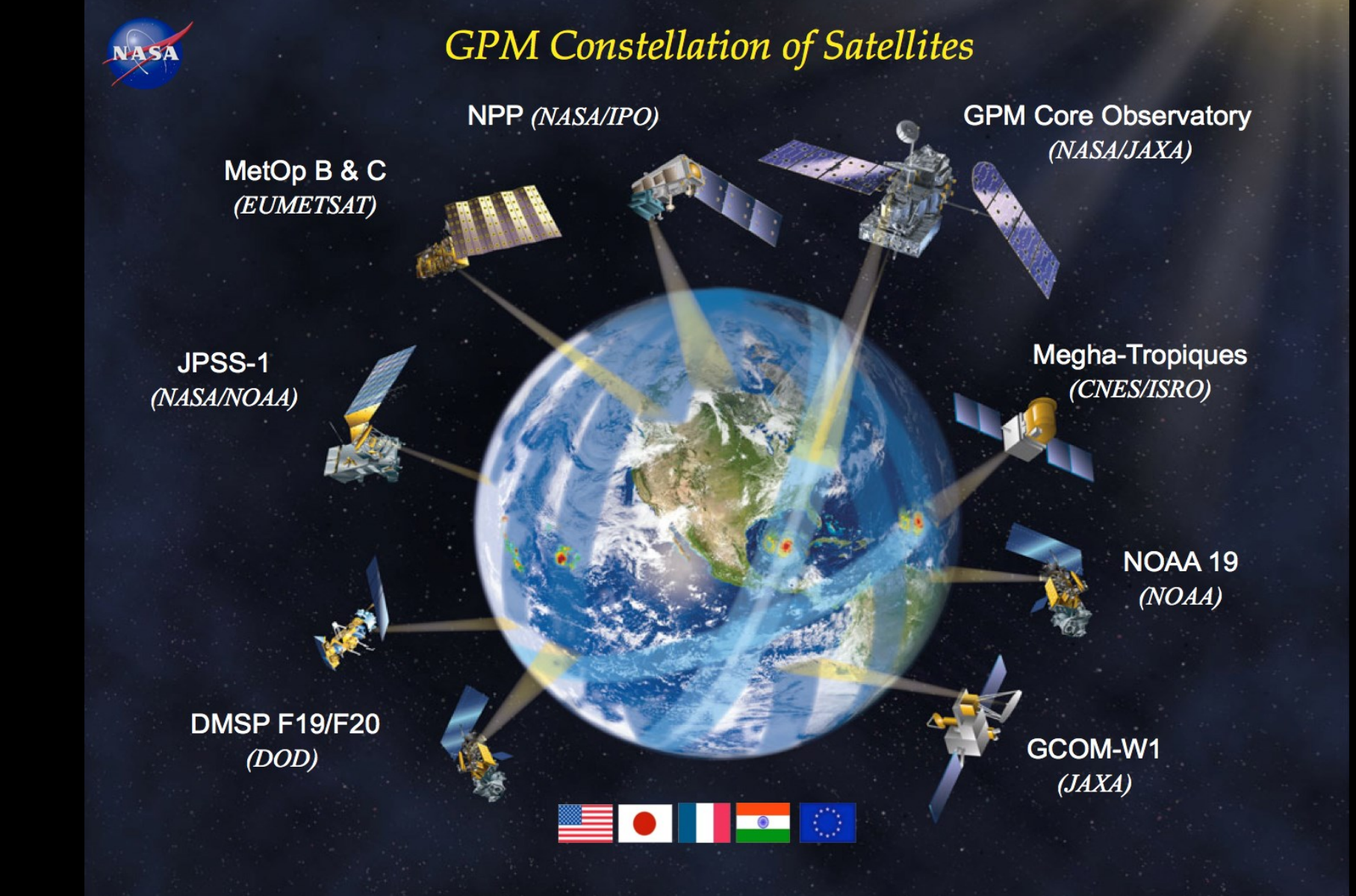

Limb-sounding

Figure 9-40:

Limb-sounding geometry for a sensor at height H above Earth viewing at angle θ below the local horizontal resulting in a tangent height h_t

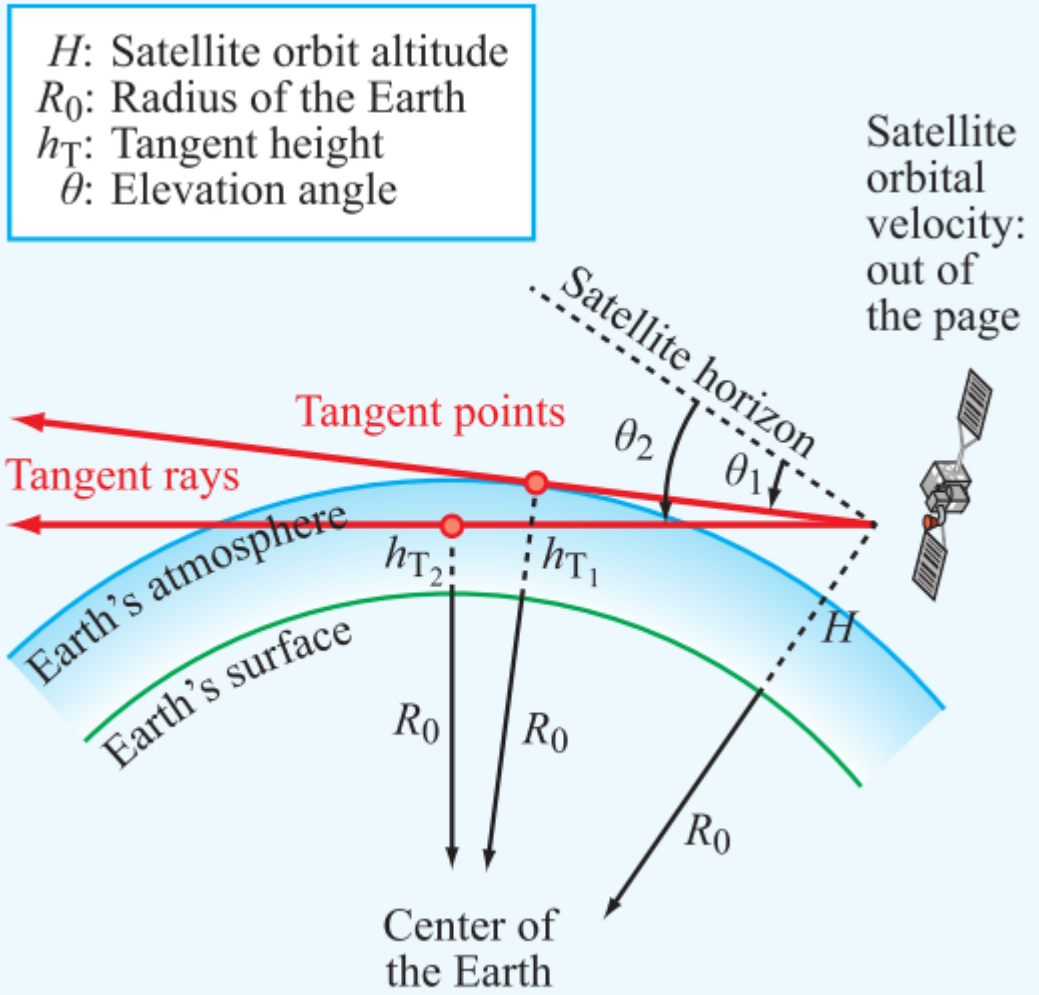

From: Microwave Radar and Radiometric Remote Sensing, by Ulaby and Long, 2014, with permission.

GPS Radio Occultation

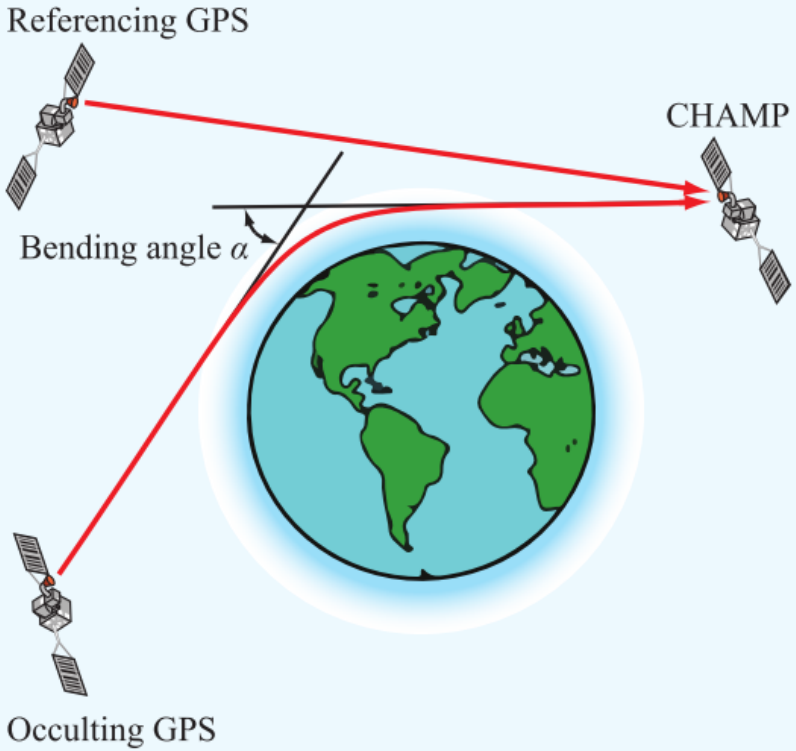

Figure 9-49: Occultation scenario for a low-Earth orbiter [Wickert et al., 2002].

From: Microwave Radar and Radiometric Remote Sensing, by Ulaby and Long, 2014, with permission.

CHAMP satellite

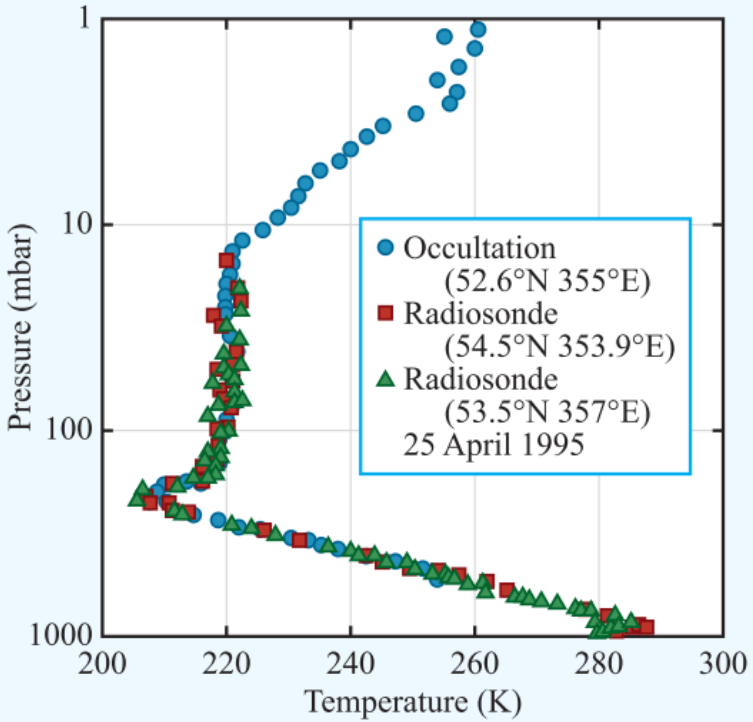

Figure 9-51: GPS temperature profile compared with two radiosondes (Yunck, 2002).

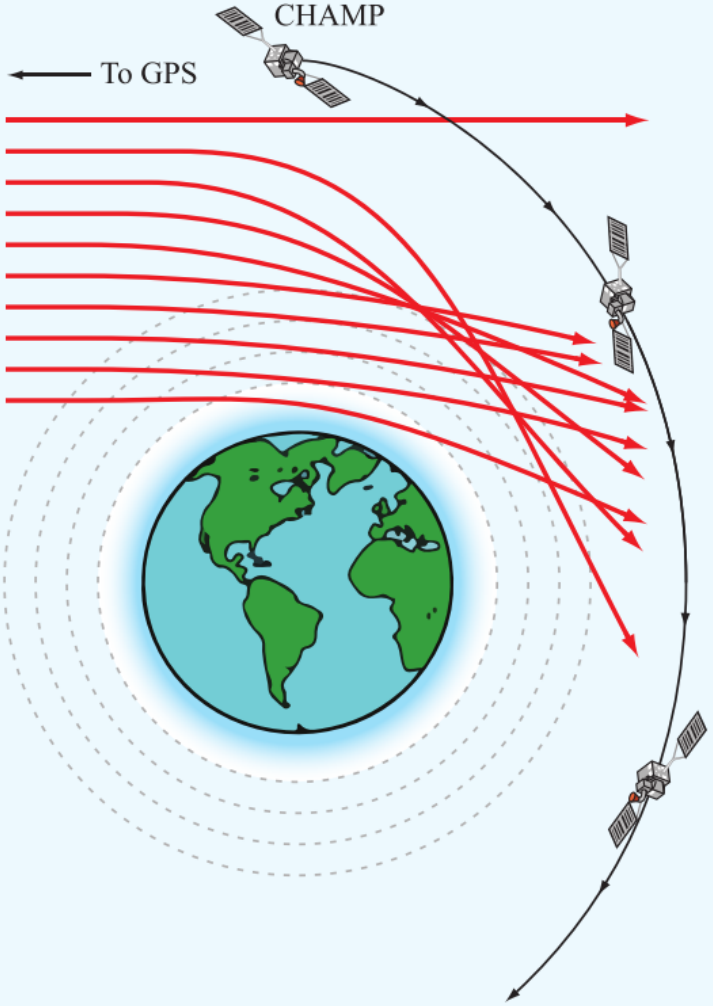

Figure 9-50: An ordered set of rays from an increasing refractive gradient with depth [Melbourne, 2004].

From: Microwave Radar and Radiometric Remote Sensing, by Ulaby and Long, 2014, with permission.

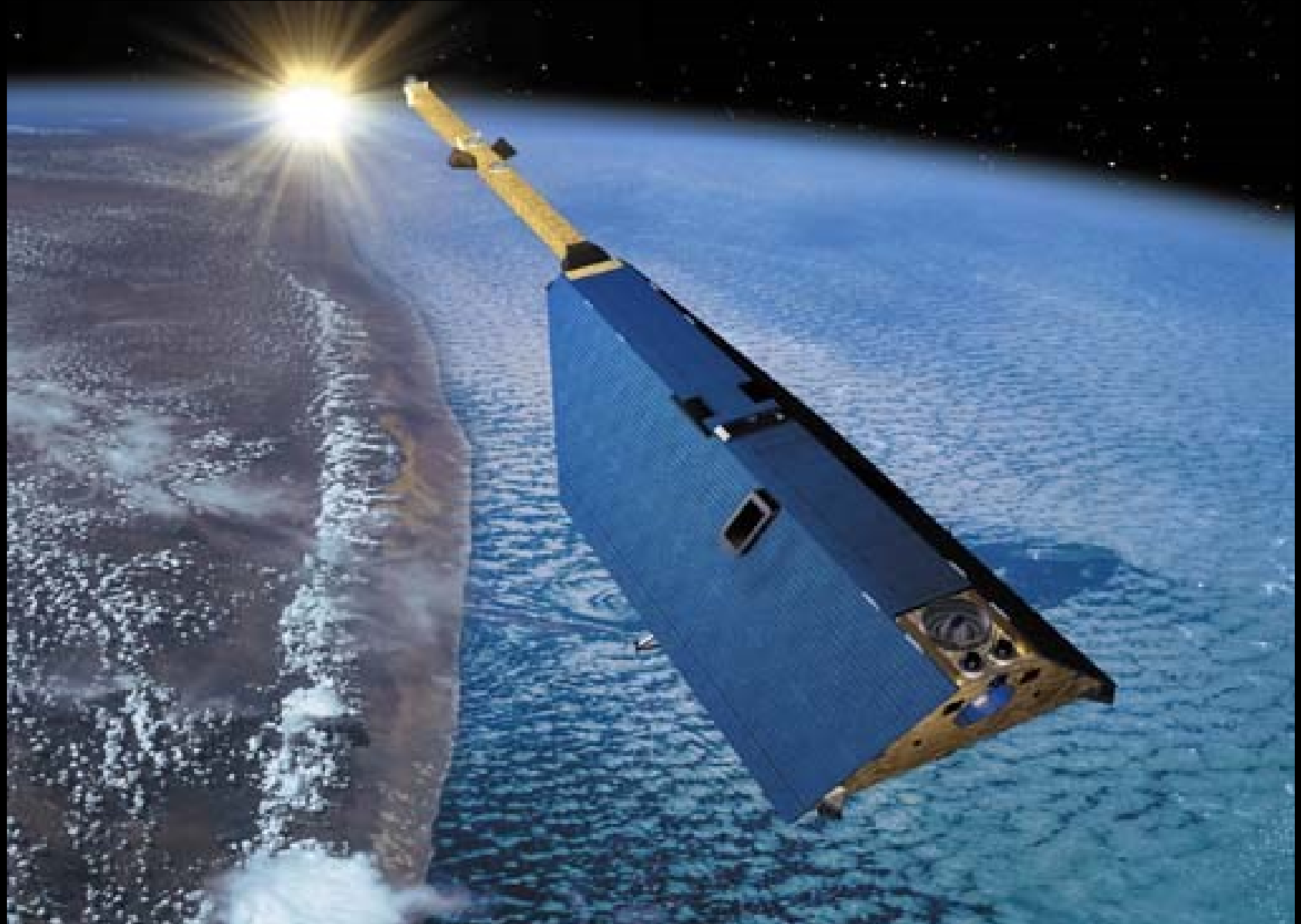

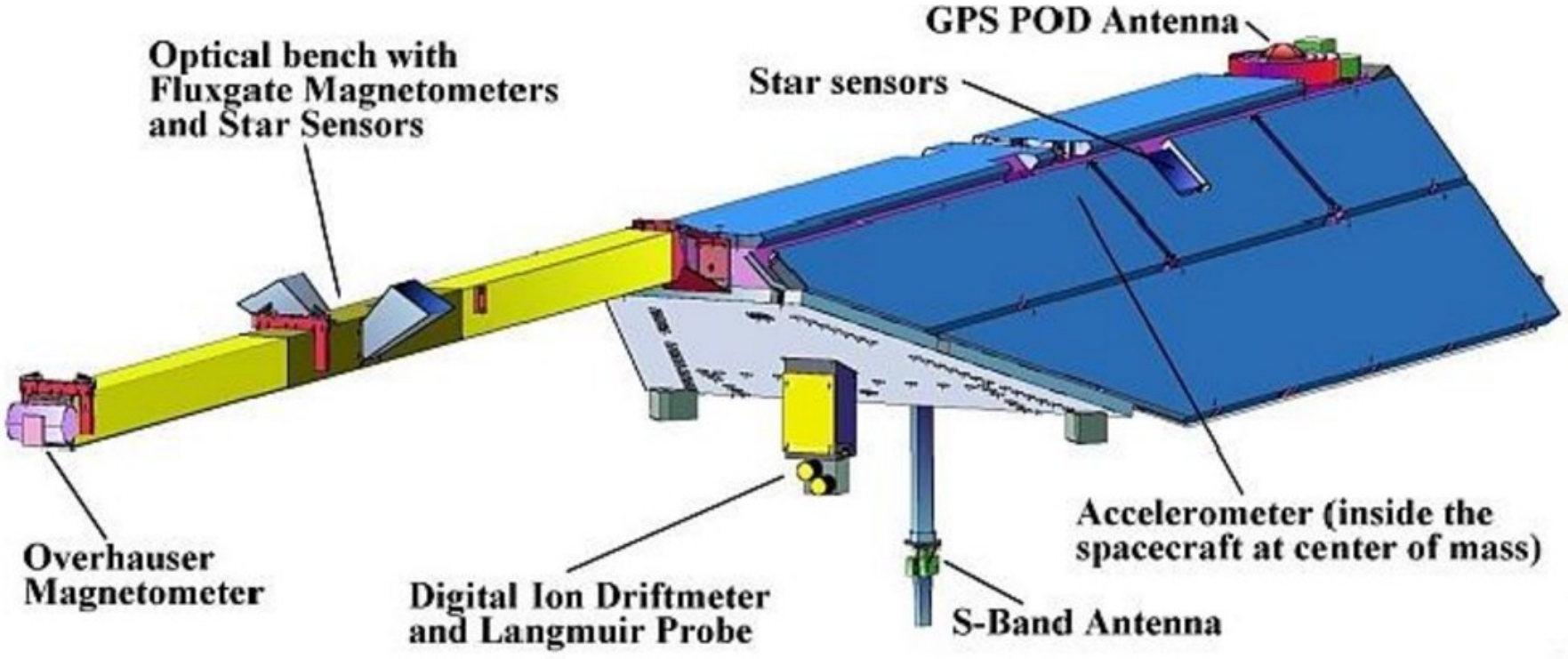
GPS POD Antenna
Optical bench with
Fluxgate Magnetometers
and Star Sensors
Star sensors
Overhauser
Magnetometer
Digital Ion Driftmeter
and Langmuir Probe
Accelerometer (inside the
spacecraft at center of mass)
S-Band Antenna

WindSat

Aalto University
School of Electrical
Engineering

WindSat
Polarimetric Radiometer

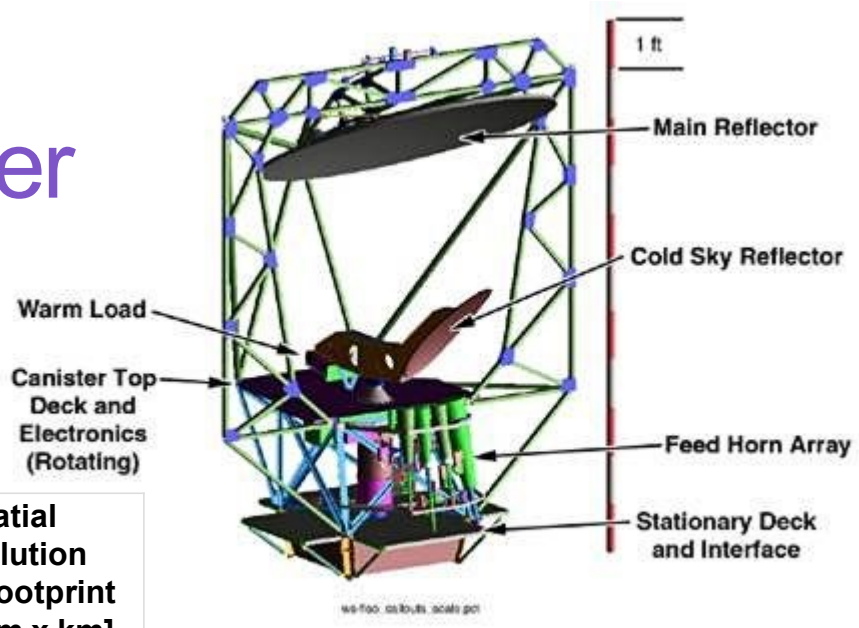

Band [GHz]	Polarizations	Average EIA[deg]	Spatial Resolution (3-dB footprint size)[km x km]
6.8	V, H	53.8	39 x 71
10.7	V, H, P, M, L, R	50.1	25 x 38
18.7	V, H, P, M, L, R	55.6	16 x 27
23.8	V, H	53.2	20 x 30
37.0	V, H, P, M, L, R	53.2	8 x 13

Summary of WindSat channels, polarizations Earth incidence angles and channel resolutions. Polarizations are listed as V for Vertical, H for Horizontal, P for +45 deg, L for Left Circular, and R for Right Circular

Aalto University
School of Electrical Engineering

http://www.remss.com/missions/windsat

WindScat data processing

Ocean Measurement	Acronym	Effective Spatial Resolution [km x km]	Channels Required for Retrieval
Sea surface temperature	SST	39 x 71	6.8 VH, 10.7 VH,18.7 VH, 23.8 VH, 37.0 VH
Ten-meter wind speed using low frequency channels	WSPD_LF	25 x 38	10.7 VH, 18.7 VH, 23.8 VH, 37.0 VH
Ten-meter wind speed using medium frequency channels	WSPD_MF	16 x 27	18.7 VH, 23.8 VH, 37.0 VH
Columnar atmospheric water vapor	VAPOR	16 x 27	18.7 VH, 23.8 VH, 37.0 VH
Columnar cloud liquid water content	CLOUD	16 x 27	18.7 VH, 23.8 VH, 37.0 VH
Rain rate	RAIN	8 x 13	18.7 VH, 23.8 VH, 37.0 VH
All-weather 10-meter wind speed	WSPD_AW	25 x 38 no rain39 x 71 in rain	6.8 VH, 10.7 VH, 18.7 VH, 23.8 VH, 37.0 VH
Ten-meter wind direction (relative to north)	WDIR	25 x 38	10.7 VHPMLR, 18.7 VHPMLR, 23.8 VH, 37.0 VHPMLR

Average of 3 days ending: 2015/02/03, WindSat, version 7.0.1

Atmospheric Water Vapor (mm)

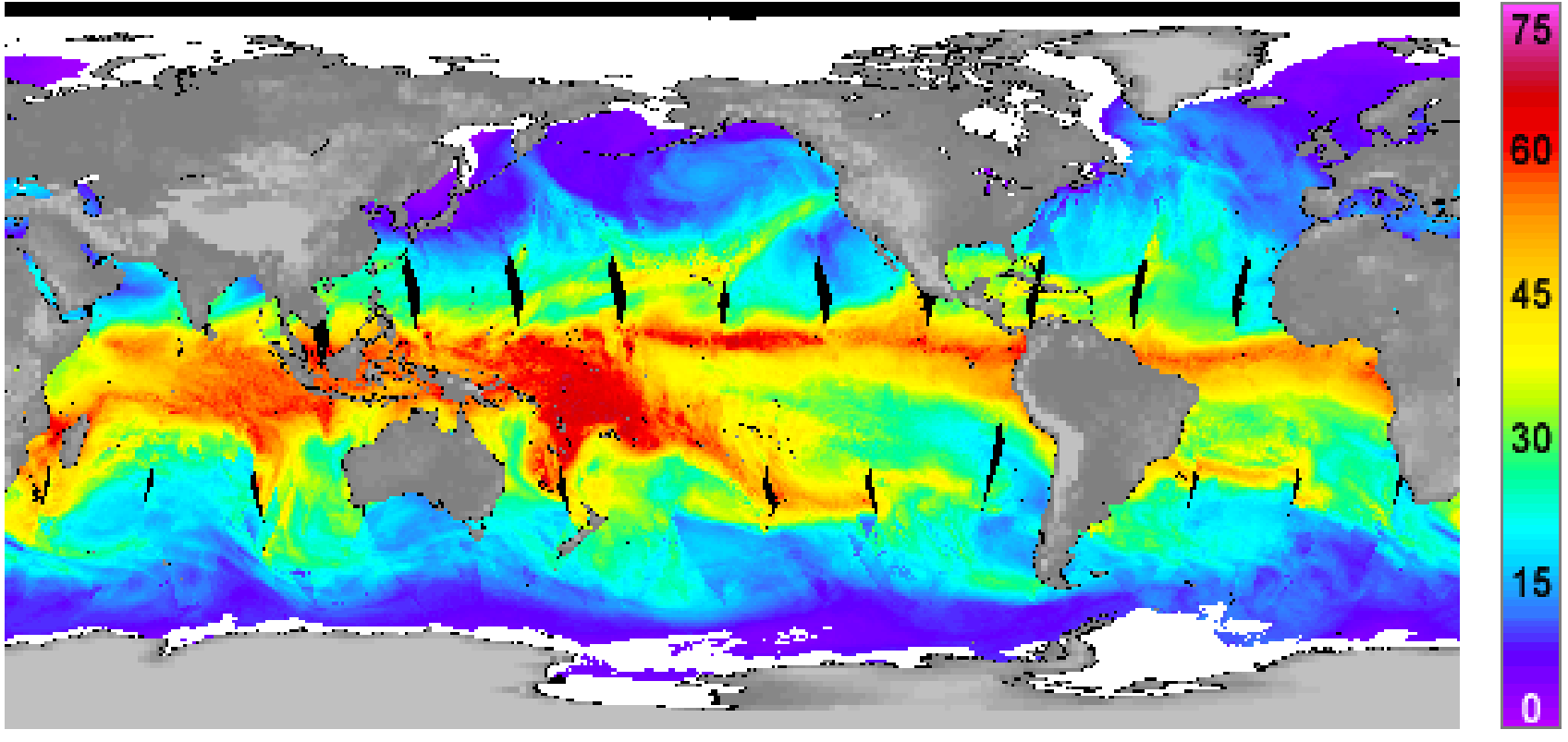

Average of 3 days ending: 2015/02/03, WindSat, version 7.0.1

Surface Wind Speed (m/s)

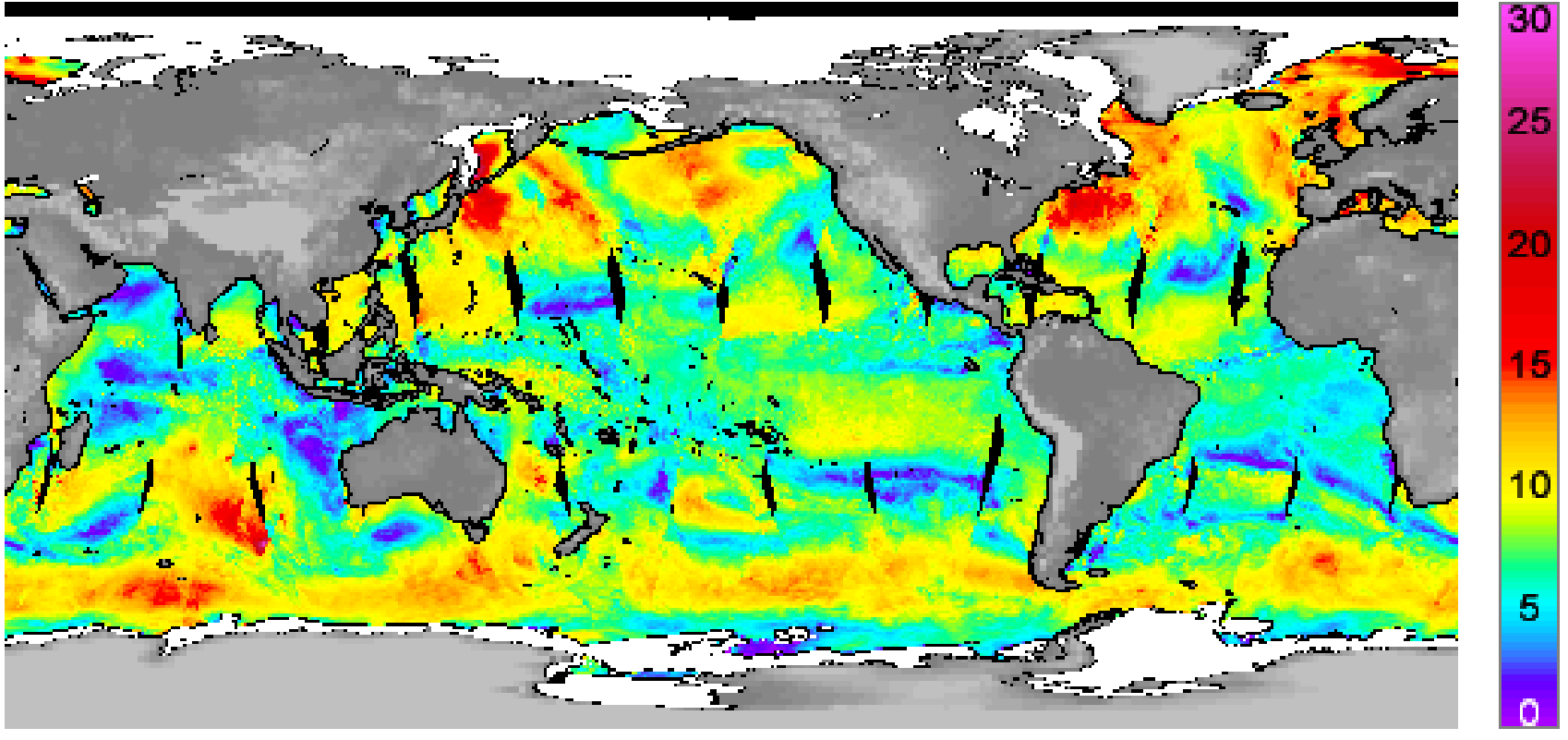

Average of 3 days ending: 2015/02/03, WindSat, version 7.0.1

Cloud Liquid Water(mm)

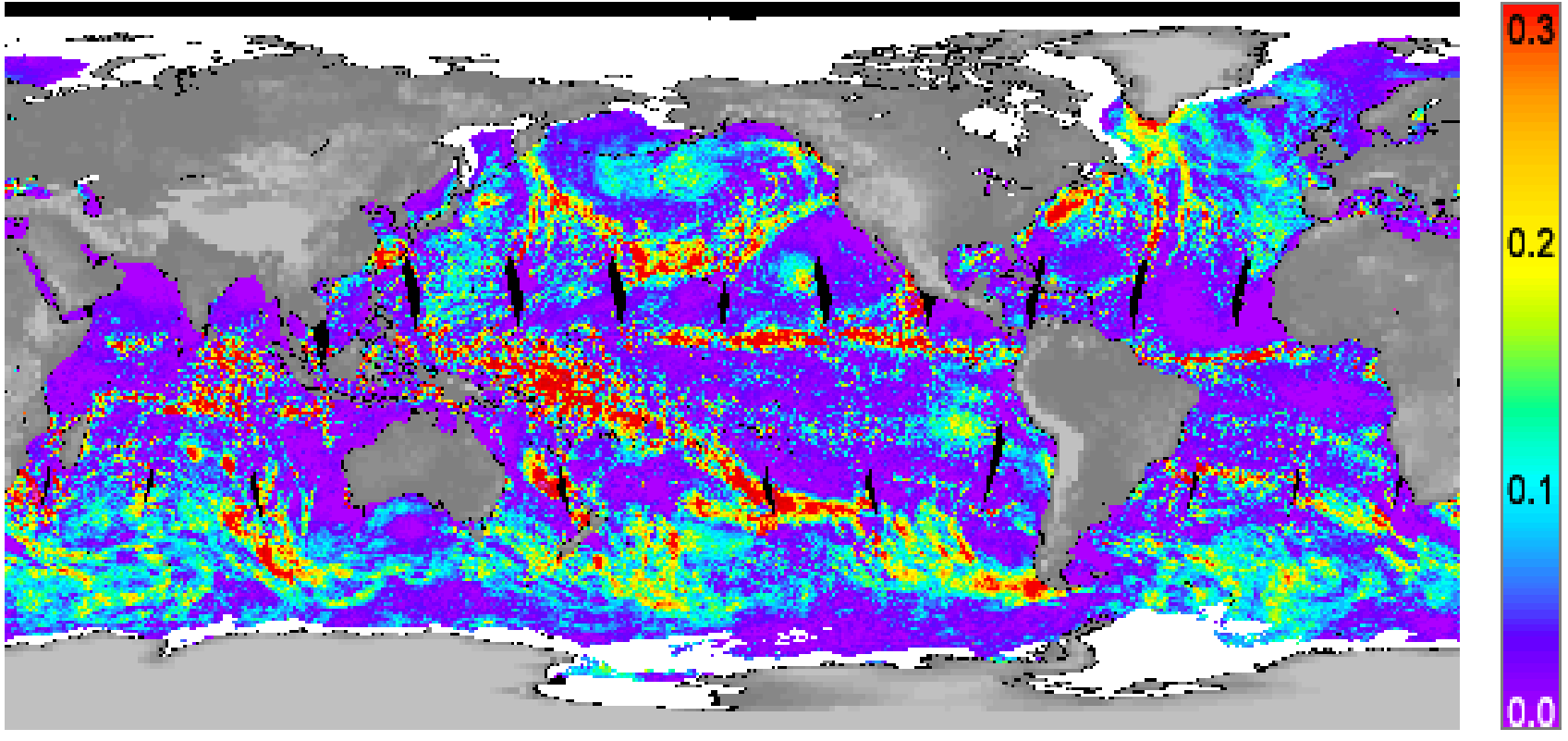

Average of 3 days ending: 2015/02/03, WindSat, version 7.0.1

Sea Surface Temp (ºC)

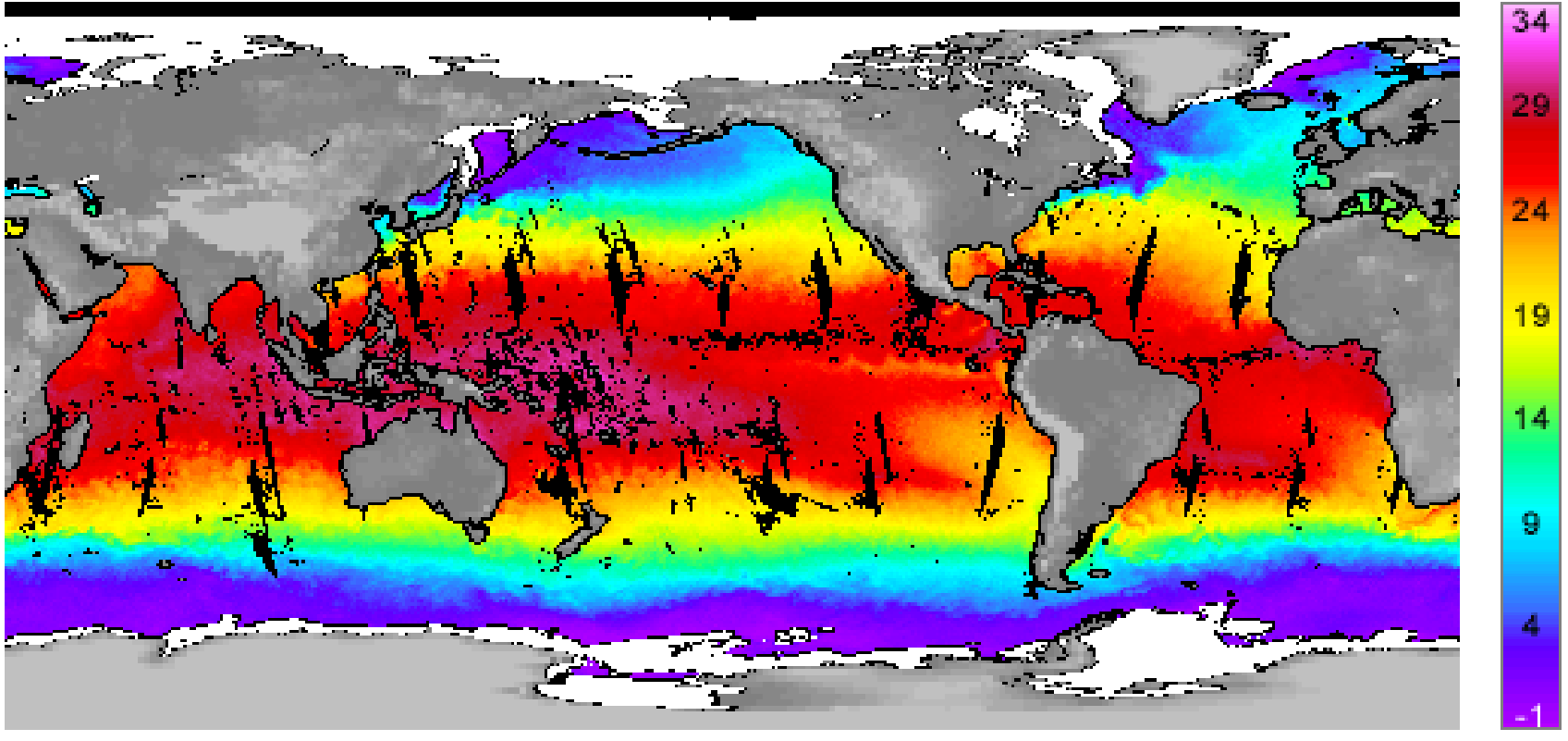

Aalto University
School of Electrical
Engineering

Small satellite radiometers

Atmosphere radiometry					
Mission	**Provider**	**Description**	**Launced**	**Mass**	**Platform**
Tropics	MIT Lincoln Laboratory; NASA/JPL	Constellation of 12 MicroMAS-2 satellites; see MicroMas-2.	2019	1 kg (payload)	3U (1U payload)
EON_MW	MIT Lincoln Laboratory; NOAA	Continuation and combination of MicroMAS / MiRaTA for high performance; Equal to ATMS channels	2018/19?	25 kg	12U
TEMPEST-D	Colorado State University, NASA/JPL, Blue Canyon Tech.	Across-track scanning radiometer (90-183 GHz); 89, 165, 176, 180, and 182 GHz.	2018	7 kg	6U (3U payload)
PolarCube	Univ Colorado at Boulder	MiniRad is a passive microwave spectrometer with 8 channels centered around the 118.7503 GHz oxygen emission line. Uses ALL-STAR cubesat bus.	10/2018	2 kg payload	3 U (1.5 U payload)
MiRaTA	MIT Lincoln Laboratory	52-58 GHz (V-band), 175-191 (G-band), and 206-208 GHz; Nadir radiometer. GPS for radio occultation; Calibration development of a radiometer using occultation	2017	4,5 kg	3U
MicroMAS-2A and B	MIT Lincoln Laboratory	12 channels near 90, 118, 183, and 206 GHz; Across-track scanning radiometer	A: 2018 B: 10/2018	1 kg (payload)	3U (1U payload)
RACE	NASA/JPL and University of Texas	CHARM is a 183 GHz radiometer; Tech development of 183 GHz radiometry (35 nm InP HEMT tech)	2014	5.5 kg (1.5 kg payload)	3U (1.5U payload)
MicroMAS-1	MIT Lincoln Laboratory	118 GHz radiometer; Transmitter failed after launch	2014	1 kg (payload)	3U (1U payload)
Ksat 2	Kagoshi University	wikipedia: "radio-frequency water vapor detector for climatology research"; K-sat 1 failed in 2010	2014		1U
CAS CubeSat Constellation	jieying He; CAS	118.75 GHz oxygen absorption line and 183 water vapor line for more than 100 channels based on high-speed digital processing technique, with a calibration accuracy of 0.5K	Not known		

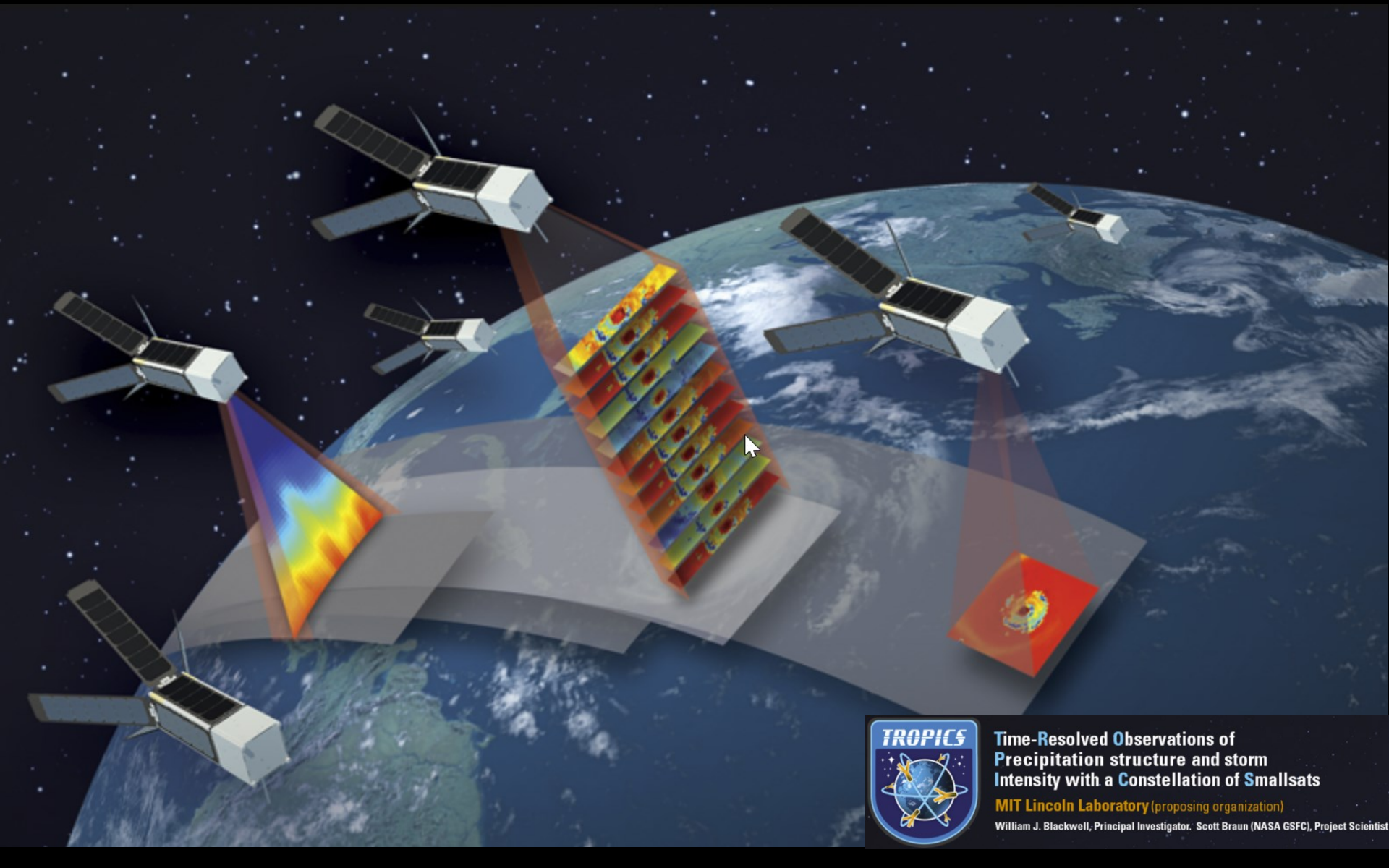
TROPICS
Time-Resolved Observations of
Precipitation structure and storm
Intensity with a Constellation of Smallsats
MIT Lincoln Laboratory (proposing organization)
William J. Blackwell, Principal Investigator. Scott Braun (NASA GSFC), Project Scientist

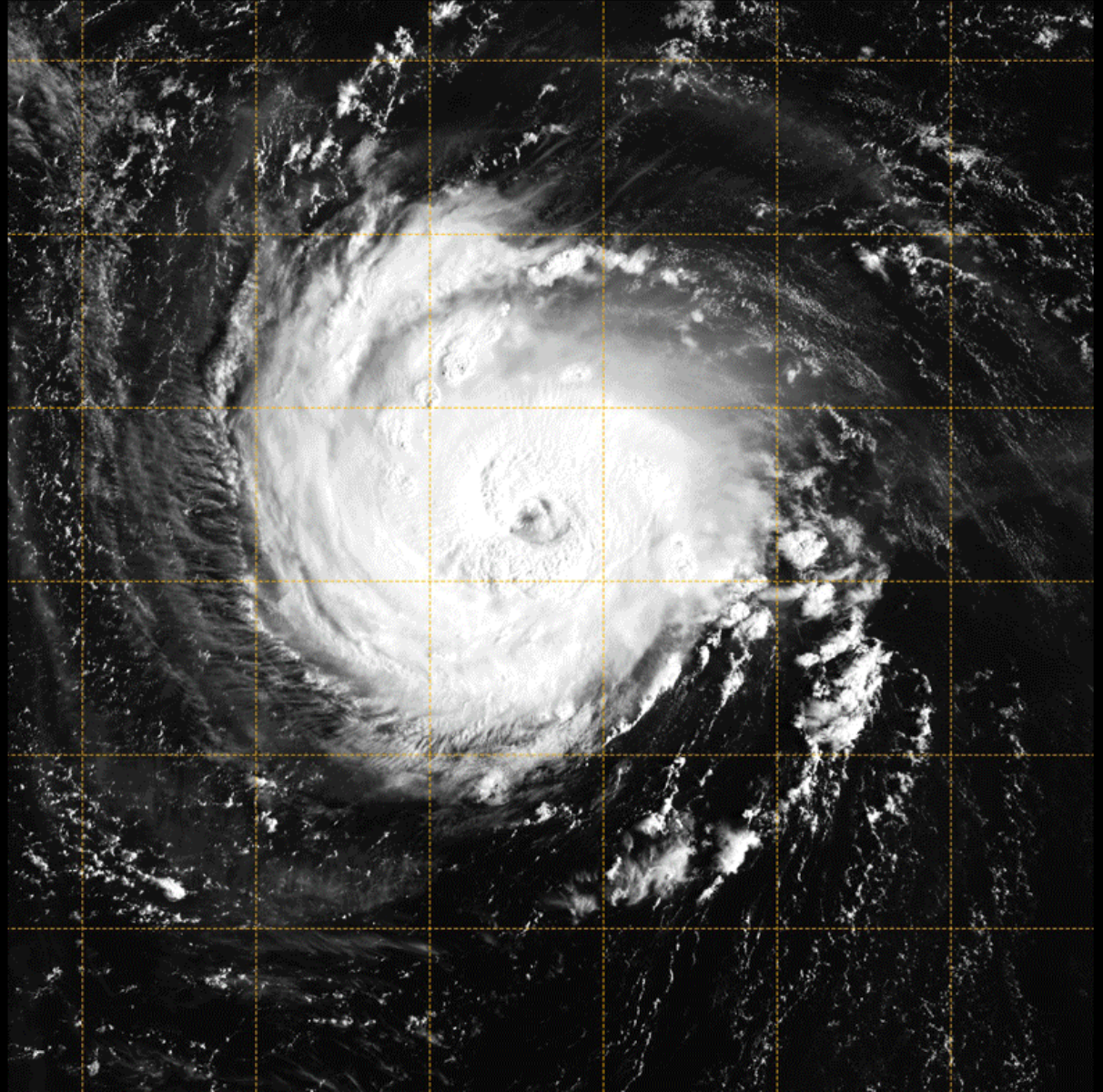

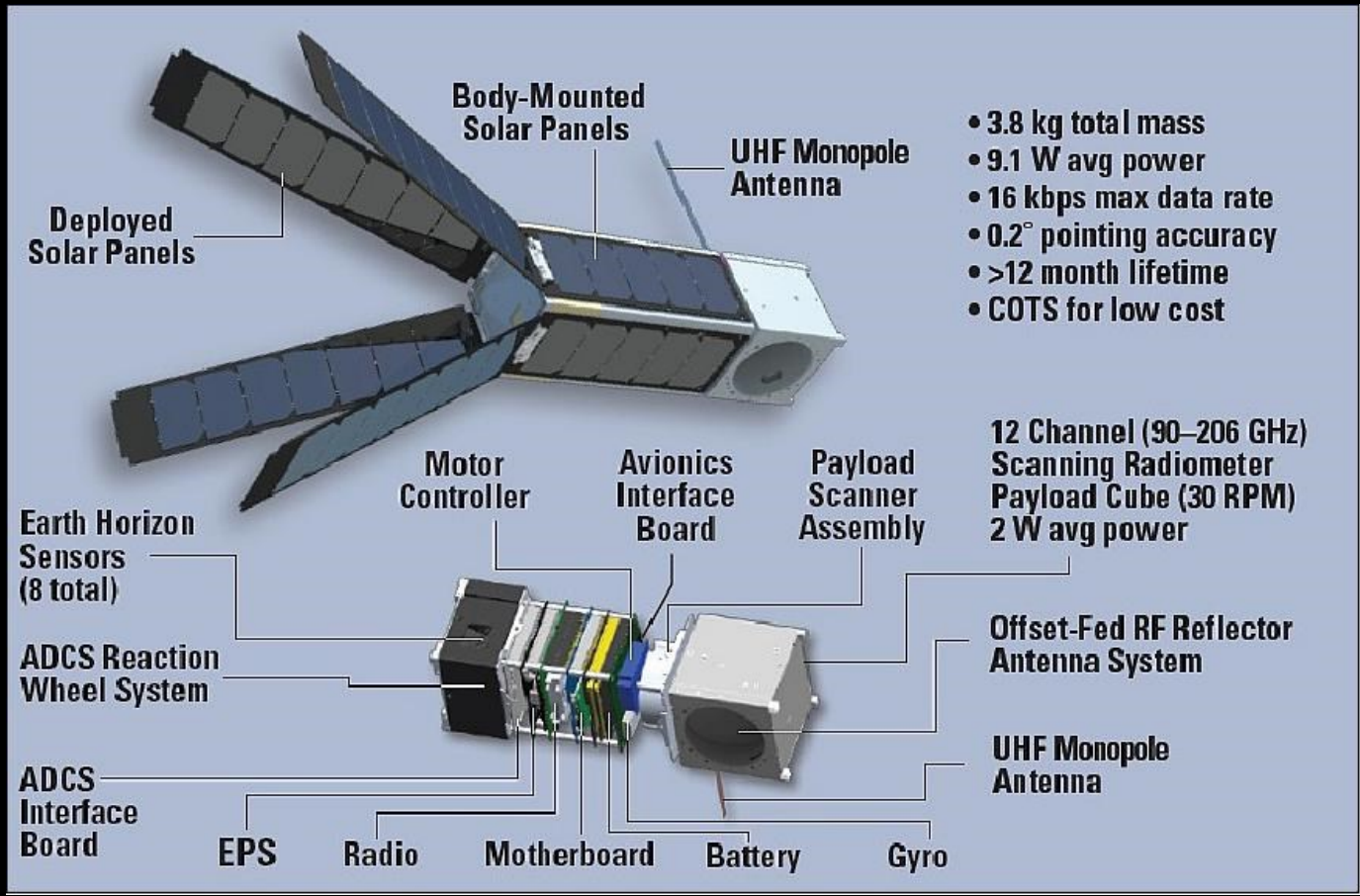
Body-Mounted
Solar Panels
UHF Monopole
Antenna
Deployed
Solar Panels
• 3.8 kg total mass
• 9.1 W avg power
• 16 kbps max data rate
• 0.2° pointing accuracy
• >12 month lifetime
• COTS for low cost
Motor
Controller
Avionics
Interface
Board
Payload
Scanner
Assembly
12 Channel (90–206 GHz)
Scanning Radiometer
Payload Cube (30 RPM)
2 W avg power
Earth Horizon
Sensors
(8 total)
ADCS Reaction
Wheel System
Offset-Fed RF Reflector
Antenna System
UHF Monopole
Antenna
ADCS
Interface
Board
EPS
Radio
Motherboard
Battery
Gyro

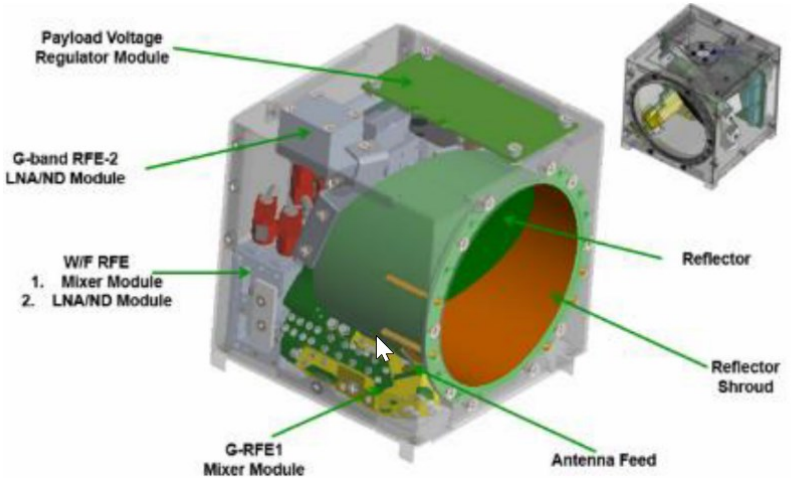

Chan.	Center Freq. (GHz)	Bandwidth (MHz)	Beamwidth (deg.) Down/Cross	NEDT	Cal. Acc. (K)
1	91.655 ± 1.4	1000	3.0/3.17	0.95	2.0
2	114.50	1000	2.4/2.62	0.55	1.5
3	115.95	800	2.4/2.62	0.60	1.5
4	116.65	600	2.4/2.62	0.70	1.5
5	117.25	600	2.4/2.62	0.70	1.5
6	117.80	500	2.4/2.62	0.75	1.5
7	118.24	380	2.4/2.62	0.85	1.5
8	118.58	300	2.4/2.62	1.00	1.5
9	184.41	2000	1.5/1.87	0.60	1.0
10	186.51	2000	1.5/1.87	0.60	1.0
11	190.31	2000	1.5/1.87	0.60	1.0
12	204.8	2000	1.4/1.76	0.60	1.0

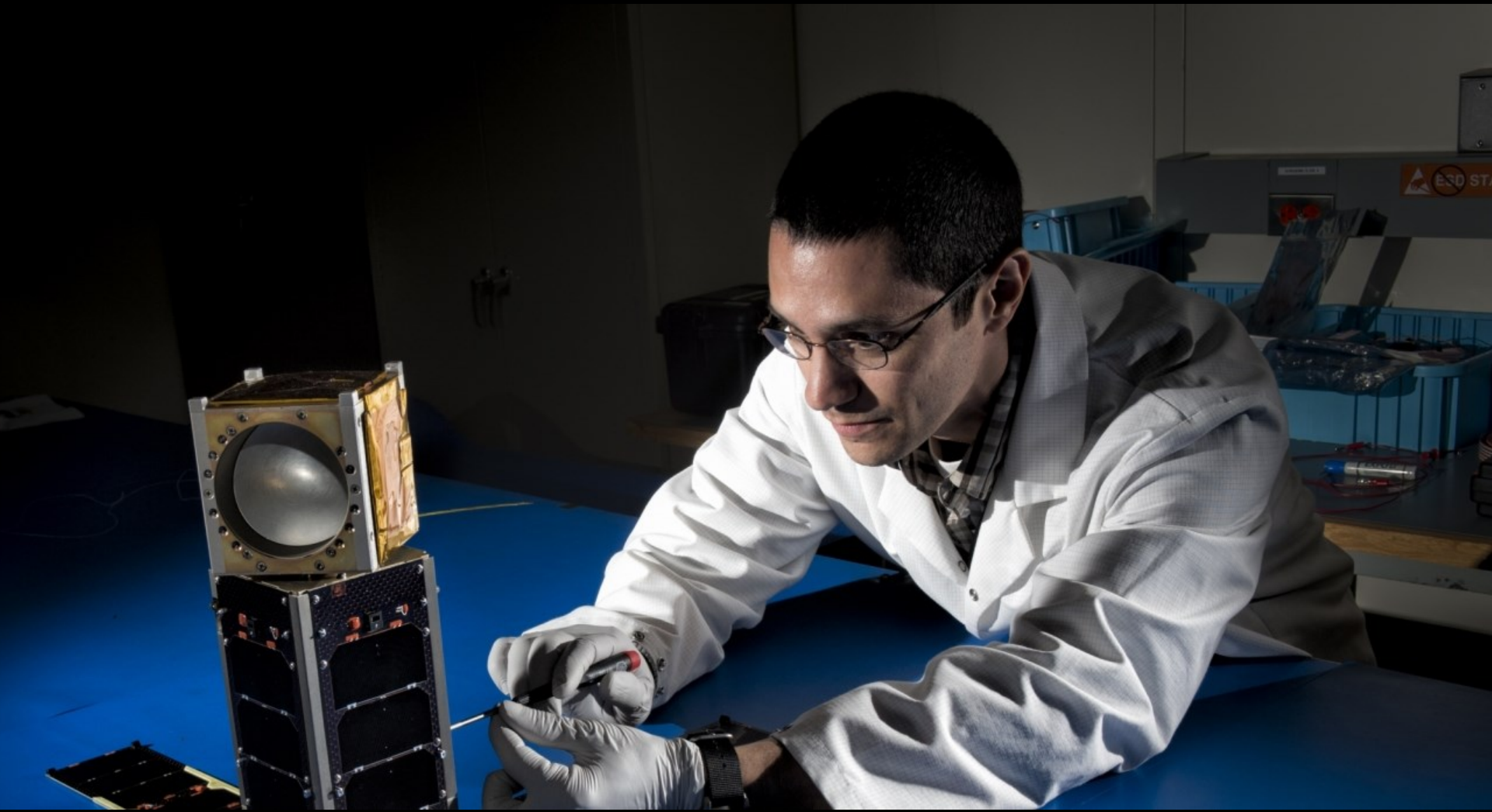

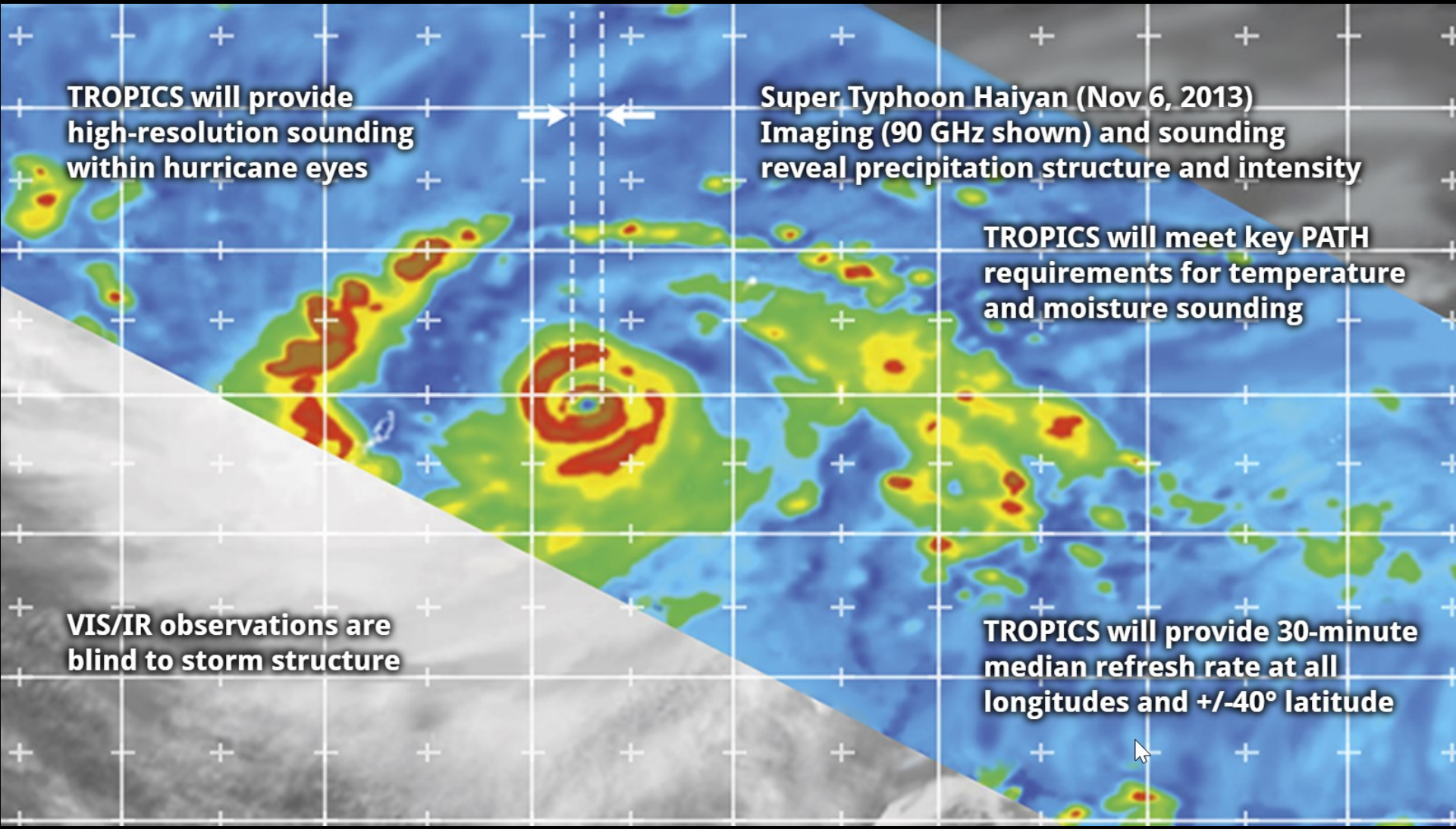
TROPICS will provide high-resolution sounding within hurricane eyes
Super Typhoon Haiyan (Nov 6, 2013) Imaging (90 GHz shown) and sounding reveal precipitation structure and intensity
TROPICS will meet key PATH requirements for temperature and moisture sounding
VIS/IR observations are blind to storm structure
TROPICS will provide 30-minute median refresh rate at all longitudes and +/-40° latitude

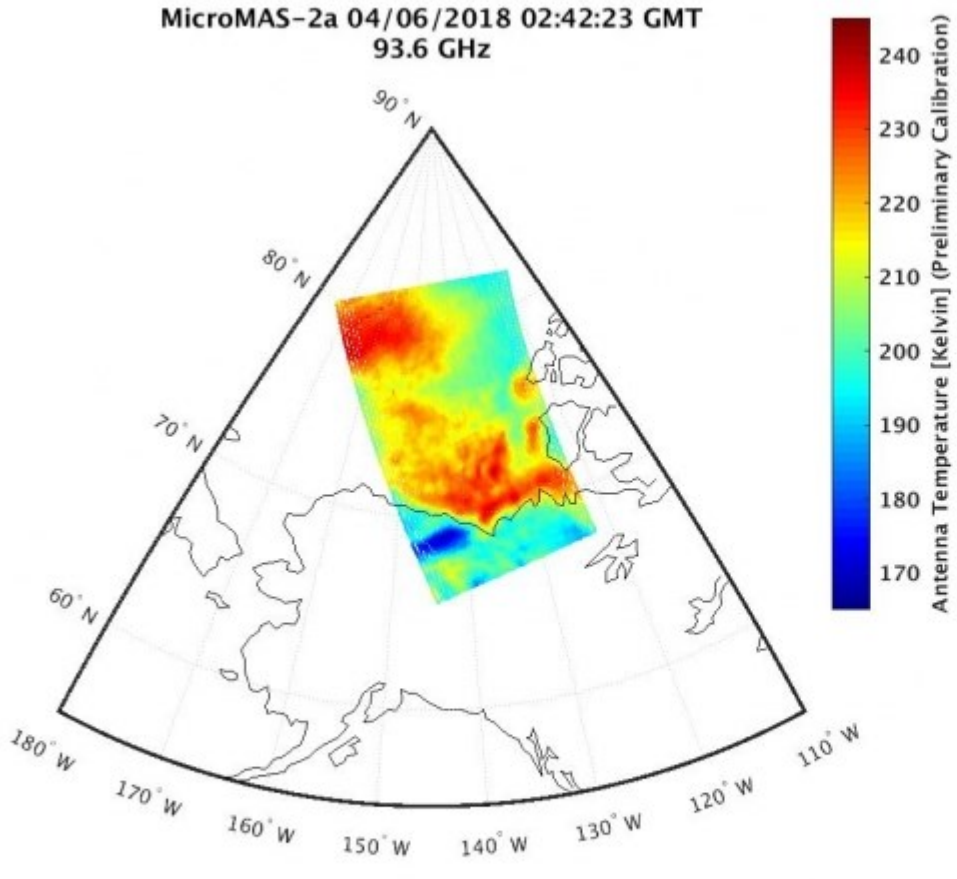
MicroMAS-2a 04/06/2018 02:42:23 GMT
93.6 GHz
90° N
80° N
70° N
60° N
180° W
170° W
160° W
150° W
140° W
130° W
120° W
110° W
240
230
220
210
200
190
180
170
Antenna Temperature [Kelvin] (Preliminary Calibration)

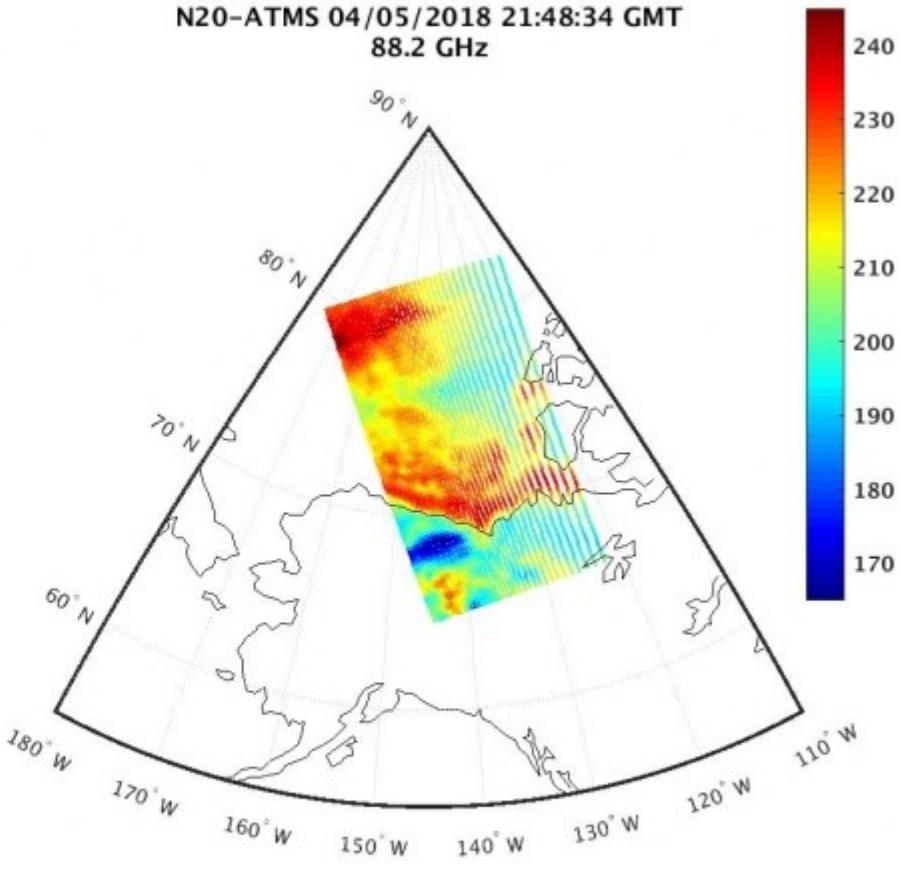
N20-ATMS 04/05/2018 21:48:34 GMT
88.2 GHz
90° N
80° N
70° N
60° N
180° W
170° W
160° W
150° W
140° W
130° W
120° W
110° W
240
230
220
210
200
190
180
170

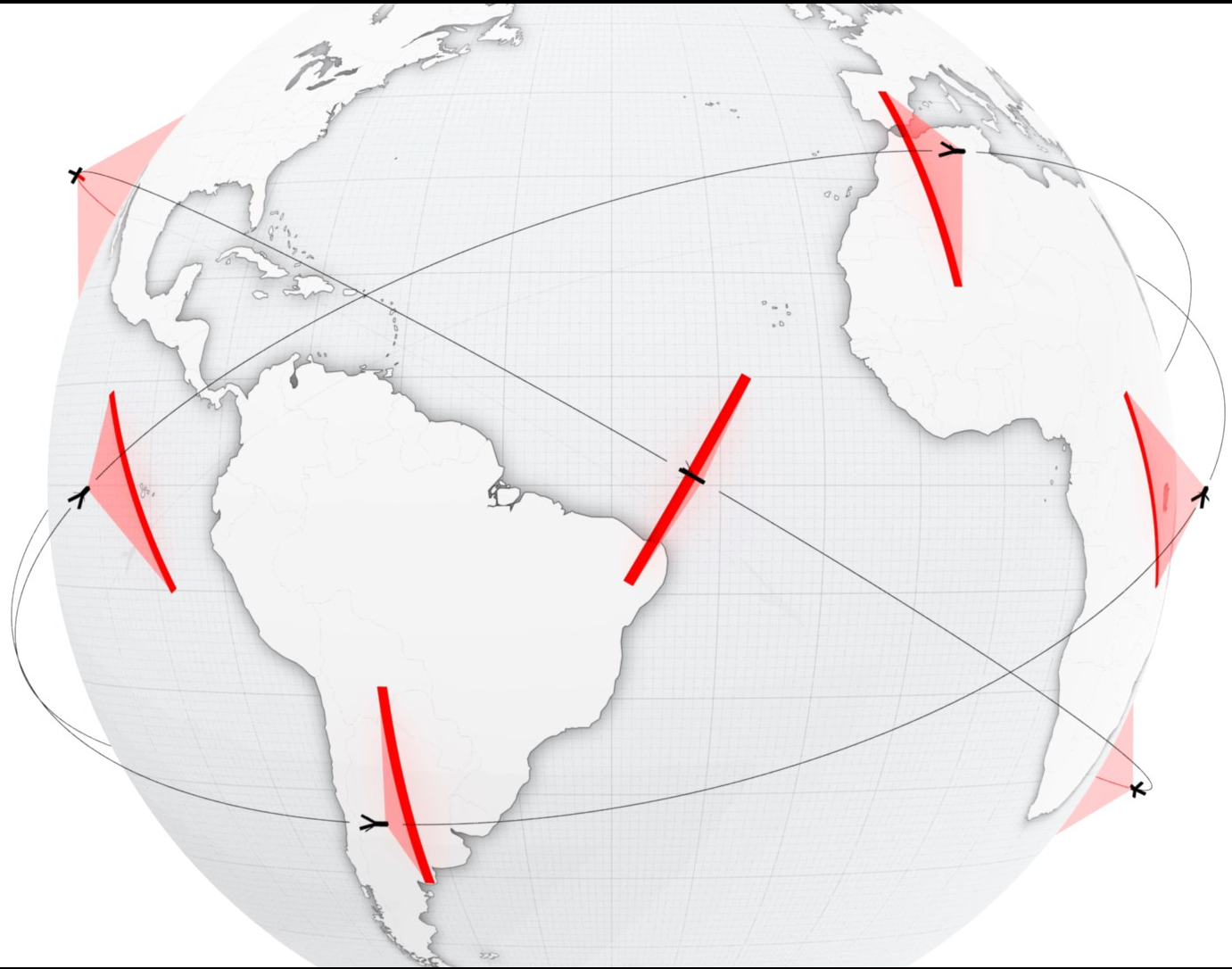

PolarCube

Channel #	8	7	6	5	4	3	2	1
IF f_c (MHz)	5000	3100	2100	1500	1100	700	400	200
BW (MHz)	2600	1200	800	400	400	400	200	100
Noise RMS (K)	0.356	0.503	0.603	0.857	0.861	0.882	1.39	2.18

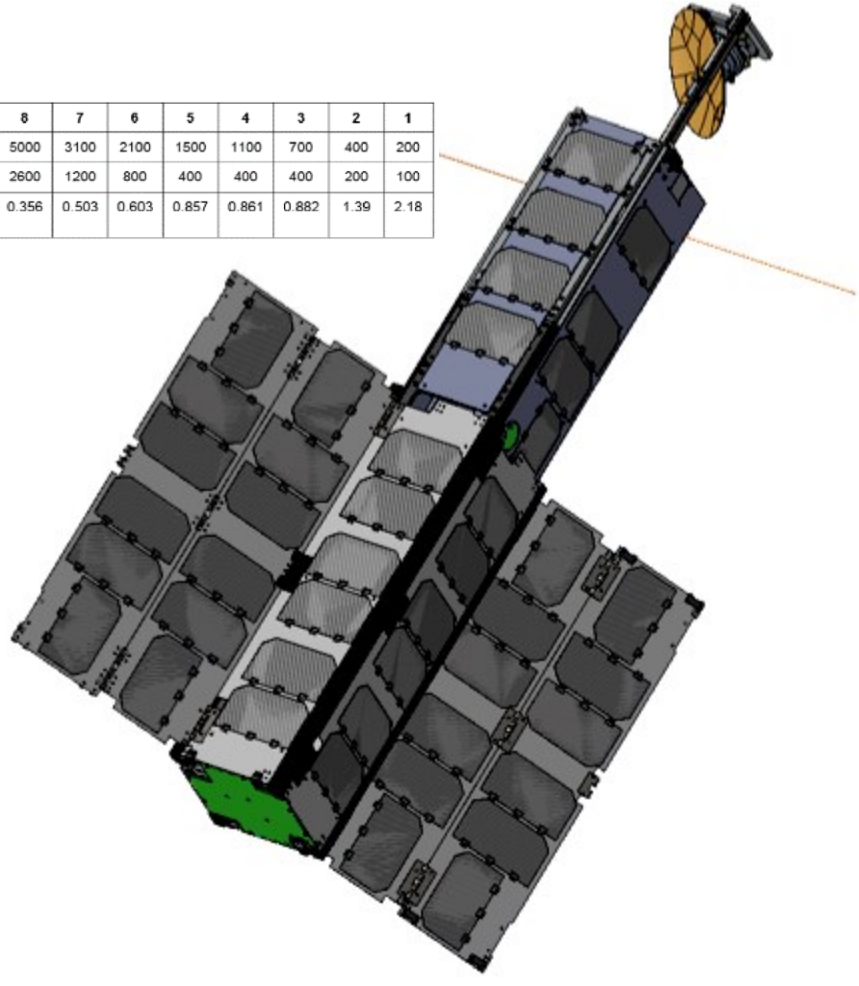

Platform: 3U Cubesat

Payload : microwave radiometer MiniRad around 18.7503 GHz

University of Colorado at Boulder

- Center for Environmental Technology
- Colorado Space Grant Consortium
- National Snow and Ice Data Center

Measures temperature, moisture, precipitation, cloud water and ice, and cryospheric surface features such as snow cover and sea ice concentration

Aalto University
School of Electrical
Engineering

CYGNSS

The Cyclone Global Navigation Satellite System (CYGNSS)

The Cyclone Global Navigation Satellite System is a space-based system developed by the University of Michigan and Southwest Research Institute with the aim of improving hurricane forecasting by better understanding the interactions between the sea and the air near the core of a storm.


+X
-Y

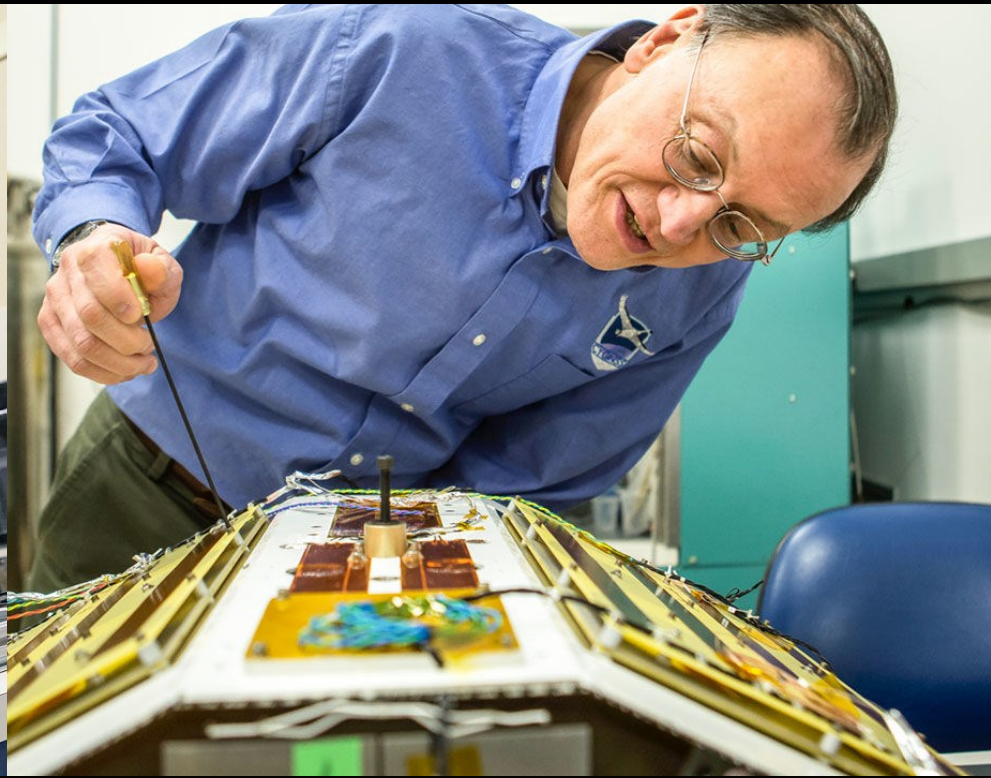

CYGNSS Level 3 V2.1 Wind Speed (2017-2018)

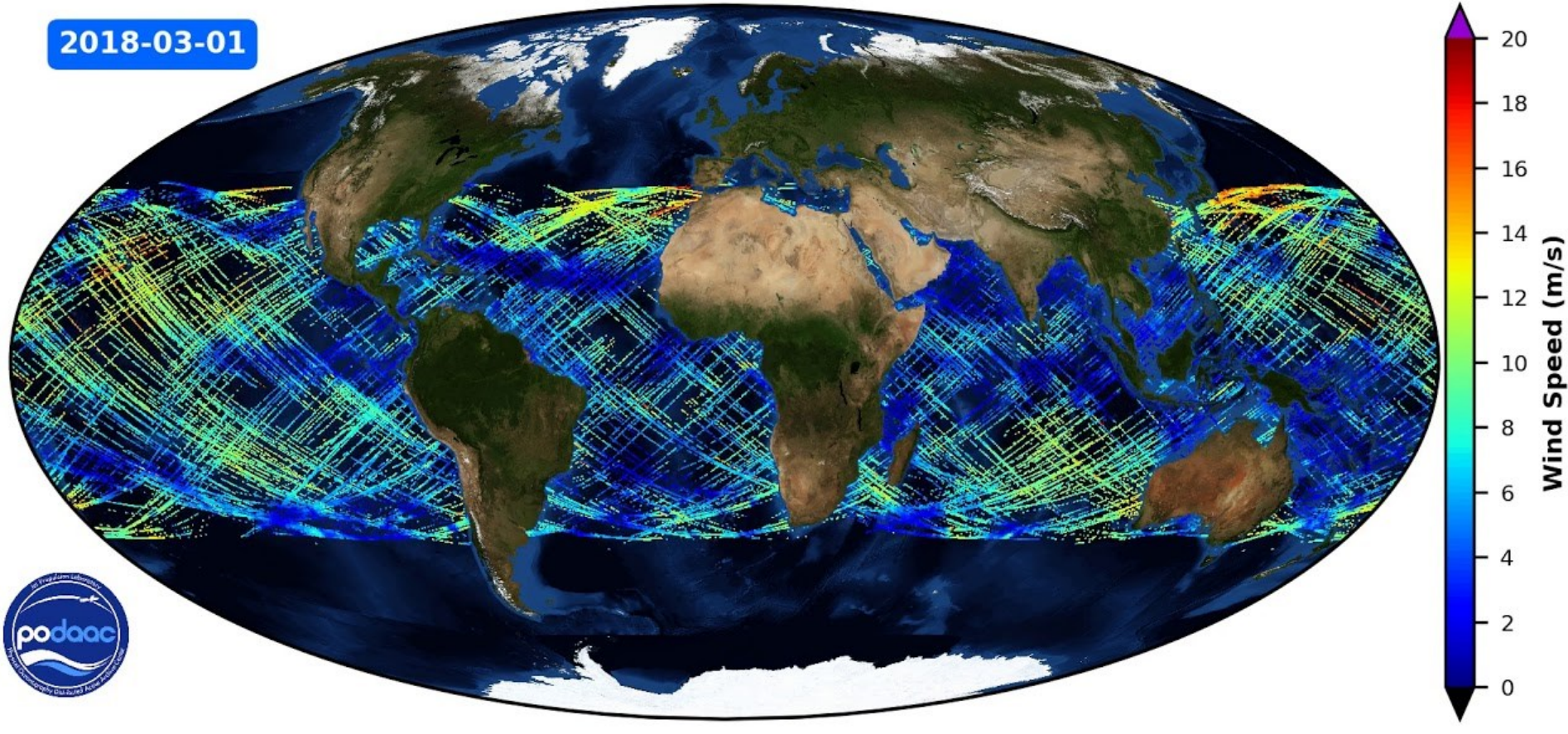

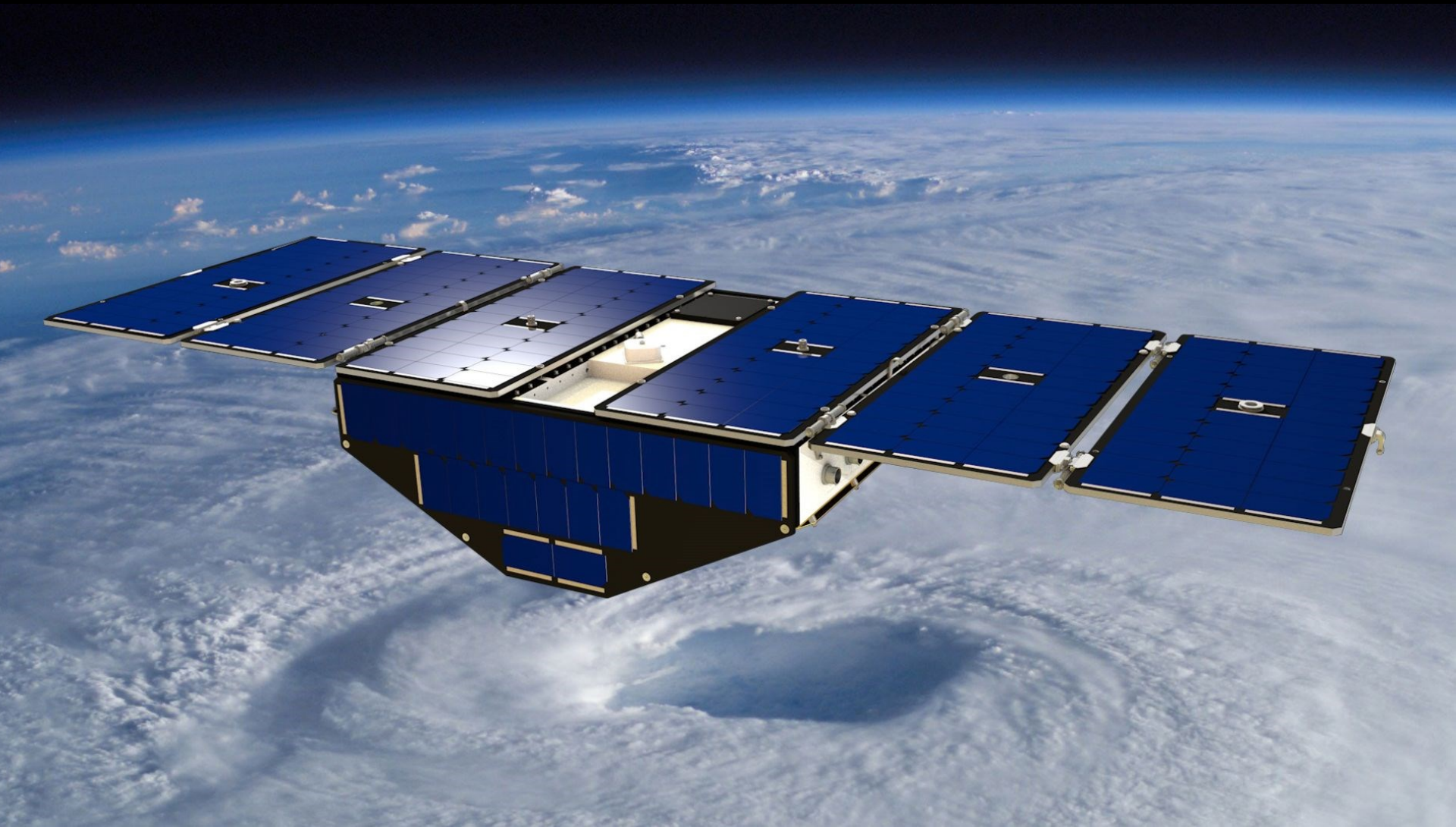

Land imaging radiometers

Aalto University
School of Electrical
Engineering

SSM/I

Special sensor microwave/imager

SSM/I series radiometers onboard 7 satellites since 1978

Frequencies and polarizations

-19.35 GHz, V + H

- 22.235 GHz, V

- 37.0 GHz, V + H

- 85.5 GHz, V + H

Mass 49 kg

Power consumption 45 W

Offset parabolic reflector:

- 61 cm x 91 cm

Reflector and feed horn antenna are mounted on a drum, rotated around its axis

Ice Motion from Passive Microwave: SMMR, SSM/I, SSMIS, and AMSR-E

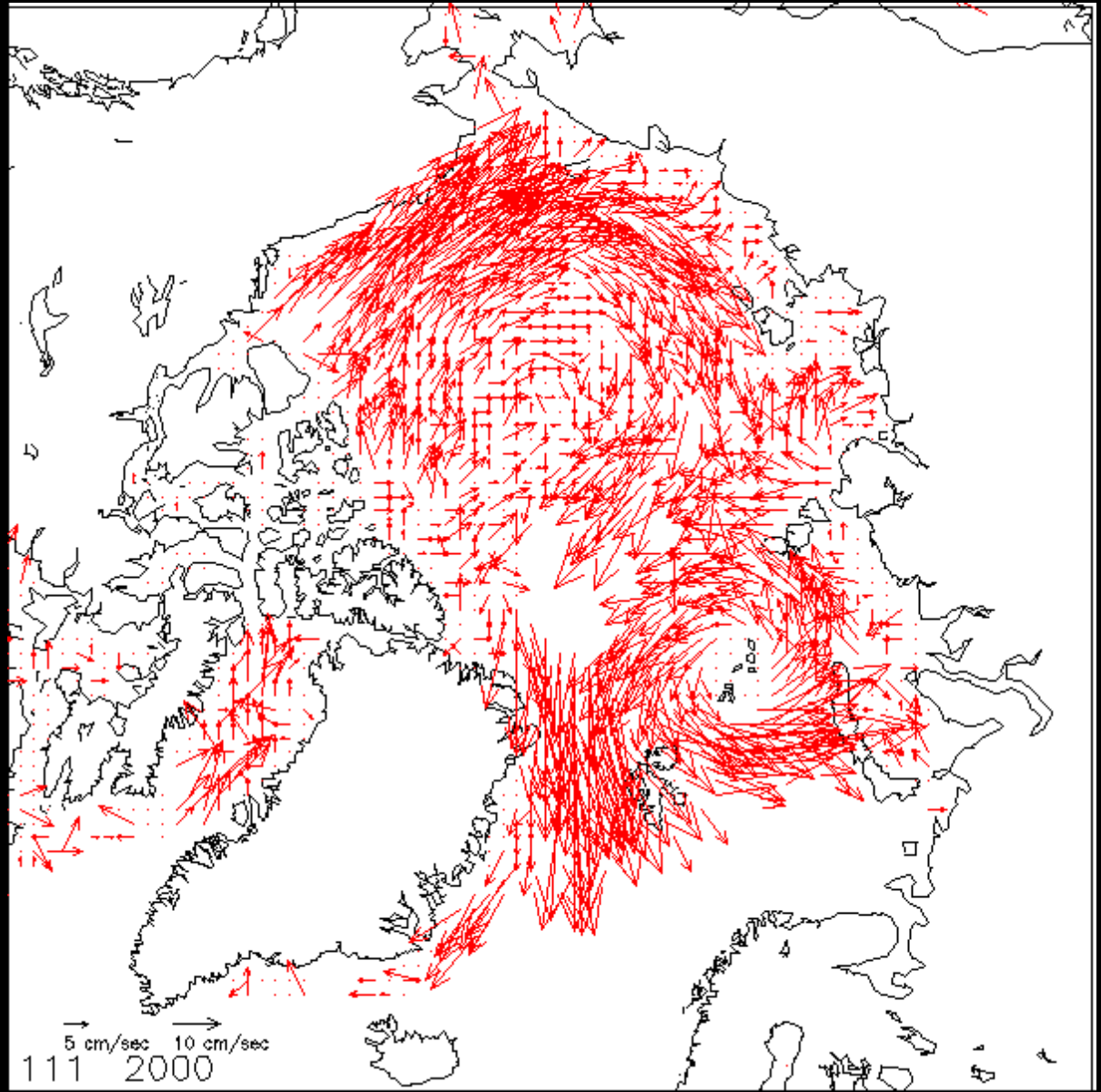

Snow Water Equivalent (FMI, Globsnow)

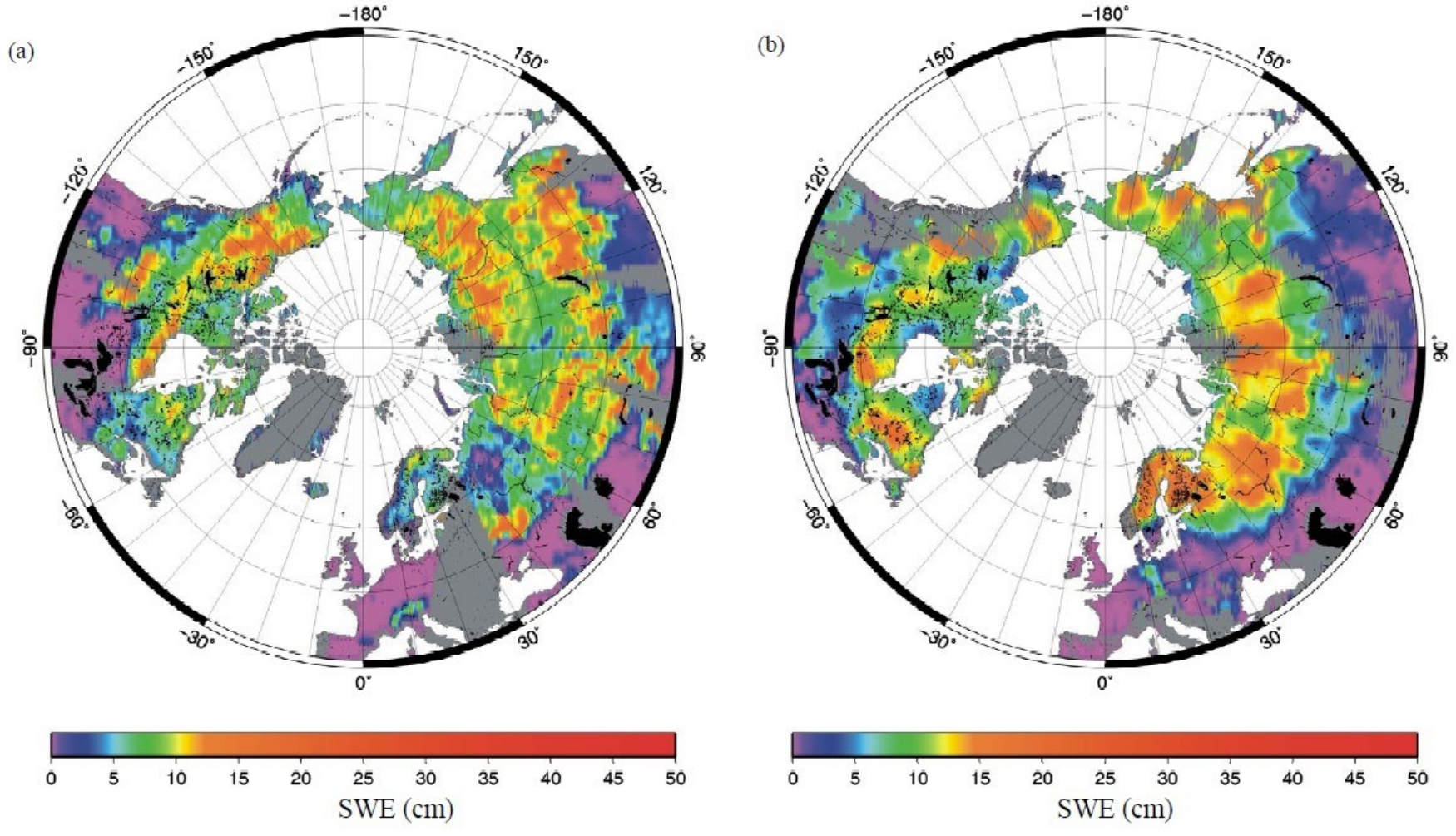

Aalto University
School of Electrical
Engineering

SMAP

Soil Moisture Active Passive

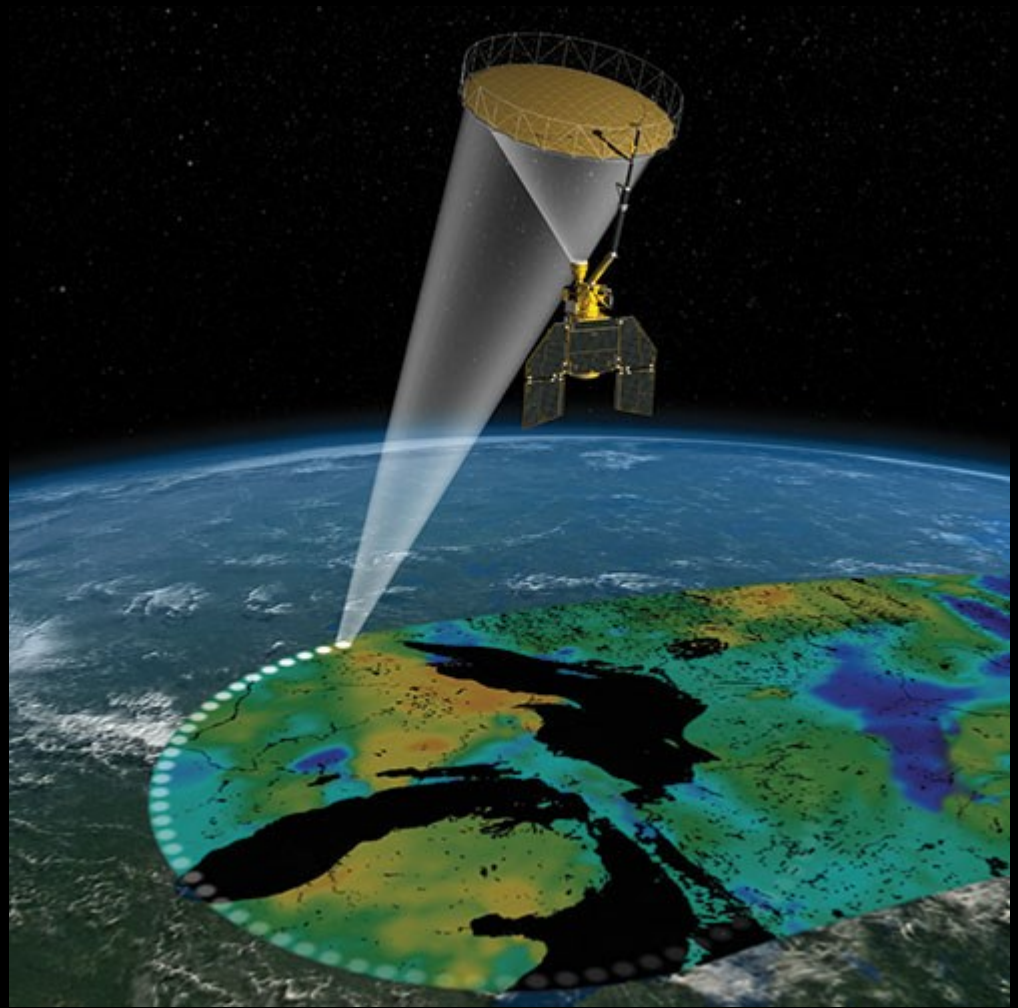

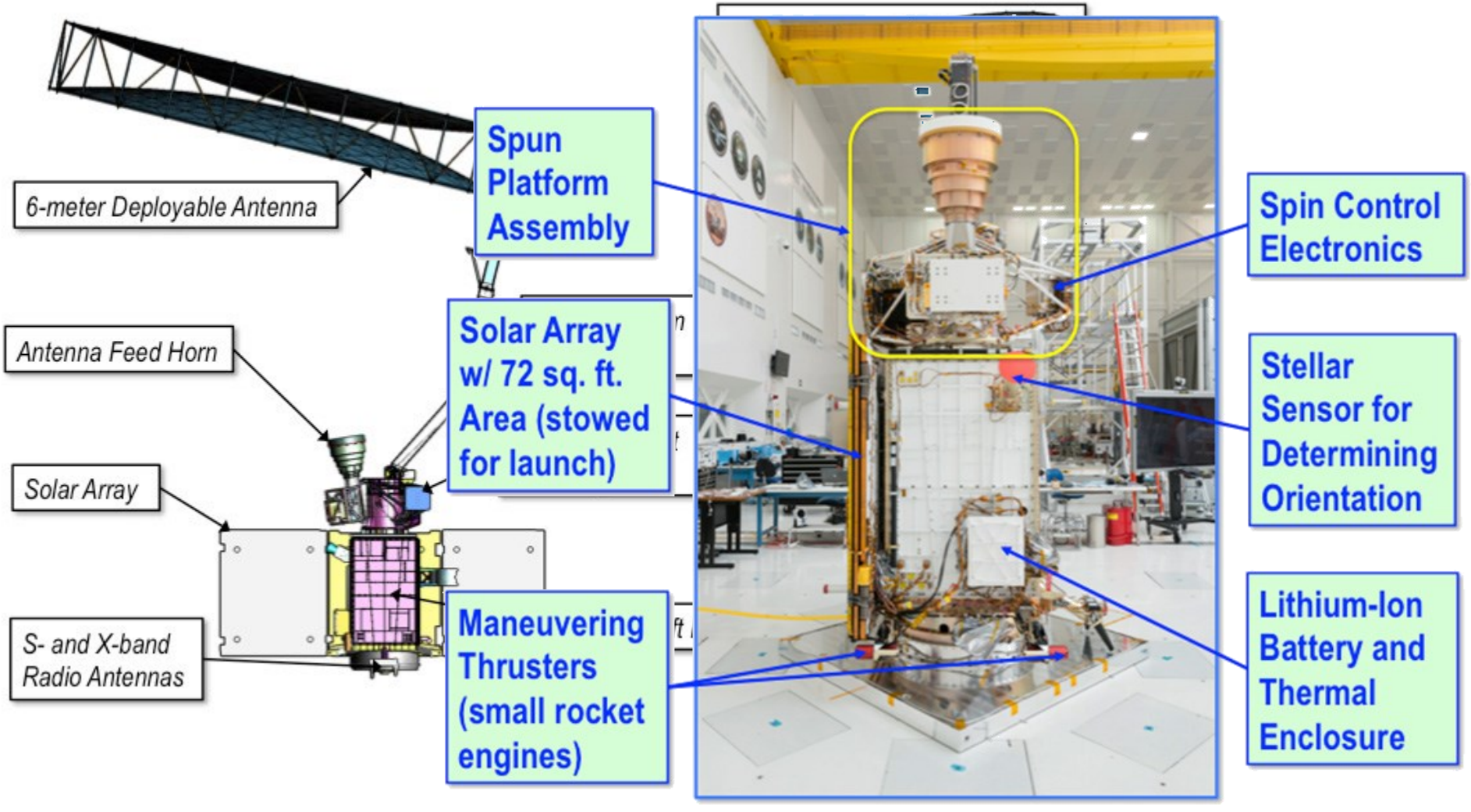
6-meter Deployable Antenna
Spun Platform Assembly
Antenna Feed Horn
Solar Array w/ 72 sq. ft. Area (stowed for launch)
Solar Array
S- and X-band Radio Antennas
Maneuvering Thrusters (small rocket engines)
Spin Control Electronics
Stellar Sensor for Determining Orientation
Lithium-Ion Battery and Thermal Enclosure

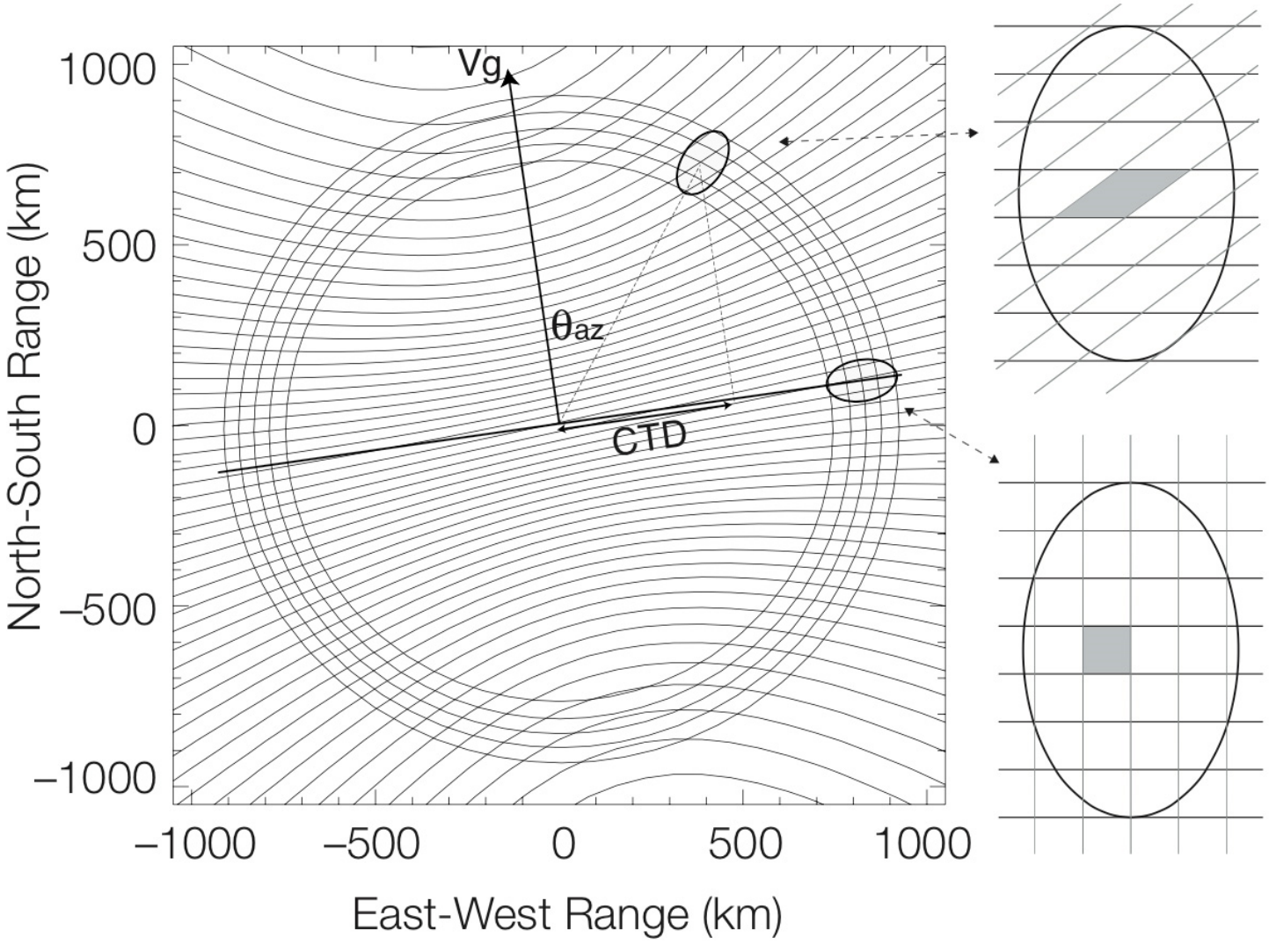
Vg
θaz
CTD
1000
500
0
−500
−1000
−1000
−500
0
500
1000
North-South Range (km)
East-West Range (km)

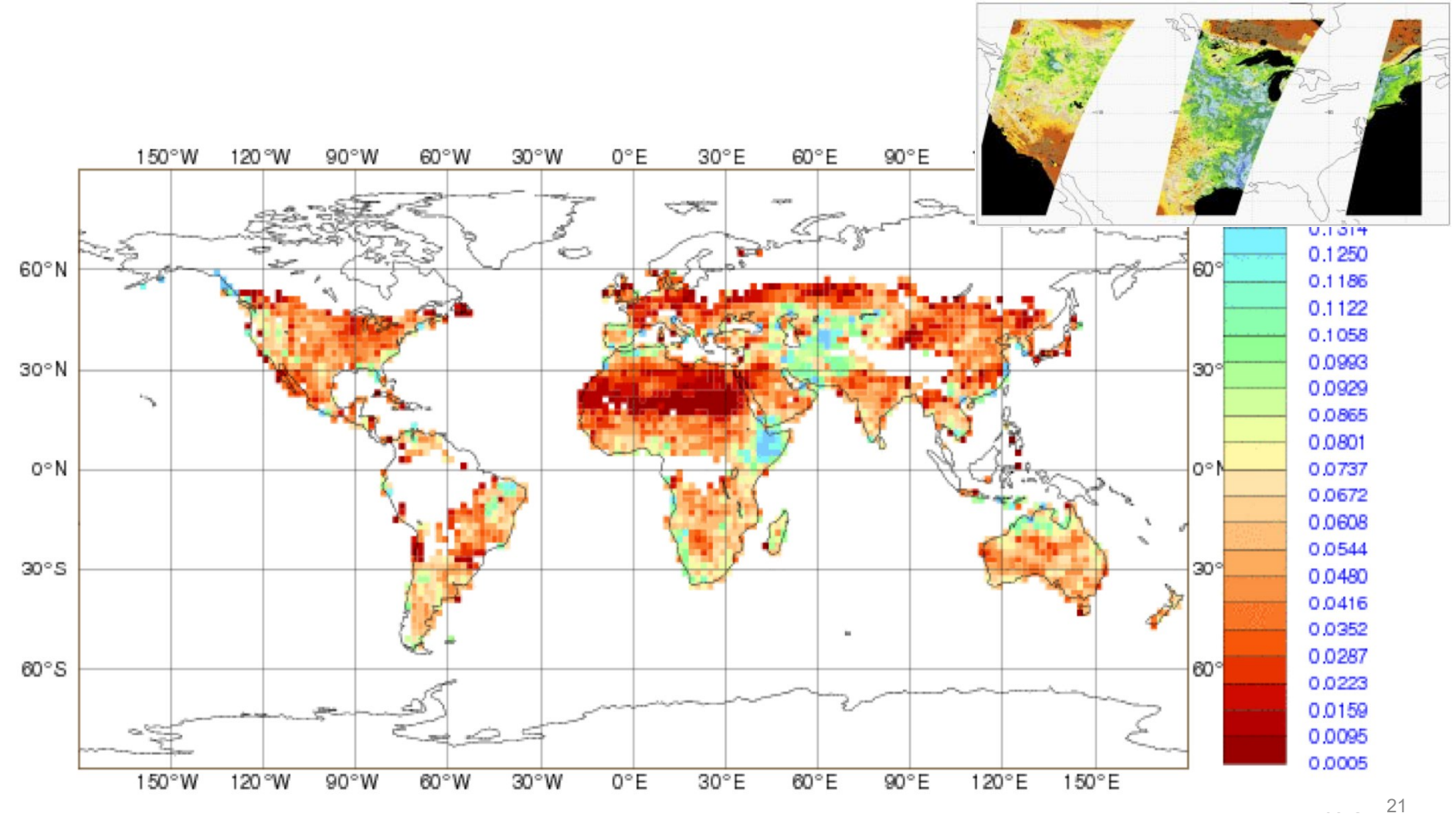
150°W
120°W
90°W
60°W
30°W
0°E
30°E
60°E
90°E
120°E
150°E
60°N
30°N
0°N
30°S
60°S
0.1250
0.1186
0.1122
0.1058
0.0993
0.0929
0.0865
0.0801
0.0737
0.0672
0.0608
0.0544
0.0480
0.0416
0.0352
0.0287
0.0223
0.0159
0.0095
0.0005

Product	Description	Gridding (Resolution)	Latency**	
L1A_Radiometer	Radiometer Data in Time-Order	-	12 hrs	Instrument Data
L1A_Radar	Radar Data in Time-Order	-	12 hrs	
L1B_TB	Radiometer T_B in Time-Order	(36×47 km)	12 hrs	
L1B_S0_LoRes	Low-Resolution Radar σ_o in Time-Order	(5×30 km)	12 hrs	
L1C_S0_HiRes	High-Resolution Radar σ_o in Half-Orbits	1 km (1−3 km)#	12 hrs	
L1C_TB	Radiometer T_B in Half-Orbits	36 km	12 hrs	
L2_SM_A	Soil Moisture (Radar)	3 km	24 hrs	Science Data (Half-Orbit)
L2_SM_P*	Soil Moisture (Radiometer)	36 km	24 hrs	
L2_SM_AP*	Soil Moisture (Radar + Radiometer)	9 km	24 hrs	
L3_FT_A*	Freeze/Thaw State (Radar)	3 km	50 hrs	Science Data (Daily Composite)
L3_SM_A	Soil Moisture (Radar)	3 km	50 hrs	
L3_SM_P*	Soil Moisture (Radiometer)	36 km	50 hrs	
L3_SM_AP*	Soil Moisture (Radar + Radiometer)	9 km	50 hrs	
L4_SM	Soil Moisture (Surface and Root Zone)	9 km	7 days	Science Value-Added
L4_C	Carbon Net Ecosystem Exchange (NEE)	9 km	14 days	

SMOS

(Soil Moisture and Ocean Salinity)

Payload:
Advanced L-band (1.4 GHz) radiometer (MIRAS)
Passive instrument
Launced 2009
Polar orbit (inclination 98º)
Period 100 min
Altitude 765 km
Mass 658 kg

Interferometric radiometer

- Interferometry tackles the **two limiting and fundamental problem** in traditional radiometry:

  1) **Impractical size** of several (even tens) meters is required from the antenna aperture at low frequencies
  → a sparse deployable array to synthesize a larger aperture

  2) **Scanning** required to cover a wide swath
  → Two-dimensional imaging within each integration without any moving parts

INSTRUMENT

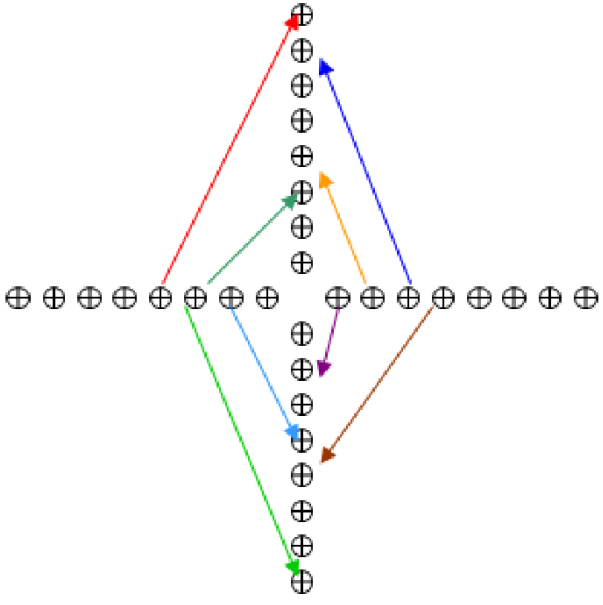

Spectrum samples

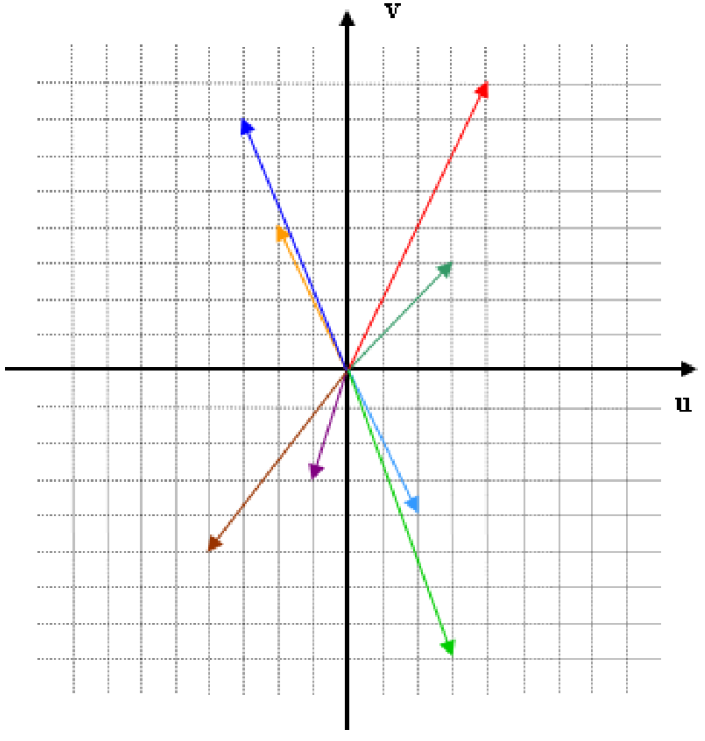

SMOS at ESTEC electrical testing

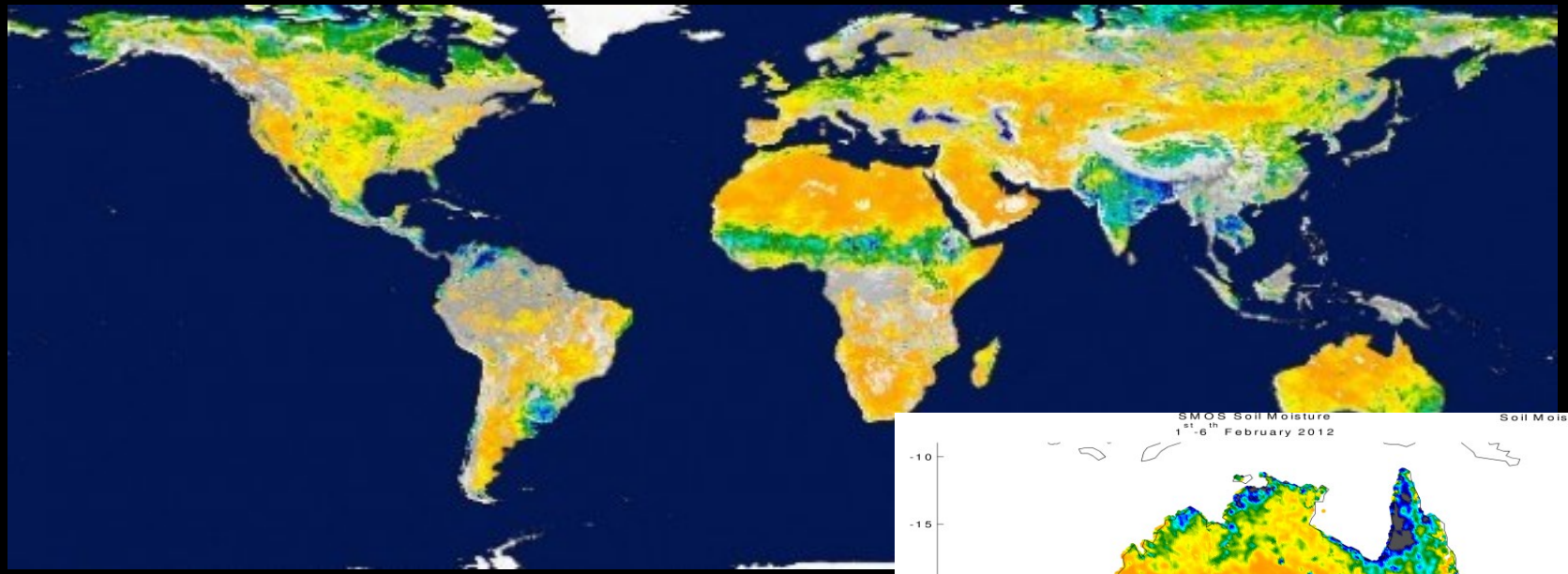

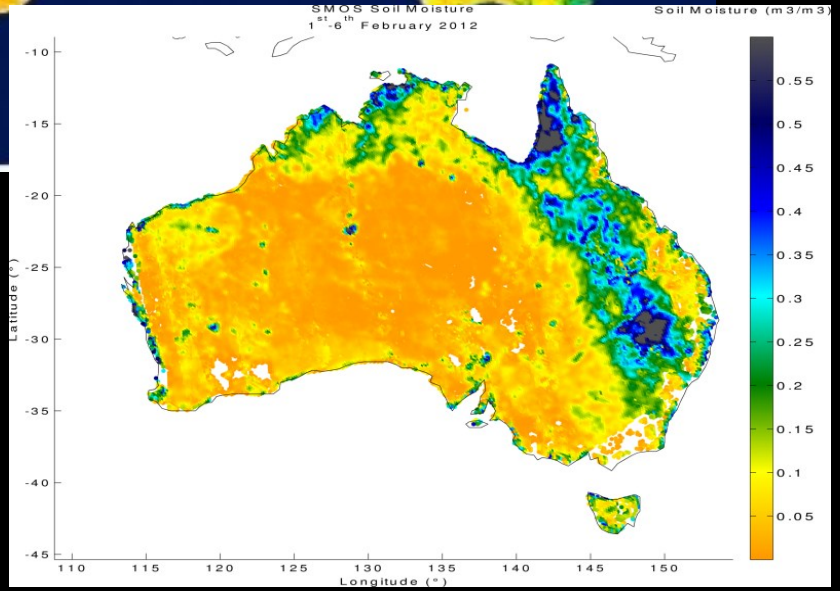

Global Soil Moisture

L-band T_B images Europe

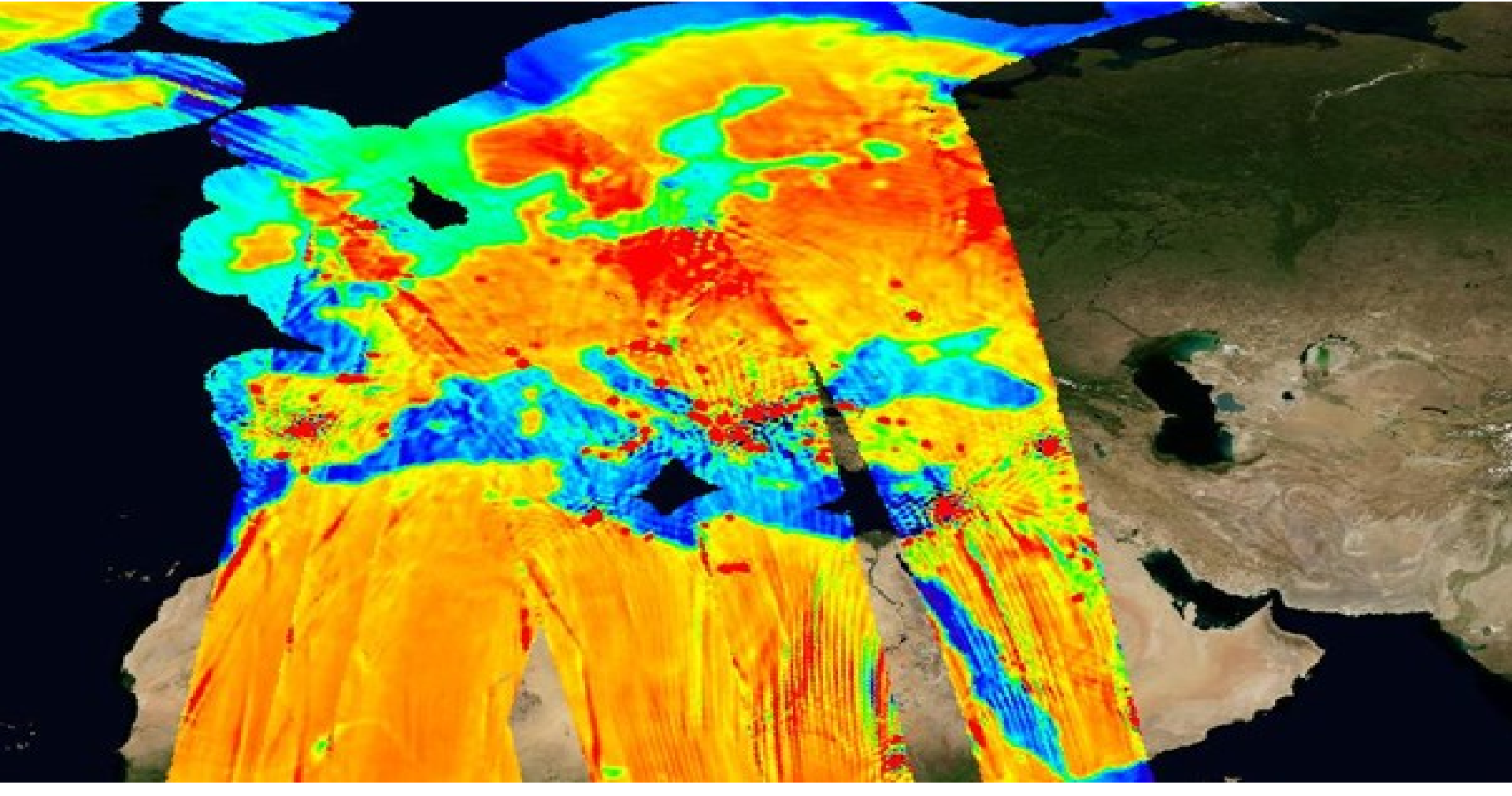

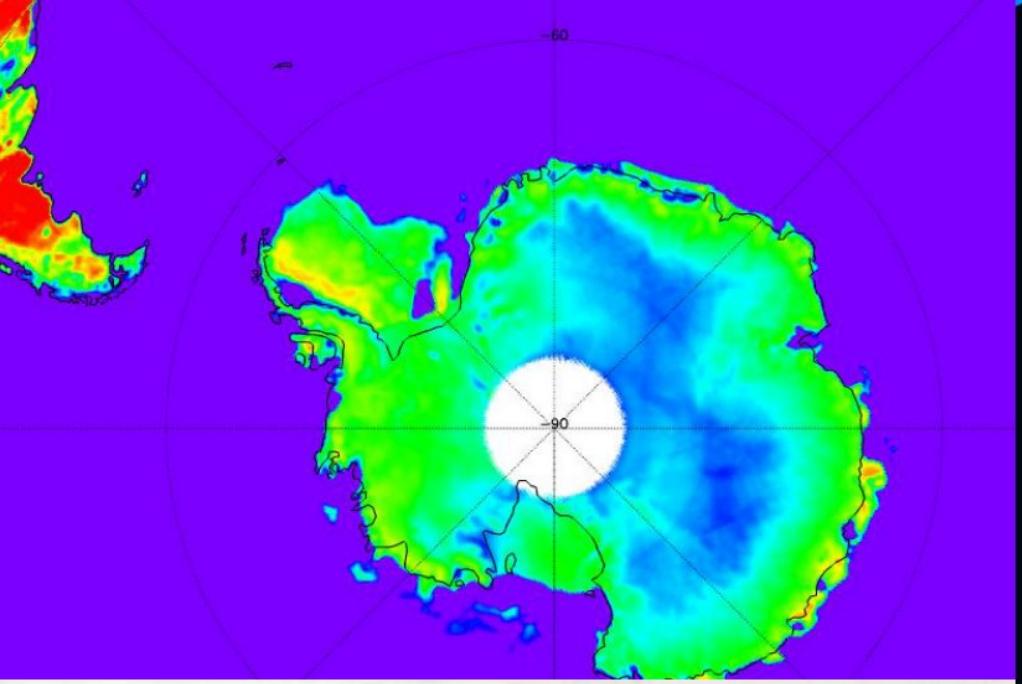
-60
-90

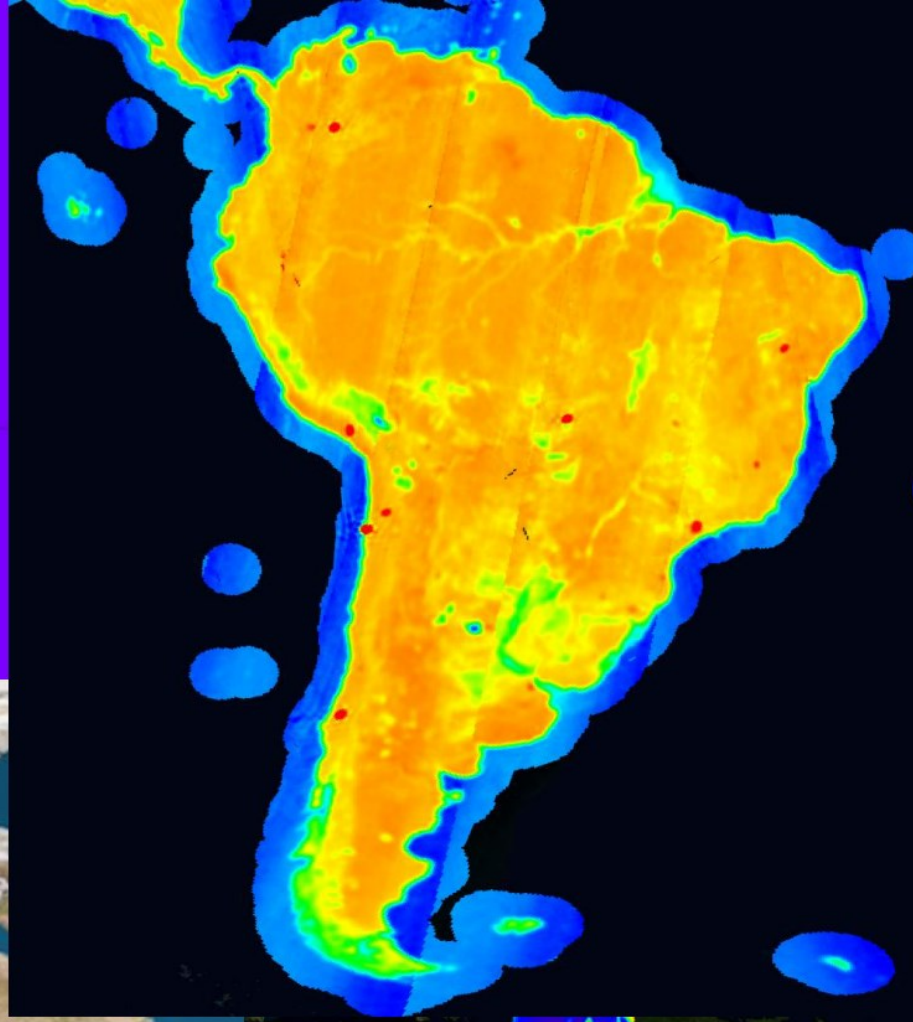

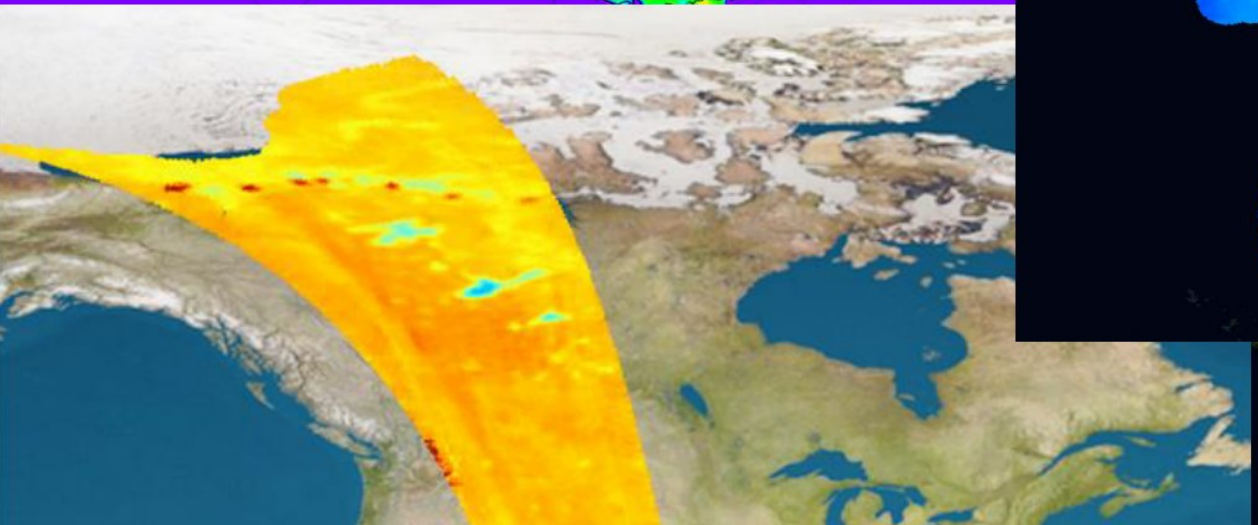

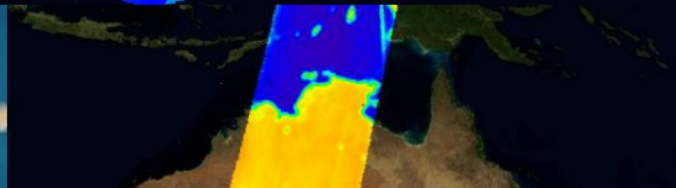

Aalto University
School of Electrical
Engineering

Radio Frequency Interference

Prohibited interferences!

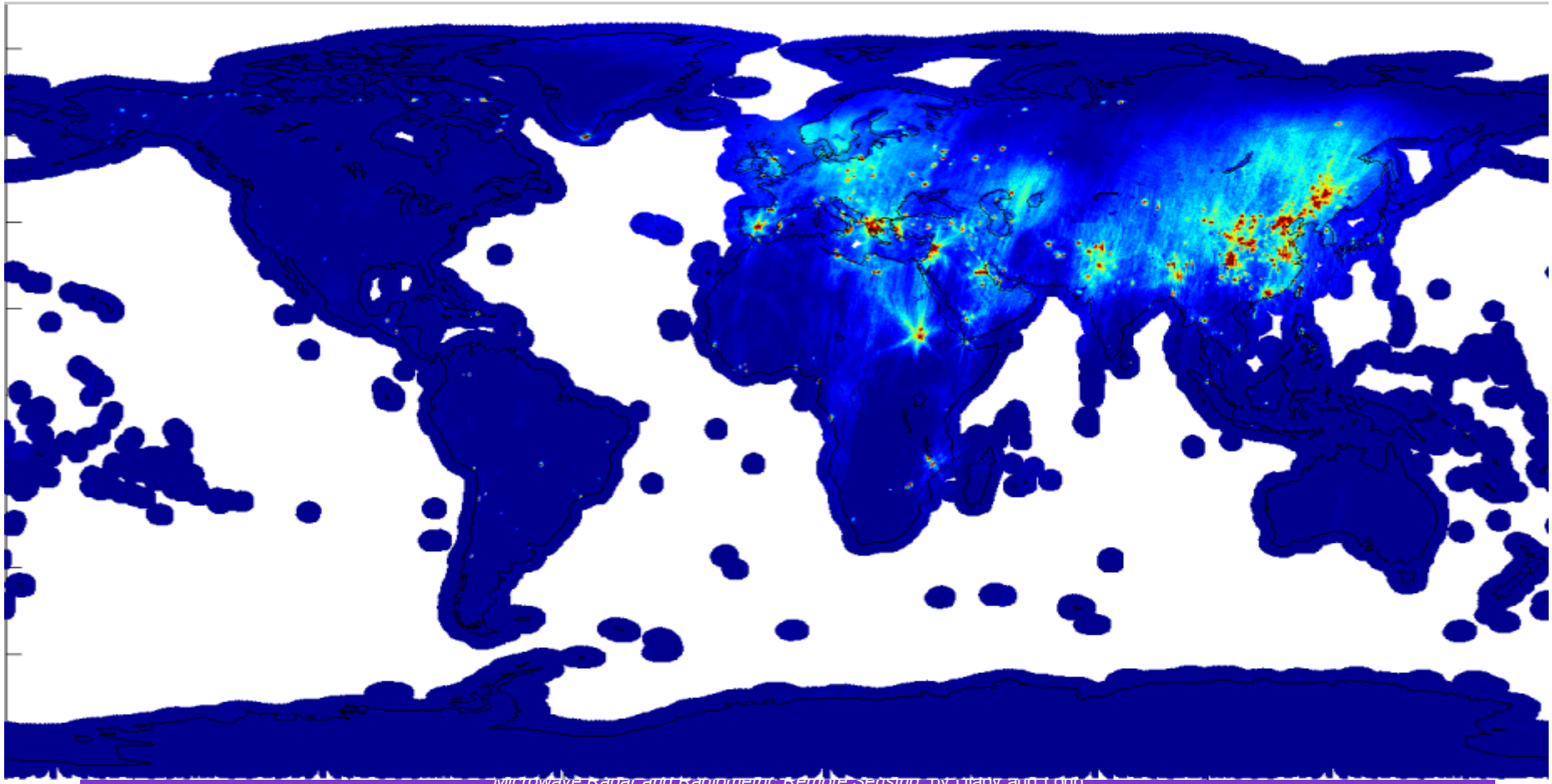

Probability of RFI in Europe!

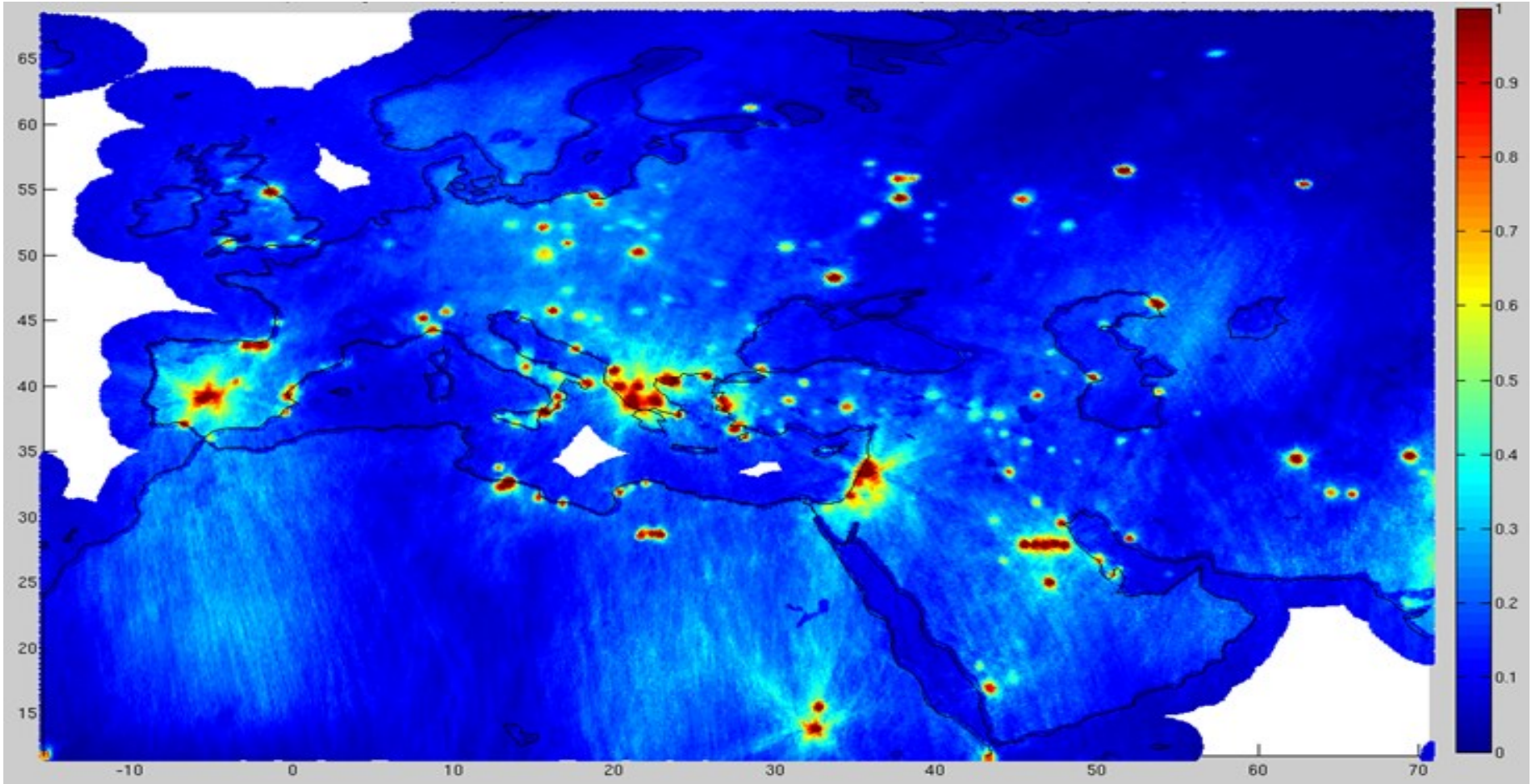

The sea ice thickness from SMOS

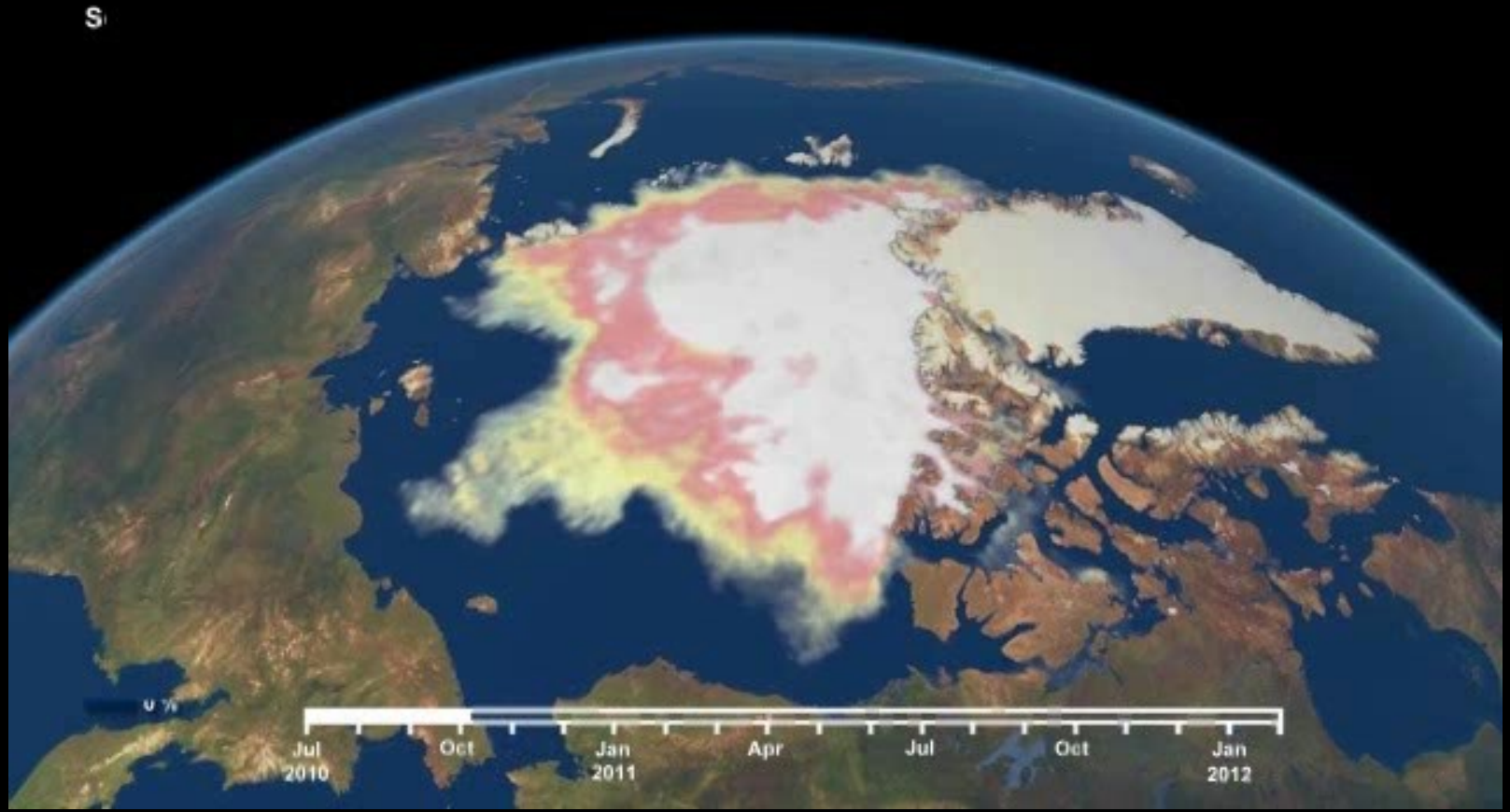

University of Hamburg / KlimaCampus / CliSAP / Institute of

Aalto University
School of Electrical
Engineering

Calibrating and verifying

Airborne systems

Primary platform of the HUT-2D is Department's aircraft

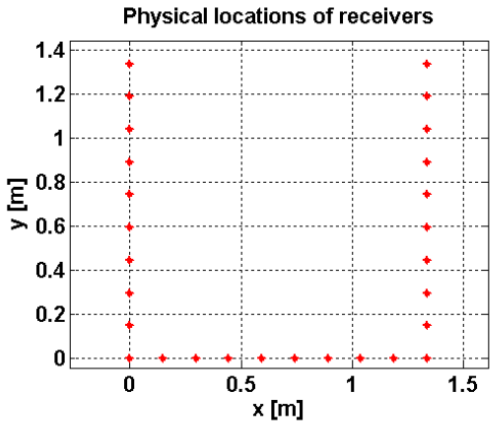

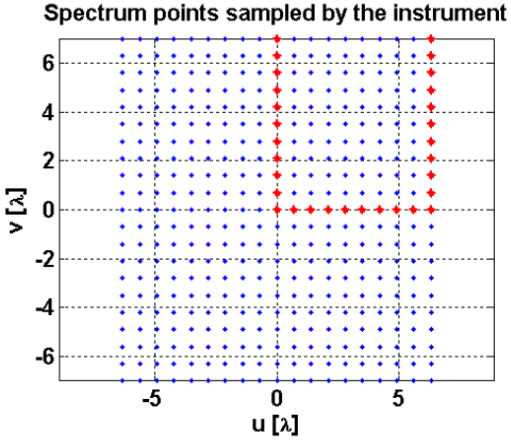

MEASUREMENT

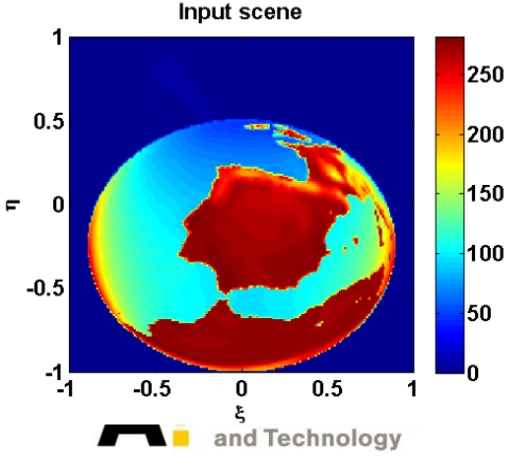

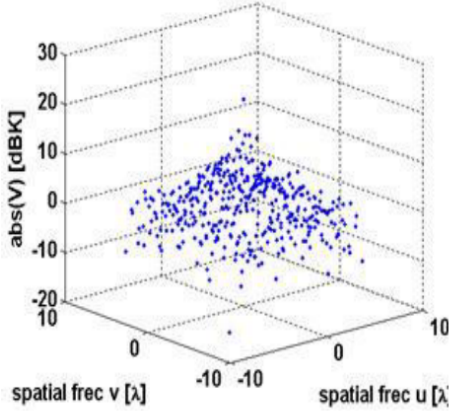

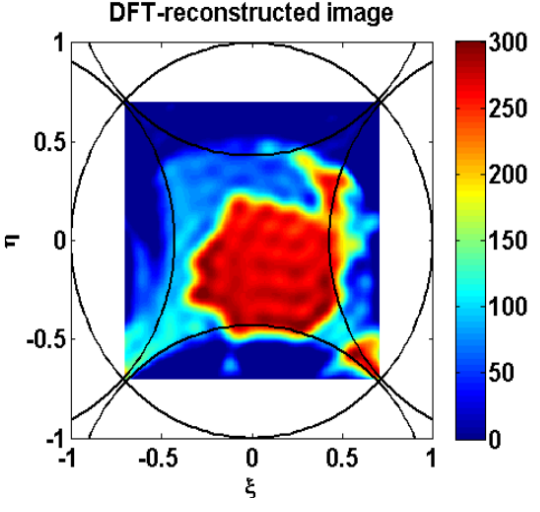

and Technology

Flying Remote Sensing Laboratory: Skyvan

- The only University-owned and operated remote sensing aircraft in Europe
- Most aircraft instruments were built in projects involving graduate and undergraduate students
- Instruments used as satellite sensor demonstrators
- HUT-2D: the world's first airborne interferometric radiometer (1.4 GHz frequency; 36 identical antennas and receivers)
- 6 – 94 GHz microwave radiometer: 14 channels
- 5.3 / 9.8 GHz quad-polarization radar scatterometer
- Imaging spectrometer 400 – 900 nm wavelength
- Infrared, video and conventional cameras
- GPS and attitude data
- Used in numerous national /international campaigns

Radiometesr mounted to airplanes cargo doorway

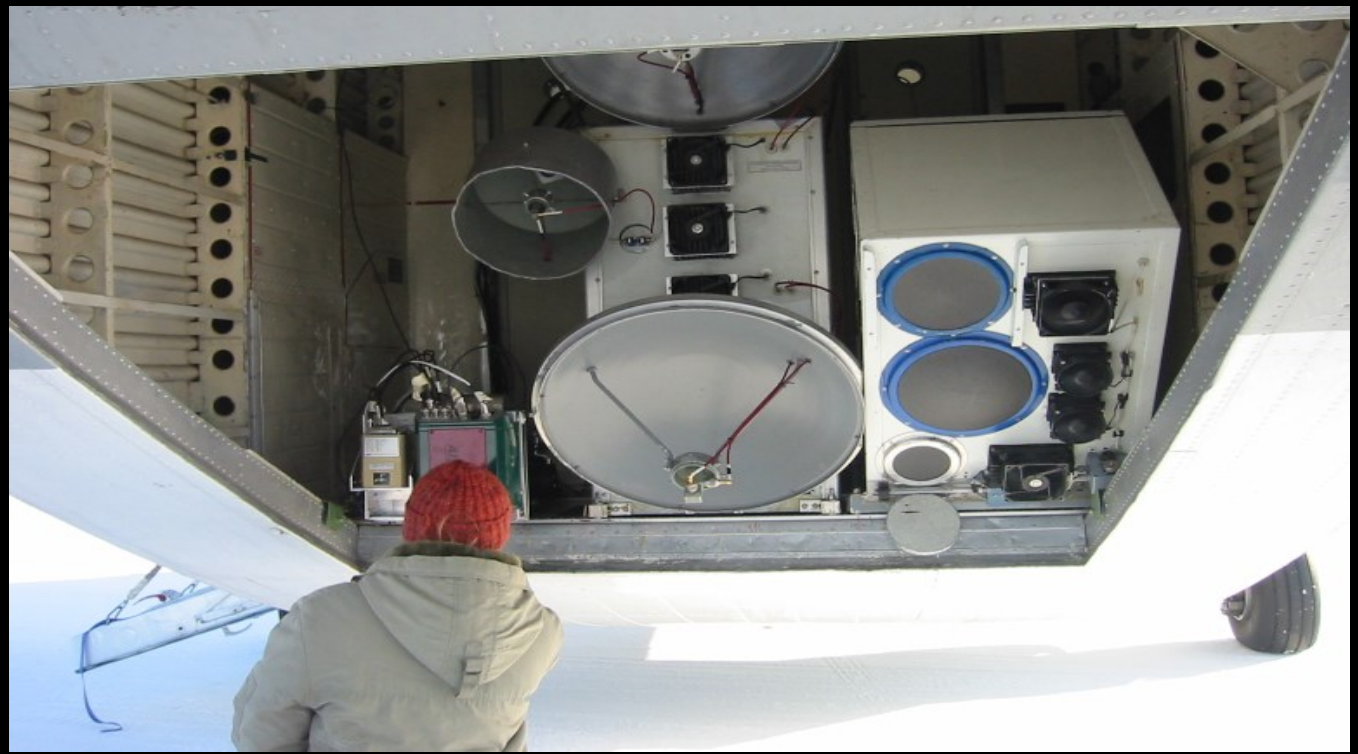

Research aircraft SkyVan

Aalto University
School of Electrical
Engineering

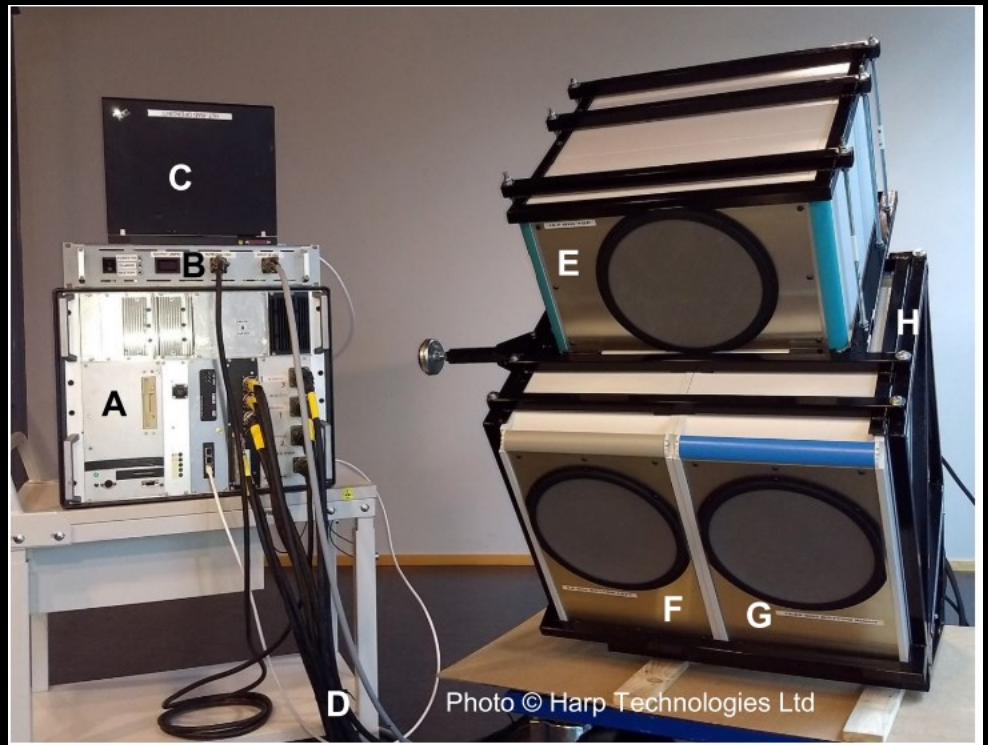

Figure 11. The overall HUTRAD 2.0 system: A) Control Processor Unit (CPU); B) Uninterruptible Power Supply (UPS); C) monitoring workstation; D) cable harness; E) 18.7 GHz receiver; F) 6.8 GHz receiver; G) 10.65 GHz receiver; H) support frame.

Instrumentation

- Refurbished HUTRAD 2.0 radiometer system
  - 6.8, 10.65 & 18.7 GHz, V & H pol
- Infrared camera (Infratec VarioCAM HDx head 600)
- Optical cameras (GoPro)
- Precision GPS and IMU
- Installation on Norlandair de Havilland DHC-6 Twin Otter

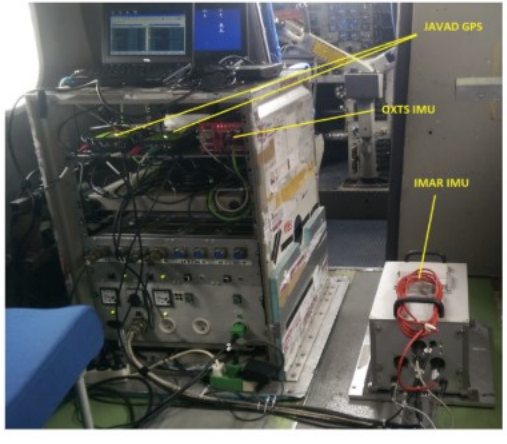

What is CIMR?

- EU High Priority Candidate Mission (HPCM):
  CIMR – Copernicus Imaging Microwave Radiometer
- Mission to support the EU Arctic Policy
- Global coverage with focus on Polar Regions
- Observed parameters:
  - **Sea Ice Concentration**
  - **Sea Surface Temperature (SST)**
  - Thin Ice Thickness; Sea Ice Drift
  - Snow Depth on sea ice and SWE on land
  - Salinity; Wind Speed
  - Many more including land (e.g. soil moisture)
- Launch 2025+

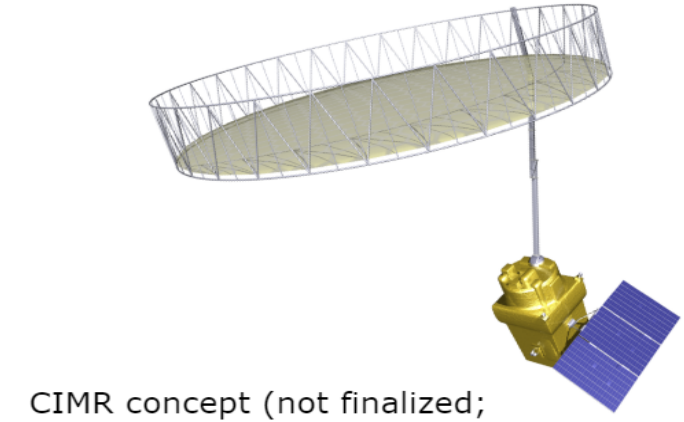

CIMR concept (not finalized; credit AIRBUS)

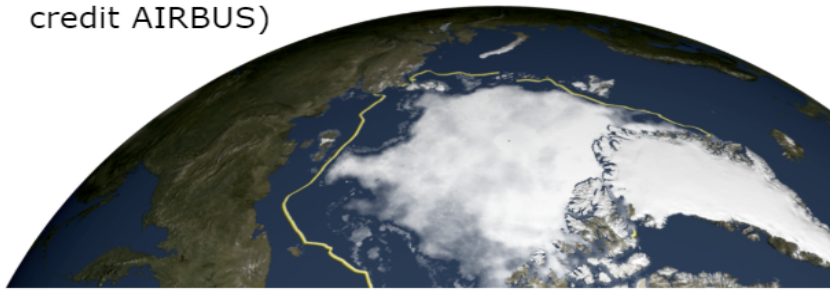

Data – Science flights

Example: Test area C on March 8, 2019

6.8 GHz V pol

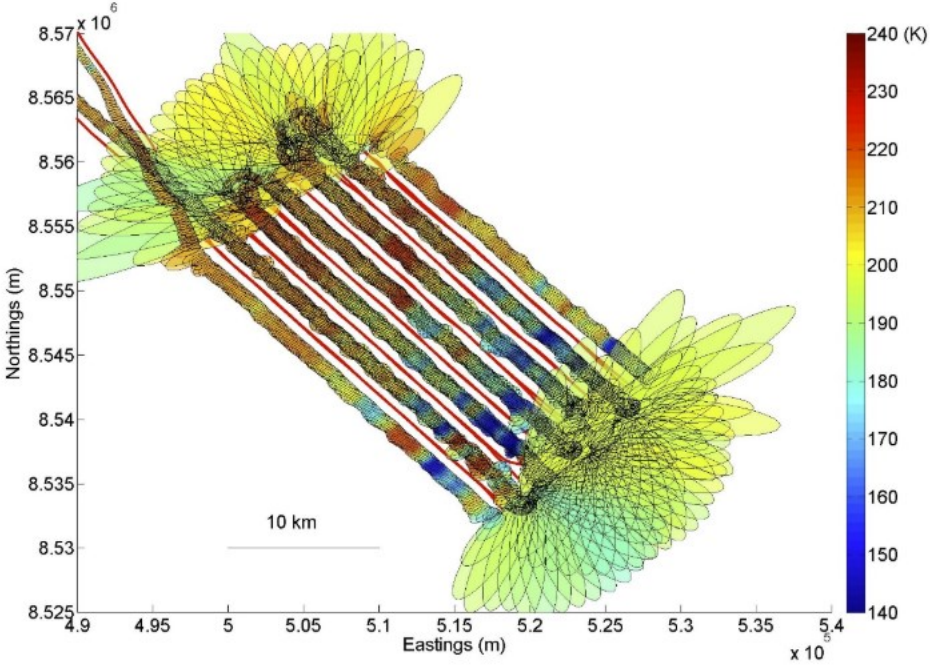

6.8 GHz H pol

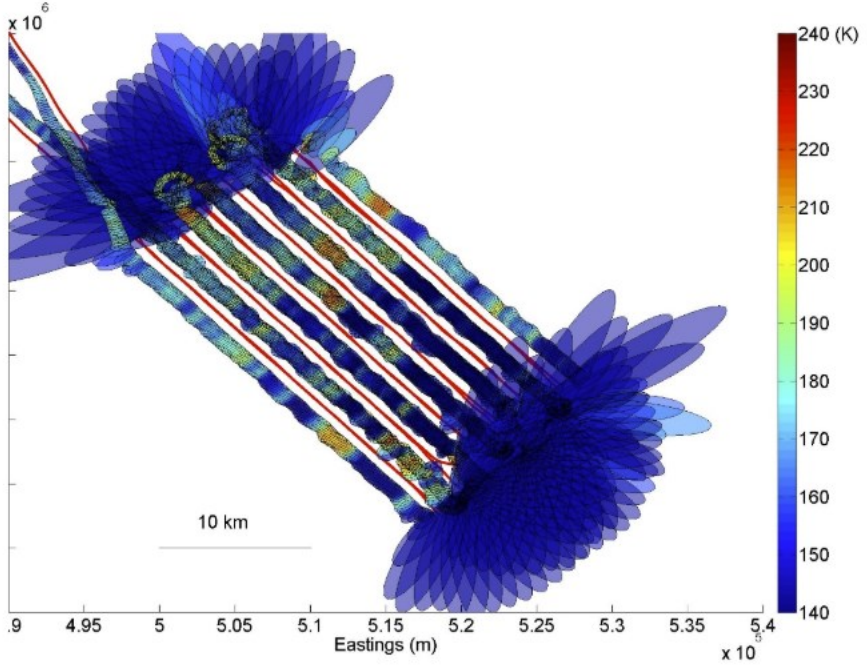

Aalto University
School of Electrical
Engineering

Calibrating and verifying

Ground measurements

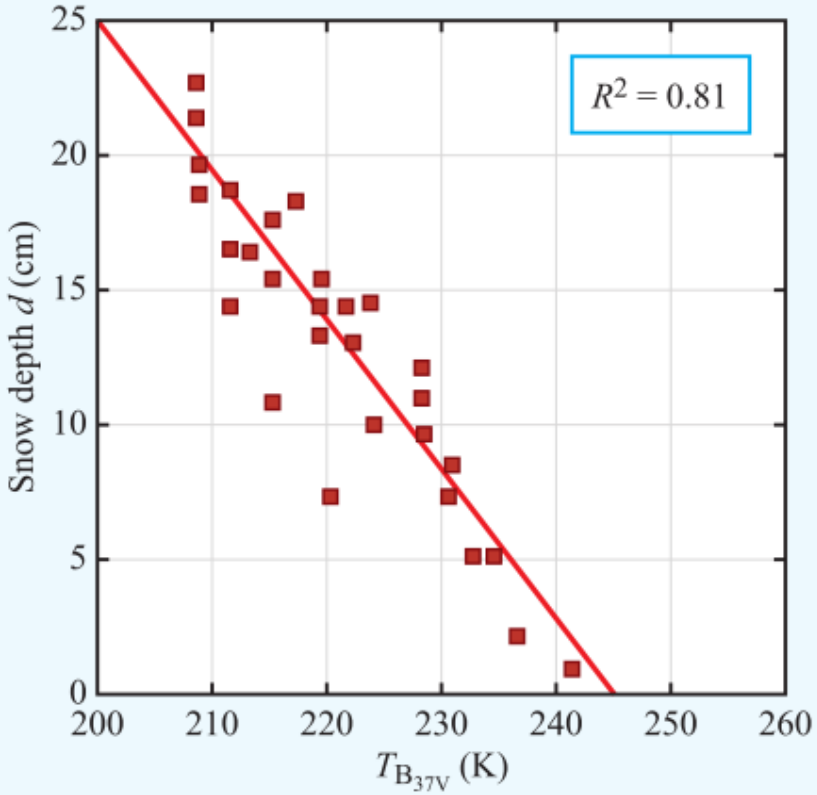

(b) Canadian high plains, 12 February 1983

Figure 12-53: SMMR brightness temperature versus snow water equivalent for (a) Russian steppes, 15 February 1979 and (b) Canadian High Plains, 12 February 1983 [Chang et al., 1987].

From: Microwave Radar and Radiometric Remote Sensing, by Ulaby and Long, 2014, with permission.

Freezing Soil map by SMOS

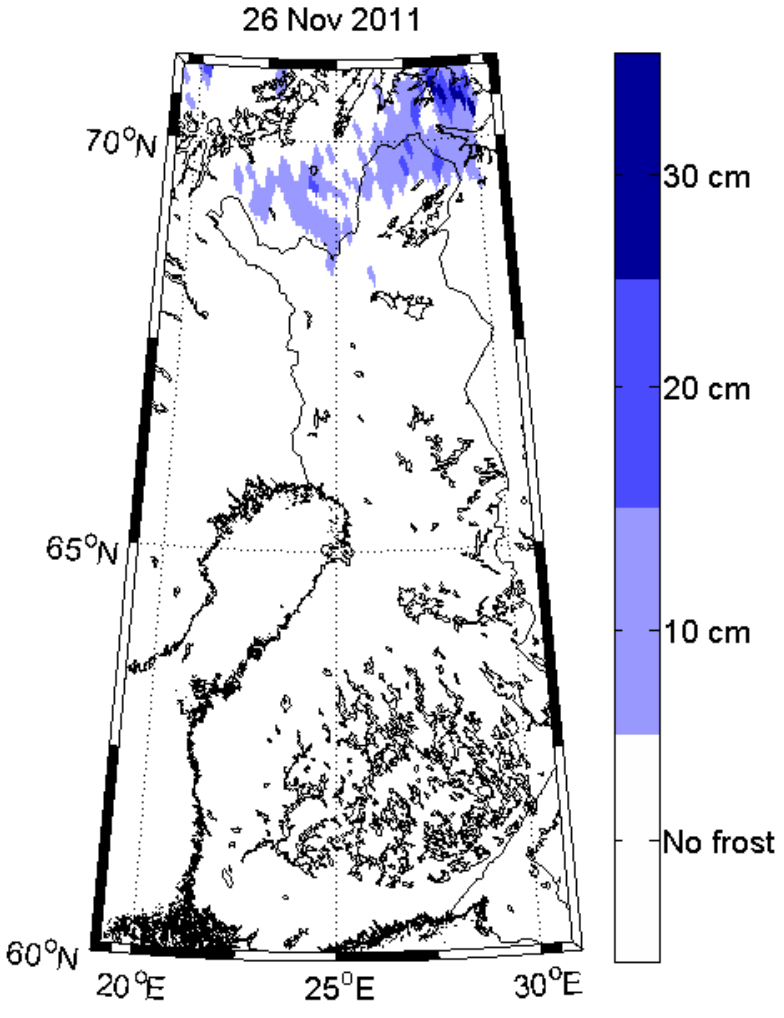

Aalto University
School of Electrical Engineering

Rautiainen, Kimmo; Lemmetyinen, Juha; Schwank, Mike; Pulliainen, Jouni; Mätzler, Christian; Kontu, Anna; Wiesmann, Andreas, "An Innovative Application for SMOS: Characterization of Seasonal Soil Freezing" EGU General Assembly 2013, held 7-12 April, 2013 in Vienna, Austria.

- Ulaby
- Long
- Blackwell
- Elachi
- Fung
- Ruf
- Sarabandi
- Zebker
- Van Zyl

Microwave Radar and Radiometric Remote Sensing